Electron scattering on radioactive ions at GANIL

A Chancé, Pierre Delahaye, F. Flavigny, V. Lapoux, A. Matta, V. Somà

Electron scattering on radioactive ions at GANIL[2]
Grand Accélérateur National d'Ions Lourds et de Leptons

<div align="right">1st December 2020</div>

Authors: A. Chancé[1,*], P. Delahaye[2,¤], F. Flavigny[3,µ], V. Lapoux[1,µ], A. Matta[3,µ], V. Somà[1,t]
* engineer-physicist in beam dynamics; ¤ physicist expert of ion trap techniques for beam production, µ physicist in structure studies via experiments of direct nuclear reactions; t physicist in nuclear structure theories
antoine.chance@cea.fr;pierre.delahaye@ganil.fr;flavigny@lpccaen.in2p3.fr; valerie.lapoux@cea.fr;matta@lpccaen.in2p3.fr;vittorio.soma@cea.fr

Contributors for discussions and future studies in 2021 about:
Radioactive ion beam RIB production
-multi-nucleon transfer, fusion-evaporation (*V.1, App. D.1*): I. Stefan[5], C. Theisen[1];
-fission; photofission (*V.1, App. D.3-4*): M. Fadil[2]
Radioprotection issues, production building: H. Franberg[2], X. Hulin[2] (***V.3***)
Radioactive ion beam production and interdisciplinary activities (working group): A. Drouart[1], G. de France[2]
Physics cases and ERL: A. Obertelli[4], D. Verney[5]
Discussions about ERL design and beam optics: W. Kaabi[5]

1. CEA-Saclay, Irfu 2. GANIL 3. LPC Caen 4. TU Darmstadt 5. IJCLab

Abstract
Electron scattering on stable nuclei represented milestones for our knowledge on nuclear properties. The purpose of the present proposal is to revive the physics of electron-ion collisions for radioactive nuclei at GANIL. Electron radioactive-ion collisions would open a new window on nuclear structure studies by collecting detailed data for ground-state density distributions and radii, transition densities to excited states and, in the long term, nuclear strength functions. These data would represent key observables directly comparable to the nuclear structure models. Taking into account the possible Radioactive Ion beams produced at GANIL with enough intensity and long enough half-life times, -soon available or possible in the mid-term future- we propose a colliding e-RI machine starting with RI beams above 10^7/s, electron intensity of $I \sim 100$ mA (up to 200 mA), energies at 500 MeV (choice between 500-700 MeV is discussed), for a luminosity from 10^{28} $cm^{-2}s^{-1}$ going up to 10^{29} with a search of potential improvement at 10^{30-31} $cm^{-2}s^{-1}$ in a later phase.

In the present document, we examine the main technical issues related to the first step of the project with standard requirements of a luminosity at 10^{28-29} (with dedicated R&D work to overcome the ion trap limitations). With the luminosity targeted at 10^{29}, the project corresponds to the performance ensuring the realization of the main physical cases, which could be reachable in the years 2030-2035. The limits over the nuclear chart are discussed, corresponding to the cases of RI beams fulfilling the requirements (combination of long lifetimes >100 ms and enough intensities >10^7/s) for the electron-RI collision experiments. From the estimate of the luminosity and of the potential technical constraints, the set of parameters ensuring the feasibility of the electron-RI collisions and the stable operation of the machine are discussed. They should be consolidated in a detailed R&D project followed by a conceptual design report.
This gives us guidelines to define the ranges of the parameters and to delineate the realistic foreseen performances and the potential evolution of the facility, envisioned to reach luminosities at 10^{30-31} in the years 2040s, s giving access to new physical cases (for the exploration of the nuclear densities of isotopes beyond the limits of the 10^{29}) and to other observable sets (like nuclear strength functions via (e,e'p)).

Background. *We recall in our document the main scientific motivations of our contribution given in March to the international committee "Nuclear structure from electron-ion collisions" [**ERIB2020**] following proposals raised in the NuPECC Long Range Plan 2017 Perspectives in Nuclear Physics [**LRP2017**] and the ETIC project studies for an Electron Trapped Ion Collider at GANIL, presented in 2015 [**ETIC15**] in the framework of the GANIL-2025 prospectives.*
We now focus on the conditions for the feasibility of the potential machine, expanding the parts describing the technical constraints, questions and challenges of the project.
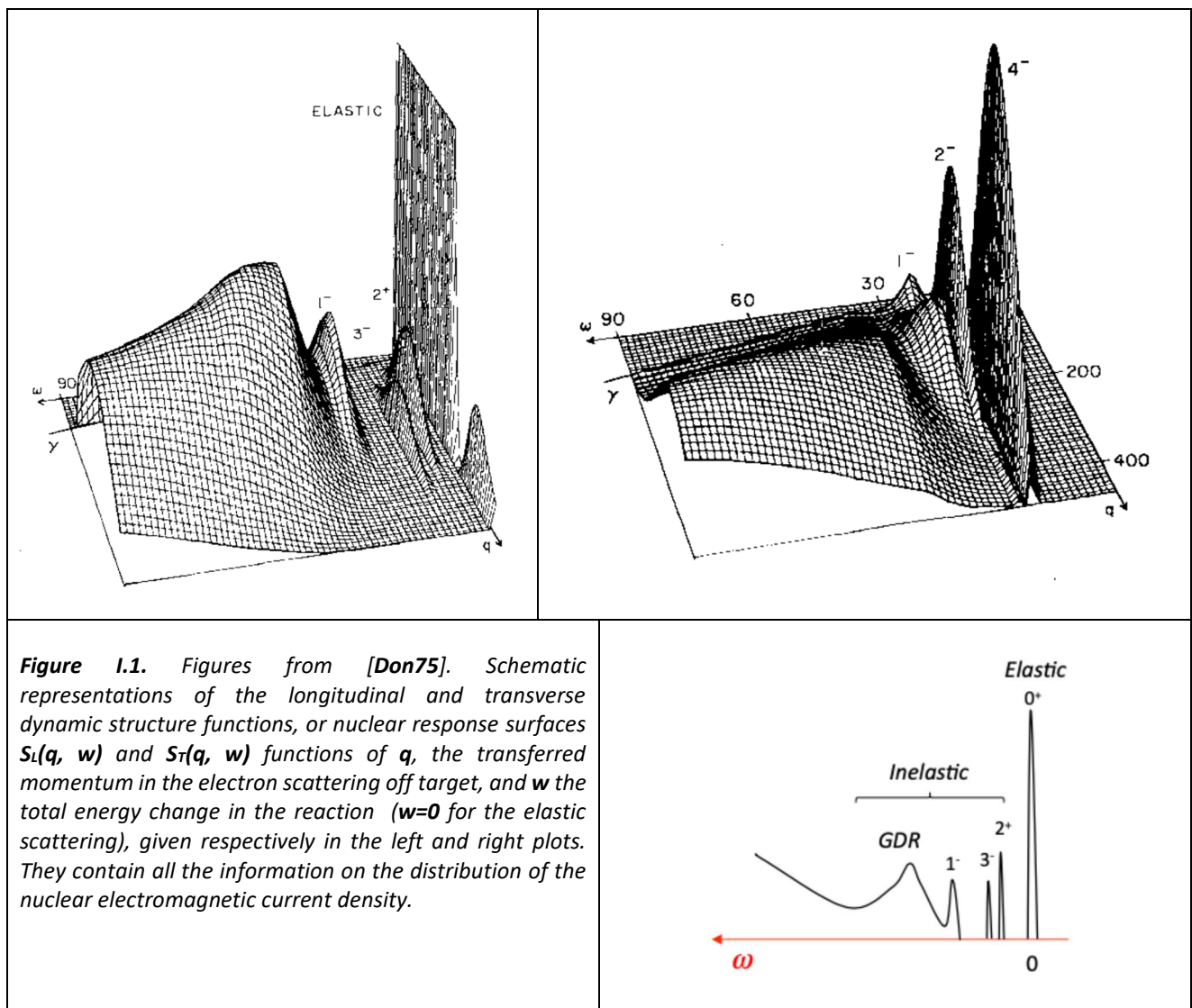
Outline

I. A microscope on the nuclear densities

I.1 Introduction. Scope and history. Past and future milestones of our knowledge on nuclear densities

Since the pioneering work of R. Hofstadter distinguished by the Nobel prize in 1961 [*Hof53*], decades of experimentation [*FroP87, Ae91*] have demonstrated that electron scattering is one of the best probes to study the structure of hadronic systems such as nuclei and nucleons. The spatial resolution offered by electron of several hundreds of MeV allows to extract a variety of spatially-dependent distributions (radial charge density, charge transition density, magnetic current distributions) very constraining for nuclear models and going beyond integrated quantities (mean square radii, electromagnetic transition probabilities).

The strength of this resolving power is illustrated in Fig.I.1 depicting the ability to go from a one dimensional excitation function of a nucleus (bottom drawing) to the full nuclear response surfaces of this system (also called dynamic structure functions) using electron elastic and inelastic scattering. Details on the variety of observables accessible using these processes will be provided later in this document but one can already easily size the gain in sensitivity offered by this deeply penetrating probe, similar (to some extent) to the jump from simple imaging to full tomography.

Figure I.1. *Figures from [*Don75*]. Schematic representations of the longitudinal and transverse dynamic structure functions, or nuclear response surfaces $S_L(q, w)$ and $S_T(q, w)$ functions of q, the transferred momentum in the electron scattering off target, and w the total energy change in the reaction ($w=0$ for the elastic scattering), given respectively in the left and right plots. They contain all the information on the distribution of the nuclear electromagnetic current density.*

The richness of the above-mentioned resolving power combined with the precise knowledge of the electromagnetic scattering process (via QED) motivated worldwide research programs of electron scattering on stable nuclei from the 50s until the end of the 90s whose solid results are at the heart of our current understanding of nuclei. To reach these achievements, intensive cross-section measurements were done

varying the electron beam energy to extend the range of transfer momenta and took place in the different facilities developed for this purpose during this period.

The worldwide panorama for these studies included in this period: in the United States, the MIT Bates Laboratory, the SLAC followed by the Jefferson Laboratory (starting, end of 90s, the research on the quasi-elastic electron scattering on nuclei and on the nucleon structure) and, for instance, in Europe, the Saclay Laboratory in the 80-90s. These labs provided most of the nuclear data we have up to now, compiled in the nuclear data tables [**ANDT87**] and used as references to discuss the ground state radii and densities of stable nuclei, and also the transition densities to excited states via (e,e') and (e,e'p) spectroscopic studies. The most illustrative and textbook results of these worldwide efforts are shown in **Figs. I. 2** and *I.3*: the elastic scattering cross section of electron on ^{208}Pb was measured on about 12 orders of magnitude and the model-independent density extracted from these data precisely down to very small radius. In *Fig. I.3*, one can see the charge density difference between^{206}Pb-^{205}Tl extracted from the (e,e) measurements.
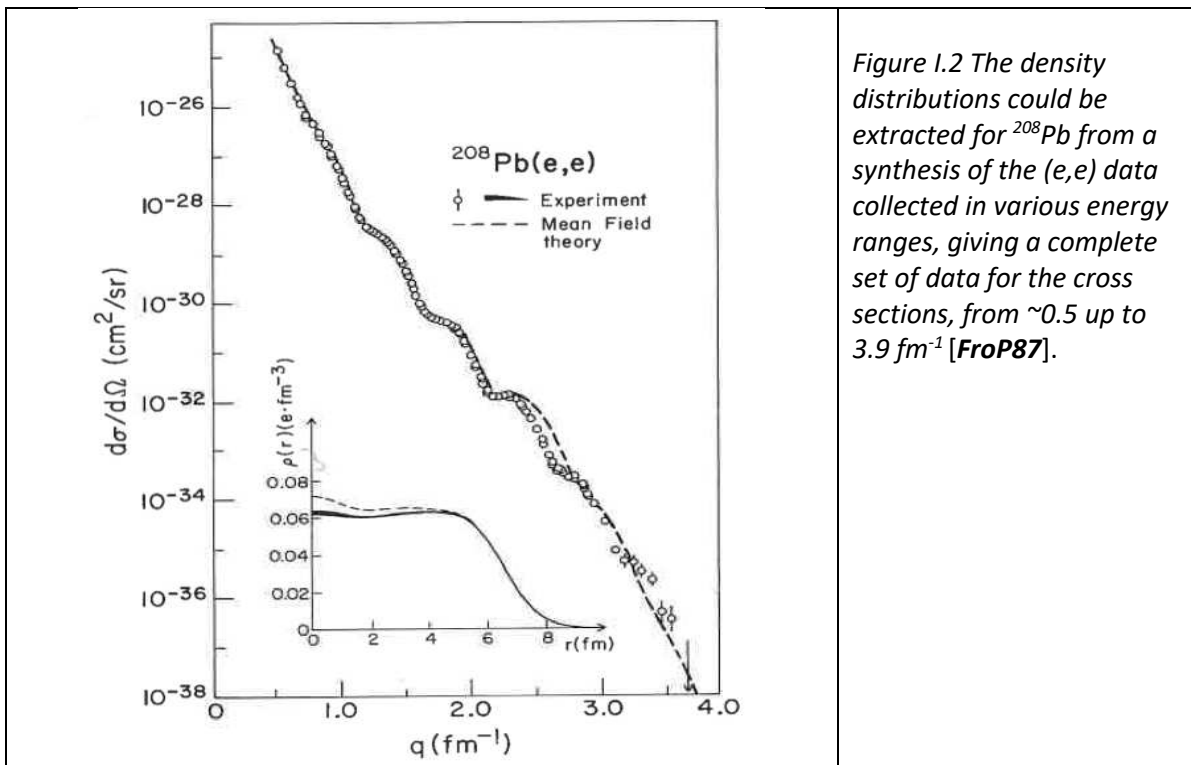
*Figure I.2 The density distributions could be extracted for ^{208}Pb from a synthesis of the (e,e) data collected in various energy ranges, giving a complete set of data for the cross sections, from ~0.5 up to 3.9 fm^{-1} [**FroP87**].*

Figure I.3. *Figure and caption from [**Fro83**]. Experimental charge densities for ^{206}Pb and ^{205}Tl obtained by (e,e) scattering at 500 MeV. Comparison of the experimental and the adjusted theoretical charge density difference of ^{206}Pb and ^{205}Tl obtained by (e,e) scattering at 500 MeV. From this charge difference, the shape of the 3s proton orbit was extracted without ambiguity. This was done using Woods-Saxon single particle radial densities of shells expected to contribute to the ^{206}Pb and ^{205}Tl difference. The extraction was validated via the experiment-theory comparison of the contributions to the cross-section ratios ^{205}Tl/^{206}Pb of the 3s, 2d and 1g shells.*

4
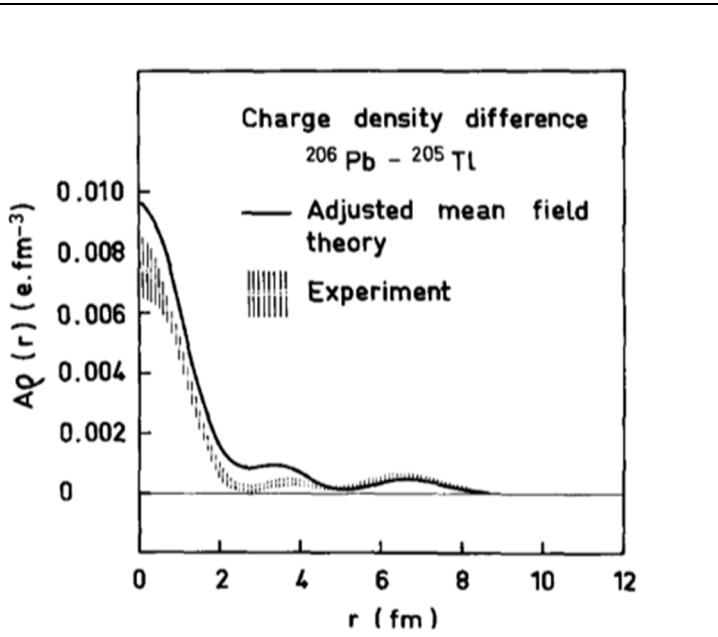
In short, the history of this research field demonstrate that electrons constitute optimal probes for the study of several properties of atomic nuclei. Their point-like nature (excellent spatial resolutions) and the fact that the electromagnetic interaction is weak (low re-scattering rates and simpler theoretical tools, e.g. perturbation theory) and theoretically well-constrained make the reaction mechanism under control. This allows a clean extraction of nuclear properties.

I.2 Next-generation nuclear structure studies with electron-RI collisions

At the end of the 80s, the area of radioactive ion beam facilities started. Since it was not possible to make targets of the short-lived isotopes, nuclear structure investigations have been pursued mainly using hadronic probes. Integrated information was obtained for rms radii of charge densities via laser/muonic spectroscopies of unstable radioactive ion nuclei, and for nuclear matter radii from RI collisions with hadronic probe (proton, heavy ion beams).

The **table I.1** summarizes the present knowledge we have on structure density observables for radioactive nuclei, from laser, muonic spectroscopy and proton scattering probe [**Diffpp**]. Despite the discussion on the accuracy of the models used to extract the information from the measurements, if we focus on the benchmark microscopic models used to obtain the structure characteristics (rms radii, moments), the precision on these values are due to the involved physical process itself.

Observables deduced quantities	Reactions-Processes *RI energies*	Intensity I Experimental conditions Precisions
r.m.s. charge radii	Laser spectroscopy Muonic spectroscopy	charge rms r_{ch} ~± 0.005 -0.01 fm
r.m.s. matter radii *matter density profile using combined (p,p) sets (various q transfer momentum ranges)*	**Interaction cross sections (p,p)** *elastic* *10 to 1 GeV/nucleon*	I > 10^4 10^6 s^{-1} inverse kinematics thick target matter rms r_m ± 0.1 fm
Neutron-skin r.m.s radii *Using known charge radii (see above)* from ρ_m and ρ_{ch}	**Combined (p,p) and (p,p')** analysis of data sets few 10 MeV/n ; wide angular range *(~10-160 deg. c.m)*	(p,p) I: 10^6 s^{-1}; (p,p') I:10^{6-8} s^{-1} inverse kinematics r_n-r_p ~ ± 0.1 fm

Table I. 1. Structure observables available for radioactive ion nuclei.

Perspectives for the form factors of exotic nuclei

Via future e-RI experiments, we propose first to investigate directly the charge density distributions of these exotic systems in which unique quantum phenomena emerge.

We plan to start an extensive program to measure (e,e) elastic scattering cross sections to extract directly the charge density distributions through a model-independent analysis and to compare them to theoretical predictions. Theory-wise, detailed densities are much more demanding than integrated quantities (such as root mean square radii) and encapsulate different correlation effects. As such, they offer an unprecedented test bench for state-of-the-art nuclear structure models. Their availability over a wide range of unstable isotopes would thus systematically provide model-independent constraints very complementary to information from other probes like (p,p) scattering.

The possibility of dealing with just a few basic constituents, the fact that correlations play a major role, the appearance of non-standard phenomena like neutron halos and their nature of open quantum systems make light nuclei particularly appealing to *ab initio* approaches. Charge radii of halo nuclei [6]He and [8]He have been measured about 10 years ago with laser spectroscopy techniques [**Wan04, Mue07**], unveiling nontrivial effects of neutron-proton correlations. Information on the charge density distribution in these systems would provide additional insight and shed light on the properties of alpha clustering.

The picture on the neutron-rich side could be complemented by charge radii measurements of certain systems that are up to now not accessible with laser spectroscopy, like [12]Be or [17]C. On the neutron-deficient side,

attention has been recently devoted to systems believed to exhibit an extended proton distribution such as ^{8}B, ^{14}O or $^{17,\,18}$Ne. At present, only the charge radius of the latter has been measured.

Conjectured central depletion in the proton density could also be measured unambiguously for systems like ^{34}Si for which the link between observables and the microscopic details of the nuclear interactions was investigated by a variety of theoretical calculations [*Theo34Si, Th34Siab*]. As shown in *Fig. I.2.1*, an elastic scattering measurement (eventually with other nuclei in the vicinity) would indicate which theoretical assumptions are consistent or not with the measured charge densities. Similarly, charge densities for Sn and Xe isotopes could be obtained from (e,e) scattering measurements and compared to *ab initio* calculations (cf *Fig. I.2.2*).
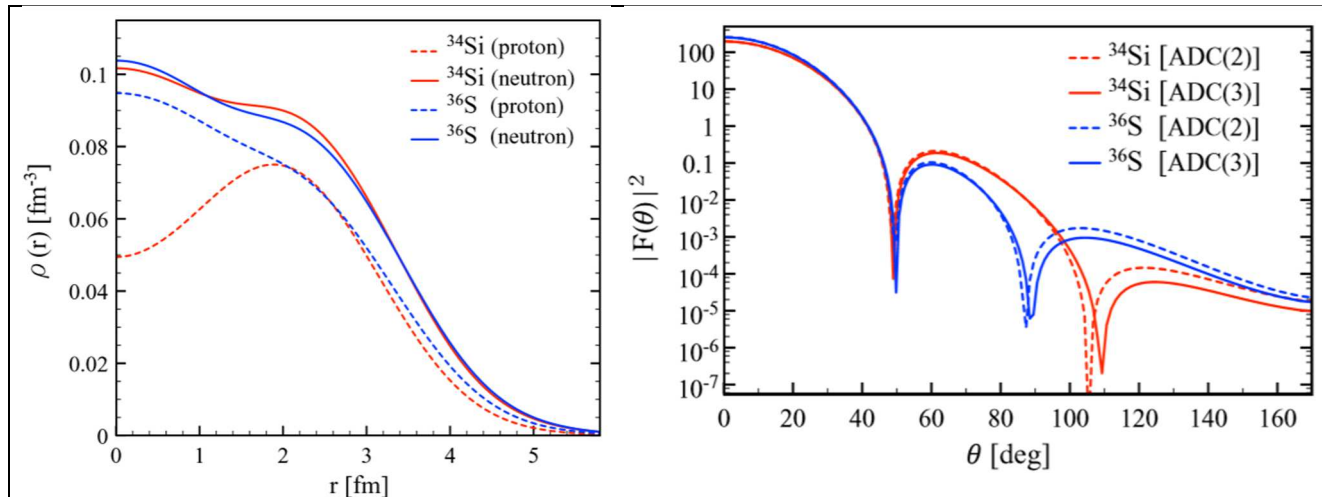

*Figure I.2.1. Figures from [**Th34Siab**]. (Left) Ab initio calculations of point charge and neutron densities for ^{34}Si and ^{36}S isotopes. (Right) Angular dependence of the form factor obtained for 300 MeV electron scattering on ^{34}Si and ^{36}S. (Results from two computation techniques ADC(2) and ADC(3) are displayed).*

Additionally, the study of neutron skins in neutron-rich isotopes would greatly benefit from the combination of electron and proton scattering data on unstable nuclei having different neutron-proton ratios. As exemplified for ^{208}Pb [*TheoNS11*], this observable helps to shed light on the density dependence of the nuclear symmetry energy of the nuclear equation of state (EoS). Differences in charge radii and densities of proton-rich mirror nuclei will also be directly measurable and helpful to characterize the isospin dependence of the EoS [*ChRms*]. These new constraints would thus contribute to improve our understanding of nuclear matter, a necessary step to model different neutron star systems [*Bau2020*], such as mergers recently identified by the detection of gravitational waves [*GW2017*] and sites of r-process nucleosynthesis [*GoBJ11*].

Progressively, the e-RI project can be widely extended to examine other fundamental questions related to shell/shape evolution by studying different electron scattering channels, or other observables, in general more demanding than elastic scattering in terms of luminosity (*see next section for detailed numbers*). For instance:

- From the (e,e') inelastic scattering cross sections, the charge transition densities can be extracted, which gives a set of observables to characterize precisely the nature of collective configurations involved in nuclear states and their mixing. This would be particularly relevant for the study of shape coexistence or high-energy resonances (giant, pygmy, etc.) [*Don75, InelExp*];

- The studies of single-particle strength in exotic nuclei is crucial to quantify its quenching by long and short-range correlations [*TheoLRC09*]; they can be performed via (e,e'p) quasi-free scattering;

- Magnetic form factors can give access to valence nucleon configurations [*Don73, Don84*]. The multipole moments peak at different q values. For instance the valence nucleon radial wave functions were extracted for ^{49}Ti, ^{51}V, ^{59}Co, ^{87}Sr, ^{93}Nb (1g*9/2*), ^{209}Bi from (magnetic) electron scattering in ref.*[PRC82TiSr], and the ^{41}Ca f7/2* orbital size was deduced from ^{41}Ca(e,e) at 145 MeV [*Ca41m90*].

The general strategy aims primarily at unveiling fundamental features related to the shape of exotic nuclei (e.g. nucleon halo, clustering, shape transitions) all being consequences of the underlying nuclear force and its modification away from stability [*SCMF03*].

Correspondingly, new theoretical tools will be put in place for electron-nucleus collisions taking advantage of the renewal of the calculations for the e-RI scattering observables. On the one hand, some of the knowledge

acquired in the past on electron collisions with stable nuclei has to be recovered and revised in light of recent advances. For instance, for the e-RI elastic scattering observables of differential cross sections and electric charge form factors we can apply the techniques elaborated in [**TheRI08**], using a relativistic eikonal approximation of the Dirac equation. On the other hand, newly developed approaches need to be adapted and generalized to the description of new processes and observables. In particular, the interpretation of the quasifree (e,e'p) scattering processes would benefit largely from a revision of the reaction mechanism to investigate final state interactions, including consistently nuclear short- and long-range-correlation effects mentioned previously [**TheoLRC09**].
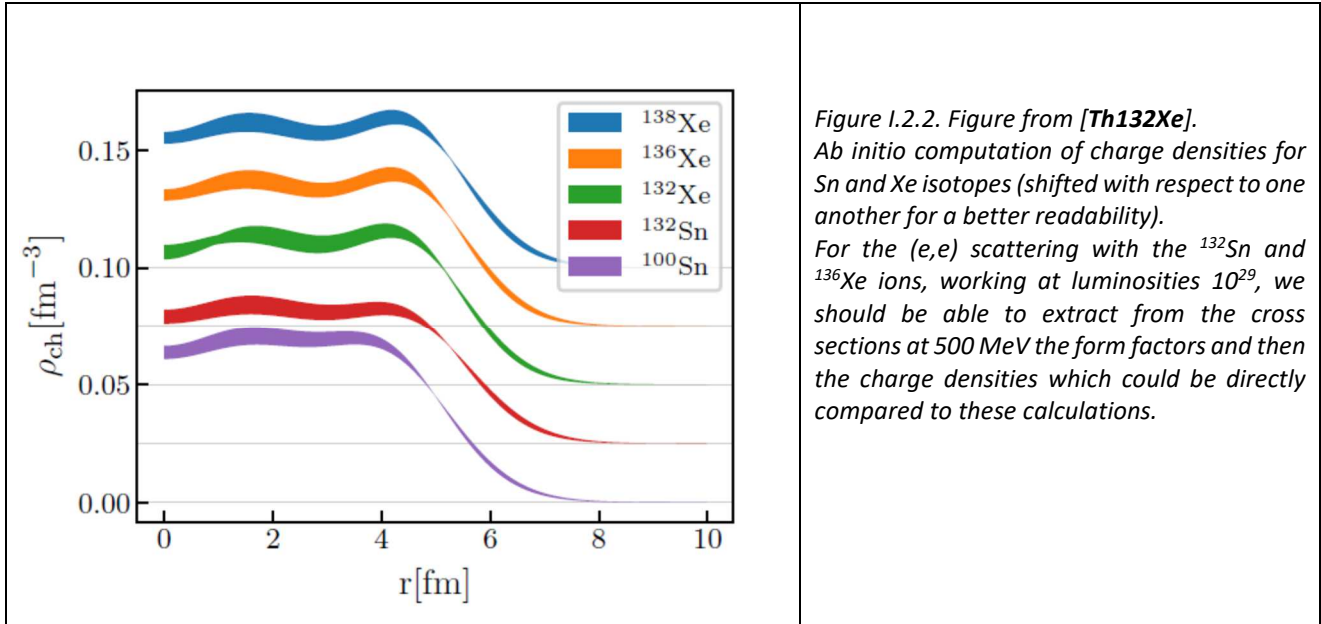
*Figure I.2.2. Figure from [**Th132Xe**].*
Ab initio computation of charge densities for Sn and Xe isotopes (shifted with respect to one another for a better readability).
For the (e,e) scattering with the ^{132}Sn and ^{136}Xe ions, working at luminosities 10^{29}, we should be able to extract from the cross sections at 500 MeV the form factors and then the charge densities which could be directly compared to these calculations.

It is worth mentioning that the main ideas discussed below on the required observables were outlined in the framework of the NuPECC long-range plan (LRP) perspective in 2016-2017 [**LRP2017**]. In this context, it was pointed out that electron beams of 400-800 MeV provide the ideal spatial resolution scale of about 0.5 fm to study charge distributions. Conclusions and recommendation of our community were written as follows:

« *Ion-electron colliders represent a crucial innovative perspective in nuclear physics to be pushed forward in the coming decade. They would require the development of intense electron machines to be installed at facilities where a large variety of radioactive ions can be produced* ».

I.3 Observables and luminosity

We recall here the main quantities, form factors and densities [**Ba74**] accessible from the cross sections [**FO66**] for the scattering of electrons on a target of Z charge. We only give here the simplified expressions, to underline the **Z^2** and **$1/q^4$** dependence of the cross sections.

For a simple case of a spin-0 nucleus, the form factor F(q) (with q the momentum transfer) is a Fourier Transform of the nuclear charge densities (ρ_{ch}) with the following integral formulae:

$$\rho_{ch}(r) = \int F(q)\left(\frac{\sin(qr)}{qr}\right)4\pi q^2\,dq \qquad \textit{[Eq.1a]} \qquad\qquad F(q) = \int \rho_{ch}(r)\,e^{i\,q\cdot r}4\pi r^2\,dr \qquad \textit{[Eq.1b]}$$

In the general case for the scattering of electrons on a spin-J finite-size nucleus, the cross sections are function of the square of the longitudinal F_L and transverse F_T form factors [**Don75**]
For elastic scattering, it can be written as:

$$\left(\frac{d\sigma}{d\Omega}\right)(q) = \sigma_{Mott}\ R_\eta\left[F_L^2(q) + \left(\frac{1}{2} + \tan^2\left(\frac{\theta}{2}\right)\right) F_T^2(q)\right] \textit{[Eq.2]}$$

with R_η= E'/E the target recoil *(mass M of the target, E'/E ~ (Mc²) /[(Mc²) + E (1- cos θ)])* and the Mott cross section detailed below.

For a spin-0 nucleus, the cross section can be expressed as a product of the Mott cross section (point charge cross section) and of the form factor $F_L(q) = F(q)$:

$$\left(\frac{d\sigma}{d\Omega}\right) = \left(\frac{d\sigma}{d\Omega}\right)_{Mott} \times |F(q)|^2 \quad \textbf{\textit{\color{green}[Eq.3]}}$$

Momentum transfer between the initial and the final electron momentum $(h\,q)^2 = [\,|p_i\text{-}p_f|c\,]^2$ (E the initial electron energy) $hq = 2\,E\left|\sin\left(\frac{\theta}{2}\right)\right|$

$$\left(\frac{d\sigma}{d\Omega}\right)_{Mott} = \frac{Z^2\alpha^2}{4\,E^2}\,\frac{(\cos(\frac{\theta}{2}))^2}{(\sin(\frac{\theta}{2}))^4} \quad \textbf{\textit{\color{green}[Eq.4]}}$$

With α the fine structure constant (~1/137), E the electron energy, θ the scattering angle in the center of mass (*c.m.*) system.

Neutron densities could also be investigated via the magnetic form factors extracted from cross sections of the (e,e) measurements. F_T can be expanded in sum of the square of the magnetic (odd) multipole M_i (I = 1 ,3, .. up to $\Lambda = 2Jo$) [**Don73,Don84**]. The extraction of the F_T form factors gives access to the entire shape of the valence nucleons, if the cross sections are measured in a wide range of momentum transfer q, this was the case for typically electron energies up to 500-700 MeV.

From the examples of the cross sections given in Fig.I.3 we can see the needed momentum range to extract the form factor. This gives the order of magnitude for the measurements we would like to transpose in the case of the radioactive nuclei.

Extracting densities require high enough momentum transfers, typically up to 4 fm^{-1} for medium-heavy nuclei (Z > 10) which means working at electron energies at least up to 500 MeV. In this case, the extreme measurement of the cross sections should go down to 10^{-38} cm^{-2} sr^{-1}. Other cases showing the limits of the (e,e), (e,e') and (e,e'p) measurements are presented in the *Appendix A*, to illustrate the requested luminosity for the various studies, on the charge ground and transition densities, and on the neutron densities.

Let's consider now the corresponding luminosities of the electron scattering on stable targets.

For an electron beam of intensity I_e (A), impinging the nuclei of a target (containing N_T nuclei) over an interacting area of S cm^2 the instantaneous luminosity (geometrical) is defined as (with Q_e the electron charge):

$$L = (I_e/Q_e) * (N_T/S)\ \text{cm}^{-2}\,\text{s}^{-1} \quad \textbf{\textit{\color{green}[Eq.5]}}$$

For instance, for stable nuclei, taking into account the electron beam characteristics with typical intensities around $1.25\ 10^{14}$ e-/s (I_e= 20 μA), a size of the spot on the target around 0.5 x 2 mm^2 and with a target thickness of 100 mg/cm^2, for A_i ~ 20 to 200, the luminosities are around 12 to 1.2 10^{36} cm^{-2} s^{-1}, corresponding to the orders of magnitude needed for the most complete studies at high momentum transfer (3-4 fm^{-1}) required for the charge density extraction. Examples of these studies done in the past on the structure of stable nuclei can be seen in **App.A**. However, to reach the charge density in simple forms like the 2 or 3-parameter Fermi density function, the measurement can be done at smaller momentum transfers, around 0.5-2.5 fm^{-1} where the cross sections are a factor $10^{6\text{-}10}$ higher, thus requesting much lower luminosities, typically $10^{26\text{-}30}$ cm^{-2} s^{-1}, depending on the type of ions (since the cross sections evolve with a Z^2 factor).

The insight one can get into density distributions depends on the accuracy of the measured form factor and the range of momentum transfer covered. This translates into luminosity constraints to access different structure observables.

Orders of magnitudes are given in **Tab.II.2** (developed from the one established in the LRP document [**LRP2017**]), with the following ranges of nuclei: light, $Z^2 \leq 100$; medium $100 < Z^2 \leq 1024$ (=32^2); heavy $Z^2 > 1024$. As an example, for elastic scattering:

- Global indicators are accessible first, like root mean square radii and diffuseness, to model densities by simple analytical functions, such as two-parameter Fermi function, as done extensively for stable nuclei reported in nuclear data tables [**ANDT87**]. This can be achieved with luminosity starting from **10^{24} cm^{-2}.s^{-1} for heavy nuclei to 10^{28} cm^{-2}.s^{-1} for lighter ones (lower Z).**

- When form factors are measured precisely over an extended momentum transfer, the charge density can be mapped and extracted via a model independent analysis [**Sick74**]. It corresponds to differential cross sections measured up to the second minimum and translates into luminosities in the range $10^{26\text{-}29}$ cm^{-2}.s^{-1}, again depending on the element.

Observables deduced quantities	Reactions (q: momentum transfer)	Type of nucleus	Required luminosity L
r.m.s. charge radii	**(e,e)** *elastic at small q*	Light ($Z^2 \leq 100$)	L: 10^{24} cm^{-2}s^{-1}
Charge density distribution with 2 parameters ρ_{ch}	**(e,e)** *First min. in elastic form factor*	Light Medium Heavy	**L: 10^{28} 10^{26} cm^{-2}s^{-1}** **10^{24}**
Charge density distribution with 3 parameters ρ_{ch}	**(e,e)** *2nd min. in elastic form factor*	Medium Heavy	**L: 10^{29} cm^{-2}s^{-1}** **10^{26}**
F_L, F_T Magnetic form factors→ Proton, neutron transition densities *Direct access to neutron-skin*	**(e,e)** *2nd min. in elastic form factor*	Odd-even Medium Heavy	**L: 10^{30}cm^{-2}s^{-1}** **10^{29}**
Energy spectra, width, strength, decays, collective excitations	**(e,e')**	Medium-Heavy	L: 10^{28-29} cm^{-2}s^{-1}
Extraction of the density distribution *using functionals (series of Fourier-Bessel functions …)*	**(e,e)** **(e,e')**	Light Medium-Heavy	**(e,e) (e,e') L : 10^{30-31}** **(e,e) (e,e') L ~10^{29-30}**
Spectral functions, correlations	**(e,e'p)**		10^{30-31} **(e,e'p) L ~10^{30-31}** cm^{-2}s^{-1}

Table II. 2. New structure observables from e-RI collisions and luminosity.

From luminosities around 10^{29} cm^{-2}.s^{-1} and higher, the study of other processes mentioned previously can be reached offering unprecedented possibilities as stated in [**LRP2017**] : « *As a long-term goal, such facilities would allow (e,e') inelastic scattering with selectivity to the transferred angular momentum, (e,e'f) electro-fission with detection of fragments, and (e,e'p) quasi free-scattering studies with radioactive ions* ».

An objective of the luminosity at 10^{29} cm^{-2}.s^{-1} is thus considered to reach an entirely new range of research and opening the way for further upgrades. Then, the long-term goal of GANIL would be to extend progressively the applicability of those methods to a broader range of exotic nuclei allowing systematic and model-independent studies leading to the build-up of nuclear data tables away from stability in the years 2040-2050s.

If we examine the requirements for the measurements, there are basic considerations on the observables and on the luminosity. Production rates of radioactive beams need to be large enough to ensure enough luminosity for the type of data we are interested in.
It is clear from the above table and from basic considerations on the feasible luminosity (more extended calculations will be given in the chapter II) that the potential test cases will correspond to isotopes produced at intensities higher than 10^7 part/s. There will be the feasible nuclei (10^{7-8} and higher) for which the detailed structure information could be reached, and, depending on the Z number of the nucleus, some intermediate test cases with lower requirements on the luminosity and on the required intensities (around 10^6).
The more difficult cases will be explored in detailed studies.
We can already identify the physical cases which will not be feasible, whatever the techniques employed and even in the case of the improvements of the luminosity: the nuclei with too short lifetimes will not be accessible for electron-ion collisions, which require nuclei with lifetime above (a few) 100 ms at least (whatever the techniques considered).
For the choice of the beam energy, we can consider that reaching 500 MeV gives us most of the essential physical cases that we want to investigate. The final choice is a compromise between luminosity, cross sections, access to high transfer momenta. The 400-500 MeV is certainly a better choice than the 700-800 MeV regime where the cross sections are lower, and better than the 200-300 MeV range, for which the electron beam properties are degraded as a function of the decreasing energy.
In summary, the main physics cases of interest will correspond to the (e,e) and (e,e') experiments done at luminosities 10^{26-28} (for nuclei with Z^2 >100, medium and heavy isotopes), leading to the extraction of the form factor at large q values (4 fm^{-1} with the incident beam energy at 500 MeV) which will give access to the charge and transition densities for the radioactive nuclei with lifetimes >100 ms and produced at rates higher than 10^7/s. The feasible Day 1 physics cases will be identified in section VI, with a list of radioactive isotopes.

To perform electron-RI collisions with enough luminosity to reach the observable of the charge densities for a large range of isotopes, two techniques have been explored: collisions between the electron beam and RIBs, or ions trapped to perform electron collisions on a target like structure.

II.1 Projects of colliders

Since the 2000s, the physics of electron-ion collisions has been part of the main international projects aiming to probe the nuclear structure of exotic nuclei [*eRIB17*]: ELISe (Electron Ion Scattering in a storage ring - eA collider) [*Elise07*] planned in the second phase of FAIR in Germany, and since 2017 the Dubna Electron-Radioactive Isotope Collider fAcility (DERICA) within the Acculina2 project [*Dubna18*] in Russia.

The ELISe and DERICA machines would have taken advantage of the increased intensities of the RIB produced with the upgrade of the facilities. However they have been pushed forward in long-term plans of the future facilities at FAIR and at Dubna, mainly because the technical difficulties inherent of the colliding techniques for an intense electron beam with a RIB between 10^6 and 10^9 were not solved, they would have requested a detailed conceptual design report followed by an expensive machine project. Moreover the e-RI facility would have requested specific running conditions and the dedicated teams to operate the acceleration of the electron-ion beams and for the tuning of the collisions. Technical complexity of the e–RI machine would have considerably increase the cost of the Radioactive Isotope facilities.

In Japan a similar project was discussed in the years 2000s along the on-going R&D for the upgrade of the RIKEN Nishina facility with the MUSES project, idea of a machine between colliding electrons and RI. As was the case at FAIR and Dubna, the project could not be launched in parallel with the RIBF facility which started its operation in 2007.

II.2 Target-like devices: SCRIT at RIKEN and the ETIC project

The alternative to the electron-ion collider machine was found with the SCRIT (Self Confined Radioactive Ion Target) [*Scrit05*] ,project launched in the years 2004-2005 at RIKEN in Japan. At that time it represented the world's first attempt of an electron-scattering facility for exotic nuclei [*Scrit04*]. It consists of a dedicated electron storage ring device with circulating electron bunches colliding with trapped ions. **The "ion trapping" phenomenon forms a local target** which makes electron scattering off short-lived radioactive nuclei possible in principle [*Scrit09*]. In the years 2008-2009, the Kyoto prototype for SCRIT reached a luminosity of 10^{26}cm^{-2}s^{-1} for 10^6 stable ions of ^{133}Cs. Some data points of the elastic scattering from Cs could be measured around the c.m. angles 30-55°. In the years 2015-2016, SCRIT became operative at RIKEN for physics runs, test results were obtained with the stable isotopes ^{132}Xe [**Scrit17**]. Note that the charge density shape was determined with an **evaluated** luminosity of 1.55 $\mathbf{10^{27}}$**cm^{-2}s^{-1}** (at E$_e$= 301 MeV) ; a few $\mathbf{10^{27}}$**cm^{-2}s^{-1}** represents up to now the current limit of the SCRIT device. The luminosity was reached with a mean electron beam intensity of **200 mA** (I$_e$ evolving between 250 down to 150 mA, at the end) and around 10^8 target ions ("numbers of ions introduced to the SCRIT with each cycle was less than a few times 10^8, **measured** by a Faraday cup").

The electron beam size was "2 mm^H x 1mm^V (σ) at the center of SCRIT".

The quality of the SCRIT data for ^{132}Xe(e,e) were sufficient to be compared to recent *ab initio* calculations [**Th132Xe**]. The numbers of the running conditions for the SCRIT facility represent some benchmarks to explore the techniques of the ion trap self-confinement to be used for the electron –RI collisions.

In the years 2015-2016, there was a project initiated by the CEA Saclay to think about a possible *Electron-Trapped Ion Collider*, ETIC [*ETIC15*]. GANIL offers the production of DC beams at low energy. The SCRIT technique fits to the existing facility. While based on the SCRIT ion-trap concept, ETIC aimed at reaching much higher luminosities around 10^{29}cm^{-2}s^{-1} in the case of 10^6 radioactive ions stored in the electron beam in the interaction region. It represents about two orders of magnitudes beyond the SCRIT capabilities. This would allow performing experiments on isotopes with smaller production rates and at the same time more detailed measurements, thus increasing the physics reach in quantity and quality. This project was explained in a workshop organized in 2016 on e-Radioactive Ion Beams (RIB) collisions [*ESNT16*].

The recently developed technique of **energy recovery linac** (ERL) was identified as a possible suitable solution to reach a luminosity of 10^{29} cm^{-2}s^{-1}. However, an R&D program (including a demonstrator) has to be done on the ETIC project, based on the ERL concept, to reach the identified performances.

In the third part of this document we revisit the ETIC project and discuss the potential technical solutions, either based on a synchrotron (evolved from the initial ETIC) or based on an ERL. Parameters of the machines are discussed to identify the possible limitations in terms of luminosity (due to technical limits of the accelerators or to the physical effects at the interacting point) or the path of improvements.

The performance in terms of luminosity are also discussed in the context of the present RIB beams, which are or will be available at GANIL. We base our physics cases upon feasible RI beams with standard techniques. If higher RI production is available, higher luminosities will be achieved.

Improved techniques, combination of various beam production modes are also considered to develop the physics case of the e-RI collisions in different regions of the nuclear chart corresponding to the foreseen "new" beams at GANIL. This is presented in parts **VI.1, 2** with the possible physics cases.

II.3 Preliminary considerations on requested luminosity and intensities for electrons and ions

Let's give a first glance to the order of magnitude for the luminosities, starting from **Eq.1.**, with rough estimation of the static collisions area and of the numbers of colliding ions/electrons, to check the overall limits due to the physics phenomena and to the present technology.

For radioactive nuclei, which cannot form a target, if we trap N_{ions} with an electron beam in a surface area S, the possibility to reach the luminosity around **10^{29} cm^{-2} s^{-1}** would require to work with electron intensity at **1.25 10^{18} e-/s (200 mA)** with typical numbers of ions above **10^7/s** considering a spot size area for the overlapping region between electron and ions of 0.1 mm^2.

The detailed calculations of the luminosity will be further explored in section III, considering the estimations of the overlap surface between ion cloud and electron beam, taking into account the ion trap efficiency, with assumptions depending on the ion charge states and on the confinement effects due to the electron beam.

From this basis, the paths of improvements for the future machine will be explained in part III, focusing on the limits of feasibility, both for the electron beam intensities which can be achieved and for the expected number of ions which can be considered for the electron-ion collisions.

However, the numbers above are the order of magnitude of the requirements for the "working conditions" of the electron-ion collisions, if we plan to measure in detail the elastic scattering cross section and to extract the charge densities from model-independent analysis (using analytical functions like Fourier-Bessel).

They are helpful also to know which radioactive ions could be included or not in our physics case and which part of the technical project has to be improved to increase the luminosity.

We could think of improving the electron intensities. But we cannot gain a factor 10 on this side.

The maximum achievable today for electron intensities is of the order of magnitude of 100-200 mA (~few 10^{18}s). It means that, provided that we could have a feasible machine at 10^{29} cm^{-2} s^{-1} the next step with a factor 10-100 on the luminosities should come from the ion trap capabilities, requiring that the numbers of trapped ions be above 10^7 up to 10^{8-9}. The reduction of the overlapping region is also a factor for the increase of the luminosity.

Exploring the running conditions, identifying the technical constraints and the beam limitations for the operation of the electron-ion collisions is the purpose of the preliminary study presented in section III.
The calculations of the luminosity with ion traps are fully discussed in part **III** and in **Appendix B**.

We explore here the technical issues in two steps: the ones on which "reasonable" values can be given (from other machine studies in the world, checking bibliography); the ones on which we have global information but on which we would need complete R&D studies. We give orders of magnitude of the foreseen realistic parameters of the machine (with the goal at 10^{29} cm^{-2} s^{-1}) and we explain the series of questions we need to solve in the future R&D projects required in 2021 with the objectives of determining the best options for the ion trap concept (storage and fixed target preparation) and the machine design.

III. 1 Definitions of the luminosity key-parameters of the project

Assuming transverse Gaussian distributions for the bunches, the **luminosity (L)** in a collider between ions and electrons would be expressed by [**LumT**]:

$$L = f_e n_e \ \frac{N_e N_A}{2\pi \sqrt{\sigma_{x,e}^2 + \sigma_{x,i}^2} \ \sqrt{\sigma_{y,e}^2 + \sigma_{y,i}^2}} = \frac{I_e}{q_e} \frac{N_A}{2\pi \sqrt{\sigma_{x,e}^2 + \sigma_{x,i}^2} \ \sqrt{\sigma_{y,e}^2 + \sigma_{y,i}^2}} \qquad \textbf{\textit{[Eq.6]}}$$

- with **σ$_{x,e}$ σ$_{y,e}$** the electron beam section -*variance value the distribution, referred hereafter as the root mean square (rms) "size" of the beam in x or y directions*- at the interaction point (IP), **σ$_{x,i}$ σ$_{y,I}$** the ion beam section in the trap; and
- **N$_A$** the number of trapped ions, **I$_e$** the electron beam intensity, **f$_e$** the repetition frequency, **n$_e$** the number of colliding bunches, **N$_e$** the number of electrons per bunch.

To simplify, if we consider circular beams, **σ$_e$ =σ$_{x,e}$ = σ$_{y,e}$** and **σ$_i$ = σ$_{x,i}$ = σ$_{y,i}$** we obtain:

$$L = \frac{I_e}{q_e} \frac{N_A}{2\pi \ (\sigma_e^2 + \sigma_i^2)} \qquad \textbf{\textit{[Eq.7]}}$$

Considering the electron beam impinging a target area of size **σ = σ$_e$ =σ$_i$**, from this expression we recover the standard luminosity for the electron beam on a stable fixed target, given in **_Eq.1 (part I)._**
If we assume that we can work with parallel beams at the IP and the same beam sizes **σ$_x$ =σ$_{x,e}$ = σ$_{x,i}$** and **σ$_y$ =σ$_{y,e}$ = σ$_{y,i}$** , the luminosity would be given by:

$$L = f_e n_e \frac{N_e N_A}{4\pi \sigma_x \sigma_y} = \frac{I_e}{q_e} \frac{N_A}{4\pi \sigma_x \sigma_y} \qquad \textbf{\textit{[Eq.8]}}$$

.
From this equation, we can consider that the lower the size, the higher the luminosity may be. However it relies on strong assumptions, we examine in section **_III.4_** their validity.
Note that the expression in **_Eq.8_** do not explicit the overlapping area (which is different from the electron beam size).
In a cylindric shape trap with Gaussian distributions, the luminosity is a function of three factors:
-number of trapped ions (**_cf III.2_**), N$_A$,
-number of electrons (**_cf III.3_** beam intensity, control of the instabilities, control of the beam size), I$_e$
and
- size of the overlapping area between the electron beam and the ion cloud (**_cf. III.4_**):
$\sqrt{\sigma_{x,e}^2 + \sigma_{x,i}^2} \ \sqrt{\sigma_{y,e}^2 + \sigma_{y,i}^2}$. A perfect beam overlap would correspond to **_Eq.8_**.

In the next sections, we explore the limits and potential improvements of these three factors, to reach the targeted values for the luminosity.
We also investigate the validity of the various assumptions made on the luminosity expressions.

The modifications induced by the evolution of these three factors should be considered, taking into account the physical effects ruling the overlap in the trap as well as the number of trapped ions as a function of the electron beam characteristics (intensity and size). These effects will be discussed in details in *III.4*. To give a more realistic estimation of the luminosities compared to the above formula, we have carried out preliminary studies with a series of simulations to figure out the potential change on the luminosity of the relevant parameters (electron and ion beam sizes, electron intensity, number of ions injected in the trap). They are also meaningful: i) to have an overview of the limitations inherent to the ion trap phenomena, ii) to check the assumptions of the physical effects at play in the electron-ion collisions in the trap, iii) to list the unknowns in the state-of-the art ion trap description.

III. 2 Existing trap projects –achievements and limitations

Quoting the report to the technical advisory committee (RIKEN 2005) by T. Suda et al **[scriTAC05]** the SCRIT technique is presented as: *"*the EBIT(EBIS) technology and "ion trapping" phenomenon in the electron storage ring" and "Purpose of the numerical simulation is to expect how long ions lives in the SCRIT, how many ions can be trapped, and how much luminosity can be obtained. This calculation tells us that 10^7-10^8 ions is acceptable at the SCRIT, of which the length is 130 mm, the lifetime of the SCRIT is order of second when the electron beam current is several hundreds mA."

In the test reported for the stable Cs *[Scrit09]*, the luminosity was obtained as follows*:* "At an average electron beam current of 75 mA, we measured the scattered electrons from the trapped Cs ions with the ion injection–trap–ejection cycle, whose trapping time was set to 50 ms to simulate short-lived nuclei. Elastically scattered electrons from the trapped Cs ions were clearly observed. Using the known elastic scattering cross section, the luminosity of 1×10^{26} cm^{-2} s^{-1} was deduced at the average electron beam current of 75 mA with 10^6 trapped ions". Note that the physicists working on SCRIT at RIKEN have identified limitations of their own machine [*Scrit16w*] in terms of ion trap injection and electron beam instabilities, and they are in search of other technical solutions. For the trap R&D studies, we would benefit from a close collaboration with these experts of SCRIT in Japan (*M. Wakasugi et al, Kyoto University*) to develop an optimized ion trap techniques for our project at GANIL. The increase of luminosity will also require working with experts of the electron beam and ion-trapping phenomena.

To overcome the limitations for the luminosity, we plan to organize an important R&D work on the optimization of the trapping techniques. We have identified several paths of R&D:

- increasing the number of trapped ions, by optimizing the injection and extraction of ions thanks to an RF trap structure guiding the ions to and from the interaction region;

 - working on the overlap efficiency between ions and electrons, by optimizing the spatial distribution of the ion cloud and by controlling the charge state distribution (multiplication) thanks to a regular recirculation of the trapped cloud in a buffer gas in a separate trapping area;

-working on the trapping instabilities using cooling down techniques to reduce ion-ion collisions, ion heating processes.

The regular recirculation of the cloud in a buffer gas would permit to overcome the problems of the spatial charge effects of the plasma in the ion trapping area. If demonstrated, this technique of recirculation would enable an important increase in the number of trapped ions for the ion trap project for GANIL with respect to what was done so far in SCRIT [due to the slowing down of the ions, for SCRIT, only species with long $T_{1/2}$ (more than few 100 ms) can be stored].

III. 3 Options of the electron accelerator facility

As in the ETIC project [*ETIC2015*] three types of accelerators for the electron beam can be envisaged, we briefly summarize their characteristics, performances and limitations.

1) Linear electron accelerator

Such a facility avoids many circular accelerator complexity (acceleration chain) and limitations as the space charge (SC) tune spread, the intra beam scattering (IBS) emittances growing, the Touschek beam life time, the dynamic aperture at injection, and so one. Moreover, a linear accelerator allows, by switching the beam, to use, at the same time or at different times, many experimental areas. The project can then be envisaged in an evolution way.

A linear accelerator, based on XFEL technology [2007], composed with 5 modules, allows obtaining the working energy range, 500MeV up to 750 MeV. At these energies, the transverse emittances are about 2-1 nm.rad. But, even with optimized accelerator and beam parameters (repetition rate, bunch charge, beam sizes and so one) the luminosity remains lower than the targeted value. The main limitation comes from the average beam power above 10 MW, which is very RF demanding.

2) Circular electron accelerator

The case of a circular collider, which can work up to 700 MeV, was already explored, and a first draft plan (with beam optical characteristics) was delivered [**ETIC15**]. The main limitation comes from the IBS. At low energy (less than 700 MeV), the IBS becomes an issue. It limits the stored intensity and thus the luminosity. A solution was proposed to use harmonic cavities to make RF gymnastics. That is more expensive and requires more studies. This option, for a substantial increase of luminosity, includes the reduction of beam sizes at the interaction zone $\sigma_{x,y}$ and/or an increase of number of trapped ions N_A, and electron beam current I_e. A circular electron ring will merge the problematics of synchrotron light sources and of circular colliders. As mentioned previously, a proper design implies the control of many characteristics of the circular accelerator

At these working energies, a double bend achromatic (DBA) lattice, comprising 24 bends, with distributed dispersion, reaches the equilibrium emittance of a few nm.rad or less.

Another possibility is to organize the arc bends as multi bend achromatic (MBA). Solutions with 24 bend magnets, combined or non-combined, was studied to reach the luminosity goal. A solution without combined bends was investigated in detail in the ETIC project; we revisit this solution relaxing some of the constraints on the beam size, which modifies significantly the design of the synchrotron collider.

3) Energy recovery linac

An energy recovery linac (ERL) has the same advantages as a conventional linac. In addition, the operation cost is less expensive. Moreover, with the same RF budget, it gives the possibility to increase the average intensity of the beam by more than an order of magnitude.

The use of this technology implies some challenges. Thus, a high average intensity has an impact on the needed performances of the source and the injector. The transverse beam stability must be less than the micrometer. RF cavity design, working in CW mode, should minimize the beam break-up instabilities (BBU) while maintaining a high Q_0. The emittance growth, due to the synchrotron radiation during the transport, should be as low as possible [**Erl14**].

Nevertheless, a number of projects (*4GLS, BERLinPro, eRHIC11, LHeC12* see refs. [**projE**]) intended for the production of synchrotron radiation or nuclear physics and high energy physics, are based on this concept. The parameters of some of them can be directly adapted for the e-Ion collider.

A solution using an ERL has also been considered. The desired luminosity is achieved by adopting the parameters of projects studied currently worldwide. Studies show that the intensity limit due to the BBU instability, which is one of the main intensity limitations, can be larger than that is needed for ETIC.

This solution does not have the drawbacks of synchrotrons which makes it particularly attractive. It is more interesting than a conventional linear because it consumes less power. Furthermore, as the bunch length is of the order of some pico-sec or less, ERL principle was envisaged in many synchrotron radiation source projects of high brilliance and FEL projects of 4th generation and so this solution can interest a wider physics community. The ERL principle is a fairly recent technology and R &D is necessary, so a demonstrator should be proposed as first step. A special effort must be performed on the electron source quality.

Note that for the three options very small beam sizes at the IP (a few μm) request to squeeze the beam optics in the interaction region and thus this leads to a complicated lattice with reduced tuning capability.

Such an R&D platform was discussed in the context of the PERLE *"Powerful Energy Recovery Linac for Experiments".* This project aims at building an ERL prototype (the proposed site would be located at IJCLab, University of Paris-Saclay) for the Large Hadron electron Collider (LHeC) with a high current (15mA) and high energy (up to 450 MeV) using a multi(3)-turn design [**PERLE18cdr, EICUG2019**]. The adjunction of an upgraded photo-fission source to this ERL, could represent a technical option to perform the first stage of a R&D project on a SCRIT-like device at lower luminosity. However this would require to organize an expert team on the technical issues (**see below, work plan**).

For the electron recirculating linac (ERL), the IBS is not anymore a problem and we can work at lower energy. A first layout has been shown at 530 MeV. A special effort must be performed on the electron source quality.

That is why a proposal of an intermediary step was made, in 2016, with a 140 MeV demonstrator to validate some of the key points of such a machine.

III. 4 Technical constraints for the electron accelerator and for the ion trap

If the project is launched in 2021, having a one-year work with two experts of the field, we consider that the final choice for the machine design -deciding between synchrotron or ERL, giving the consolidated machine parameters-, could be obtained and explained in the detailed technical report at the end of 2021. This project is also mandatory to know precisely i) if the L ~10^{29} is definitely feasible, ii) the optimization possibilities of the machine performances, and iii) the limitations on the luminosity due to the beam characteristics and to the ion trapping processes.

Here for the present report, our purpose is to outline the main questions related to the technical options and to identify the key points for the simulations and for the benchmark studies.

We have identified the necessary inputs for the preliminary quantitative studies that could be carried out in detail during 2021:

- Realistic initial beam conditions and estimates of the dimensions of the interaction region, based on typical RIB cases;
- Number of trapped ions, emittance of the beam in the interaction region,
- Limits of the potential electron beam intensities and emittance according to the technical choices of the machine;
- How these parameters develop with time.

For the purpose of this report, we gathered in a very preliminary study first elements from which we could examine the various technical solutions (ERL, synchrotron, design of the ion trap and dimensions.

We have also checked the sets of parameters, on the basis of a complete bibliographic study. From the values reported in the articles describing the existing machines, we made simulations to reproduce the present limitations of the beam conditions (size, number of ions).

The optical characteristics of the electron beam have to be discussed taking into account the dimensions and limitations of the trap. The ETIC project was conceived to increase the luminosity by a **factor 100 up to ~1000** compared to the SCRIT technique, by increasing the machine performance on two main characteristics: the electron intensity up to **200 mA**, as in SCRIT, but with an electron beam optics, that would enable a significant decrease of the surface of the interaction volume, by a factor ~1000 (S divided by ~1000 in *Eq. 5*), for an active trap length of 16 cm. It would correspond to a rms size of the beam decreased to **0.01 mm** in the trap area.

We revisit here the ETIC project by examining the characteristics previously obtained, and give here more realistic estimates for an advanced electron-trapped ion collider.

In the ETIC project, the 10^{29} cm^{-2}s^{-1} luminosity goal was reached assuming $N_A = 10^6$ trapped ions and the electron beam intensity at I_e= 200 mA (1.25 10^{18} e-/s), with the electron beam section $\sigma_x \sigma_y$ at the interaction point (IP) of about 10^{-10} m^2 (10^{-6} cm^2). As a consequence of this very small size at the IP, the beam optics should integrate the following constraints: a transverse coupling $\kappa=\varepsilon_y/\varepsilon_x$ of 50%, the transverse Twiss functions, β_x, β_y, at the IP have to be a few 0.1 m with a horizontal emittance ε_x of a few 1 nm.rad.

Finally, such small size at the IP poses 2 types of problems:

- it increases the electron beam instability due to Intra Beam Scattering and reduces the Touschek lifetime, as readily realized in [**ETIC15**],
- it hardly matches with the best typical ion cloud dimensions one can hope for, σ_i within a few 100 μm, as realized in studies carried out for the preparation of this document. We outline the conclusions of these studies below (detailed explanations are given in *Appendix B.1)*.

We should examine the more realistic cases for the ion and electron beam optics. In the simplified luminosity expression (*Eq.8 in part III.1*) we took the assumption of the collisions between two beams with a Gaussian transverse distribution and same beam sizes in x and y directions. The beam size is assumed to be constant along the bunch at the IP: the hourglass effect is thus neglected. This assumption was made for the ETIC project where we expected that the ion beam can be captured with the same radius as the electron beam and that the number of captured ions does not depend on the electron beam current.

The studies made in the present project has shown that this assumption was too strong and that we should consider the case of the ion and electron beams with different sizes to reinvestigate the constraints, both on the electron beam optics and on the ion trap processes to increase the luminosity. We can still assume Gaussian beams. Taking different beam sizes, from *Eq. 6*, the limits on the luminosity can be seen as:

$$L = \frac{I_e}{q_e} \frac{N_A}{2\pi\sqrt{\sigma_{x,e}^2 + \sigma_{x,i}^2} \ \sqrt{\sigma_{y,e}^2 + \sigma_{y,i}^2}} < \frac{(I_e)^2}{q_e} \frac{F_{Ai}}{2\pi\sqrt{\sigma_{x,e}^2 + \sigma_{x,i}^2} \ \sqrt{\sigma_{y,e}^2 + \sigma_{y,i}^2}} \qquad \textit{[Eq.9]}$$

The advantage of this second expression is to emphasize the fact that we are driven by the largest beam size: having a very small value for the electron beam is of no interest if that is not the case with ions.

Taking into account the fact that the number of trap ions is a function of the electron beam intensity according to the ion type and reaches a maximum value, function of I_e.

We note F_{Ai} the factor for this maximum, with $N_A < F_{Ai} I_e$. The limits of luminosity appears clearly as a function of the square of the electron beam current in the inequality of Eq.7. **F_{Ai} factor is a constant** which depends on **the trap geometry (l_{trap})** and of the **mean charge state Q_m** (number with time evolution, potentially from 1^+ to 10^+ or more) to be determined with detailed studies and measurements.

It can be expressed as: **$F_{Ai} = (l_{trap}/c) / [q_e * Q_m]$.**

Moreover, since the luminosity depends on the overlap surface between the electrons and the ion cloud, it is not useful to decrease the electron emittance if the ion cloud surface is large: a large ion beam size with a small electron beam (factor 10 smaller in one x or y or both directions x,y) will result in an overall reduced trap efficiency (below 10% and even below 1%).

Discussions on the ion trap conditions

Our preliminary studies on the ion trap characteristics consisted in:
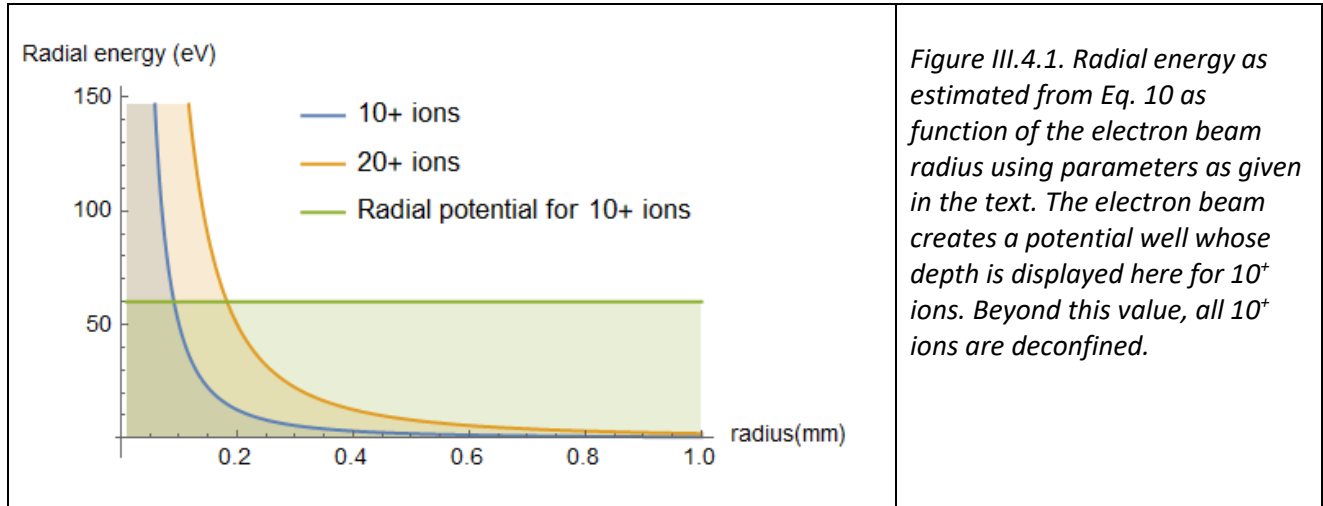- simulating the injection of a bunch of 1^+ ions freshly cooled in an RF trap into the electron beam;
- simulating the capture of such 1^+ ions in the electron beam thanks to charge breeding;
- calculating the ion temperature as a function of the charge state and trapping time and comparing it to the trapping potential.

From the first simulations (realized using the SIMION code, not detailed here), it appeared that despite a careful injection using ions cooled to cryogenic temperatures, the 1^+ ions are initially orbiting in radii of the order of 0.5 mm around the center of the electron beam. The initial radius then shrinks rapidly (< ~1-10 ms, depending on the initial overlap between the electron beam and the ion cloud) thanks to charge breeding (transformation of 1^+ to 2^+ and subsequent charge states thanks to successive electron impact ionizations): such charge transformation triggers the capture of the ions in the potential of electron beam. An important effect counterbalances this shrinkage, which is the ion heating from collisions with the electron beam. A formula derived from [**Bec81**] for relativistic electrons shows that for relatively small charge states (10^+) for a typical ^{132}Sn beam such heating rapidly counterbalance the confinement potential of the electron beam. This effect depends critically on the ion charge state and, even more importantly here, on the size of the electron beam, defining the electron density, which scales as $1/\sigma_e$:

$$\frac{dE}{dt} = 0.104 * j_e * (Q^2 / A_i) \quad \textit{[Eq.10]}$$

where E is the radial average energy of the trapped ions (dE/dt in eV/s) , je the electron density (A/cm^2), Q the charge states of the trapped ions, and A$_i$ their mass number.

The radial energy estimate is represented in **Fig. III.4.1** as a function of the electron beam size, and for a typical case of ^{132}Sn(10$^+$) trapped during 1s in a 200 mA electron beam. The radial energy has to be compared to a maximal confinement electric potential of 6 V, corresponding to a maximal axial energy of 60 eV for the ions to remain trapped. For illustration purpose, the radial energy estimate is also shown for a 20$^+$ charge state (note that in this case one has to consider a maximal radial energy of 120 eV, not shown on the plot).

Figure III.4.1. Radial energy as estimated from Eq. 10 as function of the electron beam radius using parameters as given in the text. The electron beam creates a potential well whose depth is displayed here for 10$^+$ ions. Beyond this value, all 10$^+$ ions are deconfined.

As it clearly appears from **Fig. III.4.1**, a radius well below 200 μm would inevitably yield important confinement losses, especially when considering that the potential well created by the electron beam will be progressively compensated by the space charge of the trapped ions during charge multiplication. The 10$^+$ charge state has been found to be dominant in SCRIT for trapping times as short as 200 ms for stable Xe ions. In a case of an electron density multiplied by ~25 as projected here, the 10$^+$ charge state should be attained in about 10ms, as is known from standard EBIS scaling laws: $q \sim \log (je \cdot \tau)$ where τ is the charge breeding time.

Eventually, the number of trapped ions will be limited by the ion charge state, when the electron beam is fully compensated. This is a second reason for limiting and controlling the multiplication of charge states of the trapped ions. To overcome these limitations, we propose to decrease the charge states of ions and their radial energy by regularly recirculating the ion bunch every ~10 ms in a RF trap filled by buffer gas.

From **Eq. 10**, it clearly appears that an electron beam radius of ~ 200 μm is the physical limit beyond which the ion confinement significantly degrades in the trap. With this constraint in mind, we can use **Eq. 7** (see *III.1*) **as a figure of merit to define the best parameters to aim at luminosities at least 10 fold enhanced compared to SCRIT (above 10^{28} cm^{-2} s^{-1}), using RIBs sufficiently well produced to hit the maximal trapping capacity.**

Figs. III.4.2-3 show how such objective can be attained by varying the electron beam radius and intensity, and assuming a maximal number of ions fully compensating the electron beam space charge. A typical trap length of 120 mm was assumed (see discussion below). From **Fig.III.4.2**, it is clear that an electron beam intensity of at least 200 mA is required, when considering an average charge state of 10$^+$ in the trap and an achievable ion cloud radius of 0.2 mm.
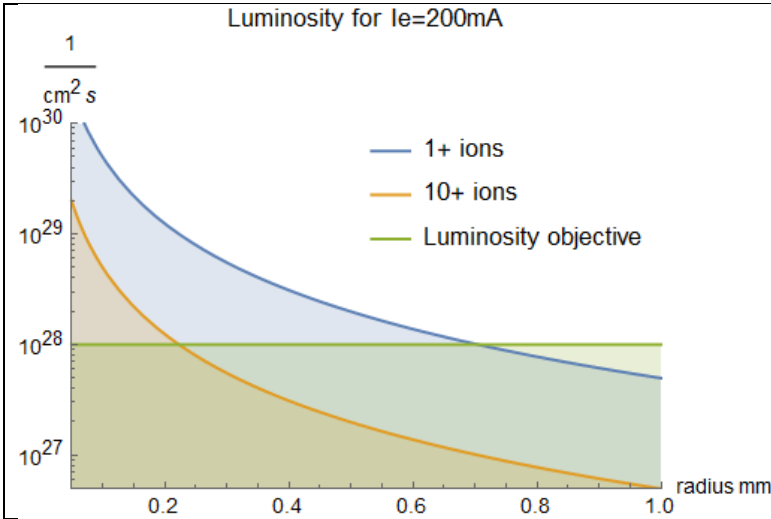
Figure III.4.2. Luminosity (from Eq.9) as a function of the electron beam radius, considering a cylindrical ion beam, with an electron beam intensity of 200 mA, and a number of trapped ions corresponding to the maximum capacity of trap (i.e. fully compensating the space charge of the electron beam).

The number of trapped ions is $5\cdot10^8$ for 1^+ ions and $5\cdot10^7$ for 10^+ ions for a 120 mm trap.
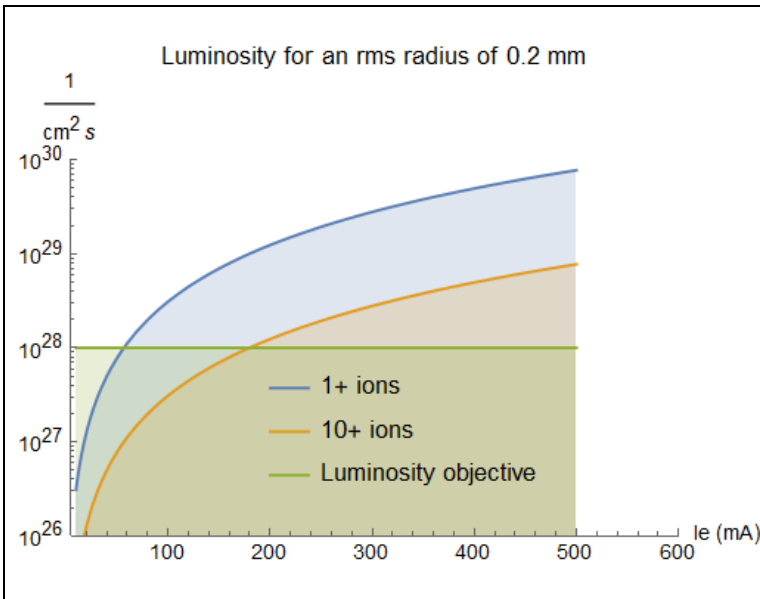

Figure III.4.3. Luminosity (from Eq.9) as a function of the electron beam intensity, considering a cylindrical ion beam, and an electron beam radius of 0.2mm.
As in Fig. III.4.2 the number of trapped ions corresponds to the maximum capacity of trap.
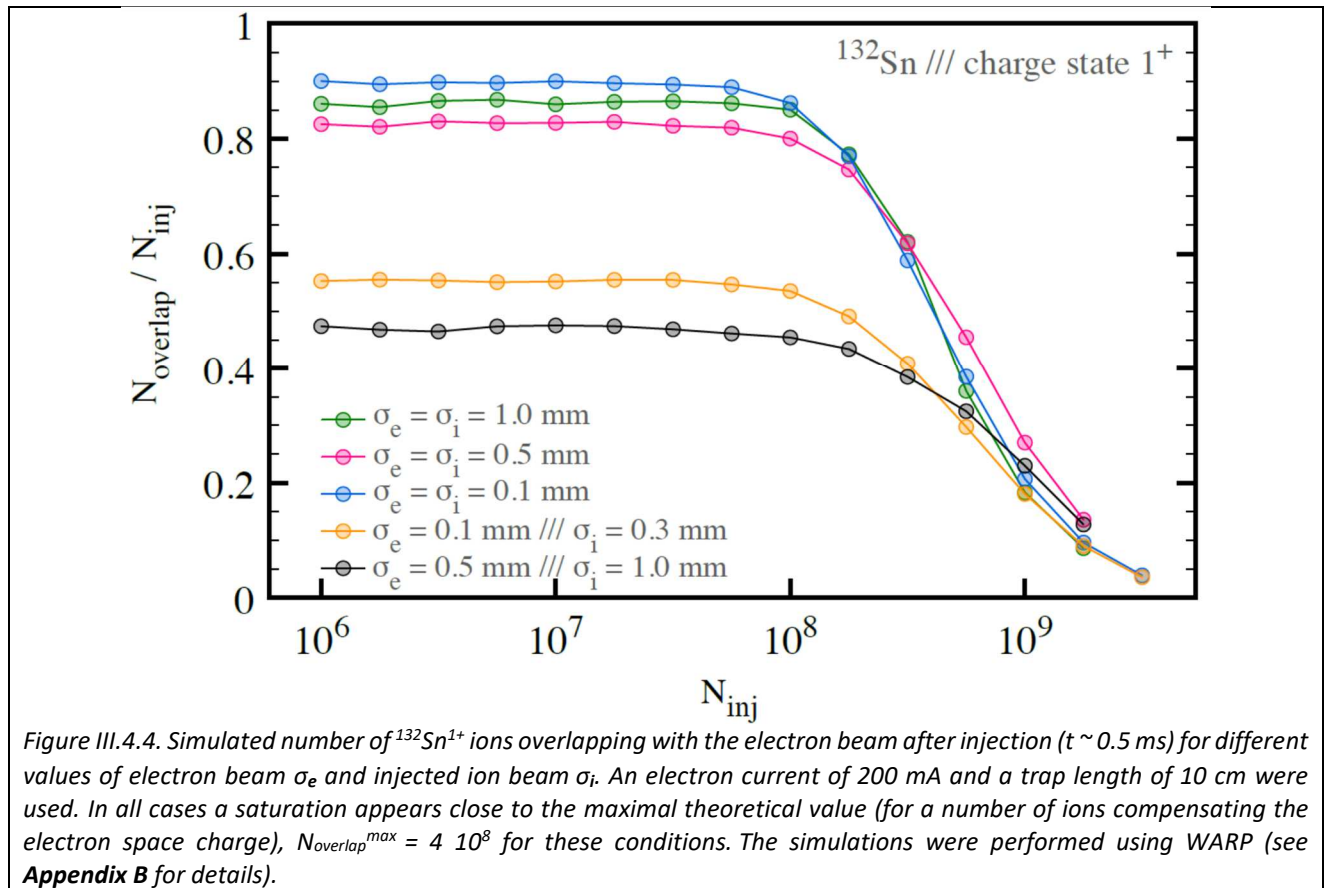*The number of trapped ions scales linearly with the electron beam current.*

For 200 mA it is $5\cdot10^8$ for 1^+ ions and $5\cdot10^7$ for 10^+ ions for a 120 mm trap.

The ion cloud minimal dimensions as derived from **Eq. 10** yield a fundamental difference with the original ETIC project, which was challenging for the electron driver (as mentioned above, a 10 μm size at the IP implied stringent IBS effects).

Reconsidering the original objectives by taking into account a 10-fold increase of the dimensions of the IP, the constraints on the electron machine are somewhat relaxed. The achievable luminosity has to be optimized by increasing the number of trapped ions rather than on reducing the size at the IP, which is another challenge.

To further validate the above considerations we have also performed dynamical simulations of the ion trapping using the WARP simulation code (see **Appendix B.2** for details). The main outcome is that, in all considered cases (i.e. varying radii of the electron beam and the ion cloud, the ion charge state, the trap length, testing different species), the simulated trapping capacity is close to the maximal theoretical capacity (full compensation between the ions and the electron beam space charge). Some examples are shown in **Fig. III.4a**, where the simulated number of ions overlapping with the electron beam is displayed as a function of the number of injected ions, for different trapping conditions. As visible from the lower curves, even when the injected ion beam has a size larger than the electron beam, a significant fraction of the injected ions ends up overlapping with the electrons (up to a few times 10^8).

These results support the use of a number of ions fully compensating the electron space charge in the estimates below. Be careful that the **Fig. III.4.4** is shown to underline the potential maximum number of ions, which corresponds to the maximum value of "N_{inj}" (x-axis) for which the "$N_{overlap}/N_{inj}$" (y-axis) is maximum and constant. The value itself of the $N_{overlap}/N_{inj}$ on the vertical axis is not to be considered at this stage since the mean value overlap depends on dynamics effects which are not yet understood and predicted at present. See *Appendix B* for discussions of the various cases. Mainly, these simulations are useful to show that the maximal

trapping capacity can theoretically be attained, after an evaporation of the ions in excess, giving some credit to the luminosity estimates done here and in the table below.

Figure III.4.4. Simulated number of $^{132}Sn^{1+}$ ions overlapping with the electron beam after injection (t ~ 0.5 ms) for different values of electron beam σ_e and injected ion beam σ_i. An electron current of 200 mA and a trap length of 10 cm were used. In all cases a saturation appears close to the maximal theoretical value (for a number of ions compensating the electron space charge), $N_{overlap}^{max} = 4\ 10^8$ for these conditions. The simulations were performed using WARP (see **Appendix B** *for details).*

We give in the table **III.4** typical estimates for luminosities, considering different achievable cases (with circular beams $\sigma_e = \sigma_{x,e} = \sigma_{y,e}$ and $\sigma_i = \sigma_{x,i} = \sigma_{y,l}$. The detection zone will be less limited with a short length trap. Compared to the SCRIT design (40 cm) the typical length could be reduced, between 10 to 20 cm. For comparison, we also give the numbers for two cases, 10 or 16 cm. Luminosities for 1⁺ are given as a reference, but charge equilibration will be at higher charge states. Going from 1⁺ to 10⁺ charge states, the number of trapped ions is divided by a factor 10, so is the luminosity. In practice, with the physical effects of the charge state equilibration and of the self-confinement the luminosities will be found between these two cases.

Ion trap Trap length (mm)	Electron beam Beam size dx*dy (mm^H*mm^V)	Ion beam (mm^H*mm^V) area overlap (%)	Electron cloud density (mm^{-3}) (charge states) →max number of trap ions (full compensation)	Luminosity cm^{-2} s^{-1}
SCRIT 400 mm	1^H*2^V	3^H*5^V 13,3%	5.08 10^4 (1⁺) →1.7 10^9 (10⁺) →1.7 10^8	2.5 10^{27} 2.5 10^{26}
e-RIB GANIL tests				
tests I 160 mm	0.5^H*0.5^V	0.5^H*0.5^V 100 %	1.32 10^6 (1⁺) →6.7 10^8 (10⁺) →6.7 10^7	(1⁺) 2.6 10^{28} (10⁺) 2.6 10^{27}
tests II 100 mm	0.5^H*0.5^V	0.5^H*0.5^V 100 %	1.32 10^6 (10⁺) →4.2 10^7	(10⁺) 1.6 10^{27}
tests III 100 mm	1.0^{H,V}	1.0^{H,V} 100%	3.3 10^5 (10⁺) →4.2 10^7	(10⁺) 4.1 10^{26}
tests IV 100 mm	0.5^{H,V}	1.0^{H,V} 25 %	6.6 10^5 (10⁺) →4.2 10^7	(10⁺) 8.3 10^{26}
tests V 160 mm	0.2^{H,V}	0.2^{H,V} 100%	8.3 10^6 (1⁺) →6.7 10^8 (10⁺) →6.7 10^7	(1⁺) 1.7 10^{29} (10⁺) 1.7 10^{28}

Table III.4. Calculated luminosities for various test cases of the ion-trap parameters and of the beam emittances, for an electron intensity of 200 mA (N_e=1.25 10^{18}/s).

These solutions have to be explored in details considering the goal of a luminosity of 10^{29} (and possible evolution towards 10^{30-31}) and all the physical beam constraints of IBS and space charge limitations at the interaction point precisely. We stress that it could be found that, after the R&D phase the targeted luminosity of 10^{29} is hardly insured, because of" amongst other effects, ion heating effect (trap issues) or intra beam collisions (electron accelerator issues related to the maximum intensity around 200 mA in the interaction point). The present known limitation is given by the SCRIT experiments that is around 10^{27} for a maximum of 10^8 trapped stable ions.

Several questions about the ion trap technique require detailed studies, including both simulations and benchmark tests with a demonstrator for a quantitative investigation of the various physical processes introduced in this section: ion heating, ion beam capture thanks to charge breeding, ion charge state reprocessing in a RF trap filled by buffer gas. The ion trapping performances such as maximum space charge capacity, overlap between ions and electrons, as well operational parameters like the possible duty cycle including the recirculation of the multi-charged ion cloud are to be carefully determined.

We underline that some of these effects are not well described or not taken into account at present in the ion trap process simulations. A demonstrator for the ion trap device is therefore mandatory to cross check the numbers found in the simulations.

The stability for the high luminosity conditions would also require to work on the accelerator machine tuning, efficiency of the ion beam transport, operating conditions of the trap (electric field stability), vacuum conditions (of the trap and of the beam lines).

III. 5 Parameter sets for the electron machine

The parameters of the electron machine are discussed here taking into account physics cases requirements and considerations of technical feasibility.

From physics requirements for the main physical cases, beam energy at or above 500 MeV (500-700 MeV) would be an ideal range.

Intensities above 200 mA together with a good trap efficiency will ensure luminosity around 10^{26-28} for all the isotopes (from light to heavy) and potential increase up to 10^{29} which would open the possibilities to access the processes at larger momentum transfer and lower rates, like inelastic scattering at large angles, and (e,e'p) processes.

Electron currents should be at 200 mA and potentially higher.

We discuss here the technical constraints on the possible solutions of the synchrotron and of the ERL.

For the ERL solution, two modes are possible, single turn or multi-turn.

In the literature, the state-of-the art ERL machines are for 10 MW beam power. Projects can be found running with maximum intensities around 100 mA (single turn) but for much lower beam energy, 100MeV. The project at higher energies than 100 MEV are for a few 10 mA (multi-turn), and in the case of a 100 mA, 500 MeV machine, the scope is beyond existing projects by a factor 5.

The increase of intensities with the ERL could be obtained using a multi-turn design, resulting in several beams of electrons at different energies, which is not what we need for the experiments: **one given incident energy for the electron scattering on the ions. Furthermore the energy has to be well defined, typically ± 50 keV at 500 MeV, corresponding to a relative energy error of 10^{-4}.**

In fact, the multi-turn design would correspond to a more compact ERL since we reduce the number of cavities (multi-path scheme) and thus the length of the straight sections.

The beam current does not increase. In fact, it decreases because we have several beams going through the cavities. The beam current seen by the cavities is thus larger but the current for the energies of interest is smaller. Moreover, because of instabilities and growth rates, we cannot afford the same average current in the cavities with multi-turn compared to single-turn schemes.

In summary, in the case of the ERL, the multi-turn does not allow reaching currents up to 200 mA. To get a larger beam current, we should keep the single-turn scheme, but the increase of intensities in the single-turn ERL requires R&D to check the feasibility at 200 mA.

We compare below the synchrotron and the single-turn ERL below in terms of the physics requirements and of the technical difficulties or advantages for the machine feasibility.

Comparison between the synchrotron and ERL solutions - *Technical constraints*

Assets-difficulties	Synchrotron	ERL
Intensity **200 mA feasible** **with synchrotron** **Not with the ERL** **(multi-turn)**	The mean currents are higher since the source and injector are not in a continuous mode and it is possible to accumulate, resulting in less constraints on the injector (the equilibrium emittance is given by the ring, with the synchrotron damping). Asset: **higher average current**.	Assets : **current stability**, there is always a « fresh » electron beam ; Energetic efficiency; better availability of the machine (no cycle to prepare)… *A demonstrator (at 140 MeV) would be needed to ensure that such currents (200 mA) can be reached with the target tolerances.*
Beam line design Detection area Stop beam	The average beam power in the dump is low. Indeed, the peak deposited power can seem high (about 100 MW) but it is deposited on a very short time (one revolution time of about 0.36 μs), which corresponds to a beam energy of 36 J. Since the beam is lost with a frequency below 1 Hz, the average deposited power in the beam dump will be below a few watts. Asset: **small average power on the beam dump**.	Assets: a stop block at lower energy (better on the radiological point of view) reduced beam dump activation
Operations Stability of the physics parameters	Overlap between the required parameter sets (acceptable one, potential)	For the electron recirculating linac (ERL), the IBS is not anymore a problem, we can work at lower energy. A first layout has been shown at 530 MeV. A special effort must be performed on the electron source quality. With an ERL the beam fluctuations can be better regulated than in the case of a synchrotron, it is easier to maintain the beam emittance parameters. Assets: out-of-equilibrium medium, **beam characteristics (emittance…) determined by the injector, no intra-beam scattering**, possibility to reduce strongly the beam size. **BBU instabilities**: unknown issues
Long-term goal machine performances Limitations	**200 mA is reachable.** Higher intensities should be studied.	A few 10 mA in multi–turn. Several electron energies not adequate. Physics requirements: one given energy for 200 mA. Around 100 mA with single-turn How to increase the intensity in single-turn?
Costs[#] Construction / Operation Feasibility	Less risks for this solution: the French community has the **know-how to reach the parameter sets** for the physics. Expert of the domain can work to define the machine design in a few-year detailed project, state-of-the-art machines are known. RF budget is reduced...	Complexity of the machine. Unknowns about the 200 mA intensities. Physics effects (IBS) have to be estimated Less expensive in operation costs?

[#]*The cost of the machine, depending on the synchrotron or ERL solutions has to be examined once the parameters of the machine are precisely defined, in the pre-detailed project in 2021, since it depends on the choice of the injector and on the elements.*

Finally, the ERL assets are numerous, but, to work with a given energy we need single-turn ERL, and the technology is not demonstrated in this case for reaching higher intensities like the 200 mA we require at the large electron energy above 500 MeV.

The initial requirement of a low emittance beam at the IP (size around 1 µm) was against the synchrotron solution. Now with a larger beam spot size at the IP (> 100 µm), the synchrotron appears as a good competitive solution to ensure the 200 mA with less risk for the development of a feasible machine.

The consolidation of the parameter sets is of utmost importance to evaluate the needs on the machine design. In the machine studies with various design options, the IBS effects and beam instability have to be carefully determined to ensure the feasibility of the machine with the parameters needed for the physics case. This step is mandatory before retaining any solution.

Whatever the electron machine design, a key point is the ion capture efficiency. The more efficient the capture is, the less intensity we need. The parameters can then be relaxed.
That is the reason why an intermediary step is proposed to host the ion trap on an existing electron machine to test the ion efficiency by varying some key parameters like the electron beam size.

If we want to demonstrate the ion capture efficiency, we would need benchmark tests, done at an electron machine which can deliver a beam size smaller than 0.1 mm (or similar to the target one), a sufficiently high average current (to achieve the saturation in the ion trap) and sufficiently high energy. We also need to have enough place to host the trap plus a detector.

A work plan could be defined with the expert group of the TU Darmstadt (following the recent studies by the MESA team working on these questions **[NimERL19]**) about the beam instabilities for various physical cases, varying the sets of parameters of the beam size, beam intensities.

Energy	500 MeV
Total length	107.372 m
Beam current	200 mA
Q_x/Q_y	16.715/8.705 -
α_c	$2.59\,10^{-3}$
Energy loss/turn	3.32 keV
$\beta_{xy,IP}$	4.08/4.15 m
$\beta_{xy,max}$	6.3/20.5 m
$D_{x,max}$	0.14 m
RF energy acceptance	2.0 %
RF Voltage	107 kV
Coupling factor	50 %
Eq. emittance (No IBS)	0.67 nm
Energy spread (No IBS)	$0.45\,10^{-3}$
Bunch length (No IBS)	8.03 mm
Hor./Vert Emittance (IBS)	1.80/0.9 nm
Energy spread (IBS)	$0.92\,10^{-3}$
Bunch length (IBS)	12.2 mm
Touschek lifetime	1.36 h

Higher than 200 mA: IBS effects could be difficult to overcome (equilibrium emittance and energy spread).
Reaching 500 mA has a cost on beam quality (and could enhance the beam instabilities and IBS effects, deteriorating the gain in intensity increase).

Other parameters of the accelerator have to be examined for the operation mode in the detailed project.

The detailed discussion on the choice of parameters and IBS effects is given in *Appendix C*.

Table III.5. Electron machine-trap parameters to reach the targeted luminosity at 10^{29} : beam parameters with IBS, trap characteristics

Note that in the detailed pre-project study for the envisioned solutions, we need to include other considerations in the discussions, to check if the proposed machine design is compatible with the following mechanical constraints of the available volume around the Interaction Point:

- including the space needed for the trap, with the known characteristics (length ~ 120 mm, with a cylindric shape, diameter to be defined) and the design of the electrode patterns (following WARP simulations and demonstrator tests of the trap, to fix the pattern);

- including the interface between the trap and the detection arrays around the beam line, the volume has to be estimated in the machine design studies. For instance in the case of the SCRIT facility the trap and injection system length is around 2 m;

- including the space needed for the detection systems.

For the typical dimensions of the area for the electron spectrometers we could consider the three spectrometer area A1 for electron scattering at MAMI facility [**Mami98**] or the HE1 Hall at ALS Saclay [**ALS80**] where "the total apparatus with carriers and shielding weighted 1000 tons and was 12.5 m high".

III.6 Possible scientific, medical and industrial applications

Once the parameters of the designed machine are defined there will a discussion with the potential users willing to exploit the electron beam for applications. For instance, having a second interaction point located in a branch of the beam line could open possibilities to make electron-matter collisions useful to characterize materials.

In **Appendix F**, we explain which potentialities can be foreseen and discussed with the groups, especially the Medical applications of very high energy electron (VHEE) beams for therapy.

At this stage of the studies of the machine we could already give *them a preliminary information on the overall possible parameters for the electron beam, to check if some adaptations of the beam line could fit their requirements for their applications, , provided that the changes are compatible with the optimized range of values we define for the sets of parameters in VI.1. The most efficient way to prospect for the potential applications would be to organize a workshop at the end of 2021, to present to the potential users the possible design of the machine and ask whether the electron beam characteristics could be interesting for them, with a dedicated beam line for instance. This would be also the good schedule to discuss some modifications of the beam line design (lengths, elements …) before entering in the CDR phase in 2022.*

IV. 1 Kinematics, transfer momenta and cross sections

Decades of electron scattering experiments on stable nuclei accumulated knowledge on the requirements and limits of a suitable detection system. We propose here to revisits them in light of the new constraints of working with unstable nuclei. We recall the requirements and the limits of the detection system, based upon the knowledge accumulated on the stable nuclei.

For most of our test cases, including elastic and inelastic scattering measurements for a large region of scattering angle (~**10 to 170 deg**) an energy resolution around 100 keV or better would be sufficient to separate the first excited state from the elastic scattering peak. At incident electron beam energies around 500 MeV, this would correspond to a momentum resolution Δ**p/p ~ 10^{-4}** (*Figure IV.1*).
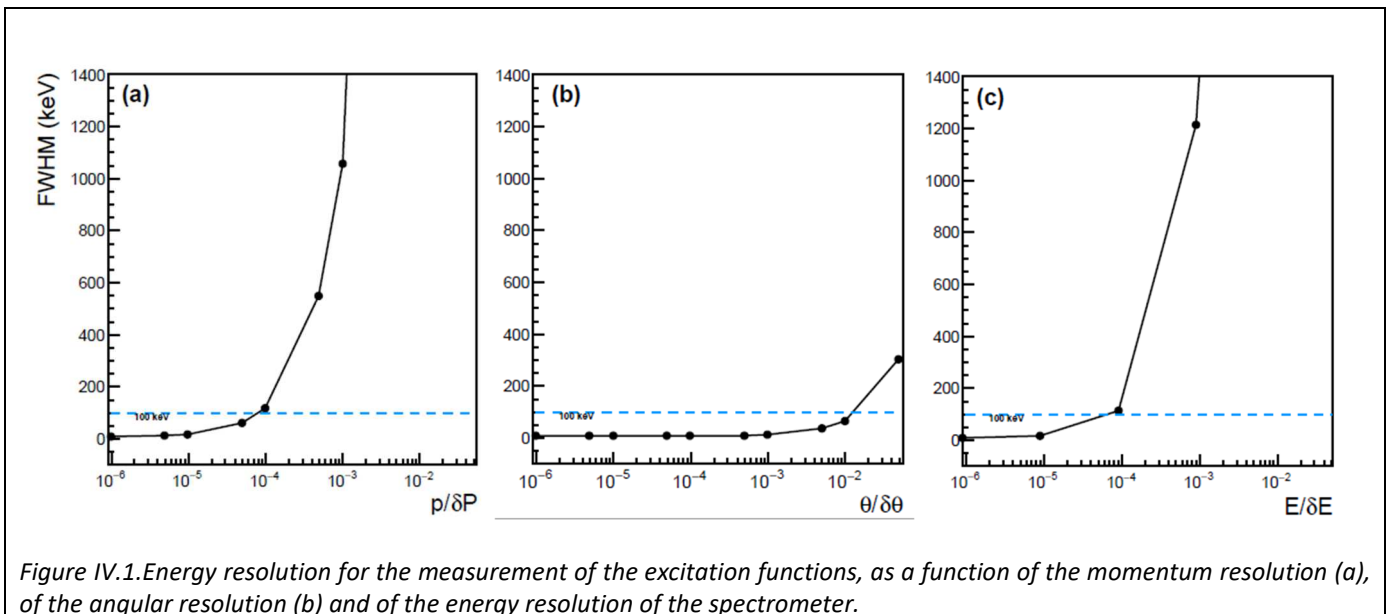The region of scattering angle would correspond to transferred momenta: **q ~0.5 to ~4 fm^{-1}**.
An angular resolution of **0.2 deg (3.5 mrad)** would guarantee granularity sufficient to draw the global pattern of the cross sections, with an angular range high enough 25° – 155°.

Low background conditions are mandatory to perform low cross sections measurements for the elastic and inelastic scattering at the largest q momenta and for the separation between inelastic processes.

Note that the equilibrium energy spread in the synchrotron is rather 10^{-3}, one order of magnitude above this value. If the intensity increases, the equilibrium momentum spread will also increase.
An energy spread around 10^{-4} is a challenge. Otherwise, some tricks should be used (for instance dispersion in the IP region) to separate the electrons in energy. This will be studied in the design report phase of the project.

Figure IV.1.Energy resolution for the measurement of the excitation functions, as a function of the momentum resolution (a), of the angular resolution (b) and of the energy resolution of the spectrometer.

In the case of coincidence experiments, for (e,e'p) measurements, the set-up will be designed to combine two spectrometers, offering large energy and momentum acceptances and good energy and momentum resolutions.

IV.2 Electron spectrometer

A variety of electron spectrometers has been designed in past experiments on stable targets. Among them we can mention the ALS [**ALS80**] in France, NIKHEF [**NIK98**] in The Netherlands, and MAMI [**Mami98**] in Germany.

The three design shared similarities, namely an adjustable angle for the spectrometer, large entrance windows to maximise solid angle, and a high momentum resolution typically around 10^{-4}. These were achieved at ALS, NIKHEF and MAMI facility with large gap, normal-conducting spectrometer, employing Dipole, Quadrupole and in some cases Sextupole elements.

The focal plan of NIKHEF and MAMI spectrometer were designed to measure the angle of the detected particle using drift chamber, not dissimilar to the ones currently used by the nuclear structure community, e.g. at the focal plan of VAMOS *[specG]* at GANIL or SAMURAI at RIKEN [*specR*], to measure the trajectory of the incoming particle.
Current expertise in building, operating, and analysing large drift chamber is a key asset of the community.
In addition Cherenkov detectors were developed in order to separate protons from electrons, allowing the same spectrometer to be used for both (e,e') and (e,e'p) studies.

An additional difficulty in our detection setup will come from the large extension of the interaction region, up to 12 cm. In comparison the MAMI three spectrometers experiment was designed to accept target length of a maximum of 5 cm. This additional constraints means the trajectory of the scattered particle may needs to be reconstructed more precisely by additionally measuring the incident position and angle closer to the entrance windows.
Typically those spectrometer were setup vertically around the interaction region, allowing them to easily rotate around the target. This design implies a typical ceiling height of ~ 10-15 m, while keeping the floor area of the experimental vault relatively small.

Spectrometer	*Configuration*	dp/p	Mom. Accept. (%)	Solid Angle (msr)	Max B (T)	Focal plane length (m)	Focal plane detection
ALS 600	D	$4. \, 10^{-4}$	+10 -30	6.7	1.5	~1.5	MWPC Cherenkov Scintillator
ALS 900	D	$1.5 \, 10^{-4}$	± 5	5.6	1.67	~1.5	MWPC Cherenkov Scintillator
NIKHEF A	QDD	$1. \, 10^{-4}$	± 5	5.6	1.43	1.05	DC Gas Cherenkov
NIKHEF B	QDQ	$2. \, 10^{-4}$	± 5	17.2	1.56	1.00	DC Gas Cherenkov
MAMI A	QSDD	$< 1. \, 10^{-4}$	± 20	28	1.5	1.73	4 DC 2 plastic planes 1 gas Cherenkov
MAMI B	D	$< 1. \, 10^{-4}$	± 15	5.6	1.5	1.77	4 DC 2 plastic planes 1 gas Cherenkov

Great care needs to be done in designing these spectrometers and their associated detections. The technical expertise for designing, building, and installing such magnetic spectrometer is currently available and the new design could take advantage of the increased in readout and processing capability of modern electronics.

(e,e'p) experiment will require at minimum two spectrometers in order to detect both the electron and the proton at different angles. In the case of (e,e') experiment these two spectrometers will be used to increase solid angle coverage.

IV.3 Heavy ion detection

The most important constraints for the detection are given by the (e,e'p) observables.
There will be the beta-decay of the radioactive beams and we will need to identify and separate the reaction products from the (e,e') and (e,e'p).
To get complete sets of data, the reconstruction of the kinematics is needed, in coincidence with the particle identification of the ejectiles, in a triple coincidence electron/proton/nucleus or electron/ photon/nucleus.
A detection adapted to the focal plane could be designed to detect either electrons or protons.

Heavy ion detection could be critical in the case of scattering experiment on unstable nuclei. Unlike stable target experiment, our target contamination could evolve over time, would it be from isobaric contamination of the injected beam, or from the beta decay of the trapped ions.
Because of these new constraints, detection of the heavy ion in coincidence with the scattered electron is highly desirable. The task is however difficult, with typical energy ranging from 2 to 5 MeV total, such ions are difficult to detect, and even more difficult to identify.

A thorough R&D program needs to be performed in order to develop the adequate identification apparatus. One could however elaborate on the property of such a device.
The low energy of this ions means their travels and detections needs to happen under vacuum and given the extremely low rates and energy deposits, the detection needs to be made in a low noise environment, not compatible with detection close to the interaction region, where delta rays are the main source of background. Ideally, a device allowing separation and transportation of the ions away from the interaction setup would be ideal, and would allow time of flight, hence mass, identification.
The Z identification is the most difficult part, where either a silicon PSA base identification (as done for the GRIT [*spGrit18*], FAZIA [*spFa17*] multi-detector arrays) would not work with current technologies, because the ions would stop within the inactive layer of the silicon wafer. Gaseous detector could be adapted to this task, and a thin windows Bragg chambers measuring the depth of the Bragg peak could be an avenue of exploration, building upon the detection expertise existing within the ACTAR *[spActar]* collaboration.

This innovative R&D program could be performed at existing low energy facilities, while the detection expertise and engineering resources already exist within the community. To this end the characterisation of the background around the target is an essential task that could be started at the only existing facility with similar target densities, SCRIT, and continue when the ion trapping device would be tested.

IV.4 Beam and luminosity monitor

Beam monitoring and luminosity detection is also a key aspect of the experiment, allowing to fine tune the ions trap at the beginning of the experiment and subsequently extract absolute cross section.
To this end, the SCRIT [*Scrit09*] experiment is emptying its ion traps regularly counting the out coming ions.
Additionally, an electron beam loss detector is placed downstream of the Interaction Region.
Both technique are useful in tuning and monitoring an experiment; similar devices suitable to our ion trap system need to be developed. This would represent an obvious topic of collaboration with ongoing development of the SCRIT experiment in Japan.

V. Radioactive isotope production

Note that for the electron-ion project, we do not plan to deal with the most exotic species close to the driplines, which are typically associated to low intensity beams and have lifetimes < 100 ms, too short for the ion trap technique.

In a first step, we plan to focus on radioactive beams easily produced at intensities at and above 10^{7-8} /s. With these rates, we should be able to measure e-RI cross sections and to extract the nuclear form factors of neutron-rich or deficient nuclei. These experiments would give rise to completely new studies of the nuclear shapes, which are not known at present, since only radii have been obtained for some species, mainly by laser spectroscopy technique.

The beams of interest could be obtained from the present GANIL/SPIRAL1 and the beams foreseen in the S^3 project as well as the ones that could be produced by photofission. Since GANIL offers RIBs without post-acceleration, it is well adapted to a SCRIT-like technique.

We have identified 5 main possibilities for producing RIBs at GANIL using presently operational drivers (CSS1&CSS2 at GANIL, SPIRAL 2 LINAC) and an additional commercial electron driver (Rhodotron from IBA). The different drivers would allow one to cover a wide range of very different regions of the chart of isotopes, which would be an indisputable asset for probing nuclear models with the electromagnetic probe, as developed here. The motivations for extending the production capabilities of RIBs by GANIL have actually been discussed in [*sp2Gan*] and [*sp7RFQ*] in a wider scope, including the possibilities of studying the most exotic nuclei at DESIR or with reaccelerated beams. The main production mechanisms envisaged in the future of GANIL are regrouped in *Tab. V.1.*

Facility	Beams, Intensities **I**	Reaction mechanism	When	Comments
SPIRAL 1	A < 80, I up to ~10^9 /s	Fragmentation	Many are ready, some to develop	Fusion evaporation possible
S3-LEB	Mid-heavy to heavy neutron deficient beams A >40 → ~270 I up to 10^6 /s	Fusion evaporation	Starting on-line development as of 2023 S^3 operation around 2026	
Gas cell/ production cave with **A/q=7 driver**	Light to heavy (N=126) neutron rich beams, with intensities up to 10^6 /s Neutron deficient heavy (A>200) ion beams, I up to 10^8/s Refractory fission fragments	Multinucleon transfer Fusion evaporation in inverse kinematics or using intense proton beams (not possible at S^3) Fusion fission reactions	* After A/q is ready > 2027 * ideally in the production building ~ > 2030?	*See **App. D.1** contribution of C. Theisen*
Fission fragments from **LINAC**	70 < A< 150 with intensities up to ~10^9 pps	Fusion reactions Light particle induced fission (p,d,3He,4He)	Production building, ~> 2030?	See [*sp2Gan*] contribution of Delahaye et al. and ***App. D.3-4***
Fission fragments from **Rhodotron**		Photofission	Production building, ~> 2030?	

*Table V.1. Main production mechanisms as envisaged for the future of GANIL ([**sp2Gan, sp7RFQ**]).*

*The more detailed description of the production modes can be found in **Appendix D**. Here we give a summary of the main production techniques which could deliver the beams of interest for the electron-ion collisions.*

V.1 Production techniques

We give the main elements about the various production techniques, a short description for each facility and a few typical yields that would be available from these.

V.1 A. ISOL
Light (A < 80) exotic beams from SPIRAL 1
SPIRAL 1 is the only ISOL facility world-wide using fragmentation of heavy beams at intermediate energies (up to 95 A MeV). This production technique permits the production of very intense beams in regions of the chart of isotopes that can be accessed by the stable beams available from CSS1 and CSS2. It delivers many of the highest intensities worldwide for neutron deficient and neutron rich isotopes of light noble gases (He, Ne, Ar). With the FEBIAD ion source recently adapted to the SPIRAL 1 targets, many more intense beams are becoming available. Beams from fusion-evaporation are additionally being developed, for complementing the production from S3 LEB (see **V.1.B**) for the DESIR program. Beam intensities estimates are available from *[sp2beams]*.
Typical beams with intensities suited to the electromagnetic probe:
^{6}He^{1+}: 2·10^8 /s ; ^{19}Ne^{1+}: 1.5·10^8 /s ; ^{23}Mg^{1+}: 2·10^8 /s.
We can underline that the RIBs produced by the so called Isotope Separation On Line (ISOL) method would be particularly suited to the studies of nuclear densities with the electromagnetic probe: the ISOL technique permits producing intense (>10^5 pps) and pure (in some cases close to 100%) 1$^+$ beams with half-lifes ranging from the fraction of s which are possible to manipulate in ion traps.

V.1 B. LINAG, Multi neutron Transfer reactions and fusion-evaporation with A/Q=7

Neutron deficient beams from S^3 LEB
The Super Spectrometer Separator Low Energy Branch (S^3 LEB) will permit accessing the neutron deficient side of the valley of stability, thanks to fusion evaporation reactions with the very intense heavy ion beams available from the SPIRAL 2 LINAC. The innovative gas cell technique, employing resonant laser ionization in a gas jet [*specS3*], will enable a quite universal but selective production of the most exotic beams (beam intensities estimates from *[sp2beams]).*
Typical beams with intensities suited to the electromagnetic probe: ^{118}Cs^{1+}: 3·10^6 /s ; ^{239}Am^{1+}: 2·10^6 /s.

MNT and fusion fission from the production building
The third cave of the production building ("versatile target ion source(s)" on **Fig. V.2.2**) is another important part of the extension proposed here. This cave is dedicated to the RIB production with the very intense A/q=7 beams from the SPIRAL 2 LINAC. Heavy ion beams at 5 to 10 MeV per nucleon enable the use of fusion fission, fusion evaporation, few nucleon transfer, and MNT mechanisms. The heavy and intense beams of the A/q injector would enable in such a cave the use of inverse kinematics reactions, which are particularly well suited to gas cell or gas catcher techniques. In contrast with the standard ISOL thick target technique, the gas cell technique permits to access exotic isotopes independently on their chemistry. A cave of this kind would therefore be very complementary to the other 2 fission caves, by granting access to fission fragments of the refractory elements Nb to Pd (Z=41 to 46), using fusion-fission reactions. The MNT reactions in gas cells provide a unique access to the N=126 region, as attested by recent projects at KEK [*spnu7*] and ANL [*spnu8*]. It would supplement S3 for the production of neutron deficient heavy isotopes by making an optimized use of fusion evaporation reactions in inverse kinematics.
Yields estimates for some beams have been calculated in the frame of the present proposition and are presented in more details in **App. D.1**. While only a limited number of isotopes with intensities sufficient for the electromagnetic probe can be envisaged by using such production mechanisms, numerous beams would become available for nuclear structure studies at DESIR or with a possible reacceleration, as envisaged in [*sp7RFQ*]. The third cave would additionally enable the use of a few nucleons transfer reactions, from which copious beam intensities would become available, 2 to 3 nucleons away from the stability valley, as attested in [*spnu9*]for light (A < 40) beam production.
Beam intensities estimates: some in target yield estimates can be obtained by measured cross sections available from literature (see **App. D.1**). A typical gas cell flat efficiency factor of ~10% has to be accounted for.
Typical beams with intensities suited to the electromagnetic probe:
^{214}Ra$^+$ (fusion evaporation in inverse kinematics): 6.3·10^9 /s^{248}Bk$^+$ (MNT): 3.3·10^6 /s ; ^{30}S$^+$ (transfer): 2·10^8 /s
The **appendix D.1** explains how the cave intended for the production building could be used for fusion evaporation production in inverse kinematics, or using more classical ISOL methods with intense proton beams. Fusion fission processes are also interesting for the production of fission fragments in a gaseous cell, which will not be feasible anywhere else. It would give access to the refractory elements (cf *Tab. 1)*.

The production yields obtained for neutron-rich isotopes of Mg, Si, Ar, Ca from Multi neutron Transfer (MNT) reactions using a ^{48}Ca beam are presented in ***App. D.2.***

V.1 C. Fission fragments from the production building

Two methods are envisaged for the production of intense beams of fission fragments:
- Light particle induced fission, using the p, d, ^{3}He intense beams from the LINAC
- Photofission, using the e- beams from a Rhodotron

Using these methods, we target fission rates of the order of $5 \cdot 10^{12}$ to 10^{13} fissions/s, which is in the order of magnitude of what is expected at SPES or ARIEL at TRIUMF for example, and what is already available at ISOLDE. We should note however that the beams from photofission are free from contaminants from neutron deficient isobars, which is an important asset of the method. The light beams from the LINAC would directly be impinging on target, with typical power of 5 to 10 kW, while a compact electron to photon converter would permit using up to 100 kW of 40 MeV electrons from the Rhodotron.

*Beam intensity estimates for **photofission***
An exhaustive beam intensity estimate has not been done for this preliminary study. Nevertheless, first calculations with PHITS, presented in ***App. D.4***, show that 50 kW of e- on a converter are enough to produce more than $5 \cdot 10^{12}$ fissions per second. The in-target yields seem also to compare favorably to neutron induced fission (phase 2) for the most exotic isotopes, although these numbers would have to be verified in a more thorough study. Typical numbers for yields should be equivalent or better (due to enhanced effusion properties) to ~ 3 times the beams calculated for SPIRAL2 phase 2 day 1 (~$1.5 \cdot 10^{12}$ fissions per second, considering 50 kW on converter, low UCx density target). In a preliminary step, beam intensities estimates are a factor 3 higher than the beam intensities calculated for phase 2 beams, available from [***Sp2beams***].
Typical beams with intensities suited to the electromagnetic probe:

^{132}Sn^{1+}: $3 \cdot 10^9$ /s; ^{134}Sn^{1+}: >10^7 /s ; ^{96}Kr^{1+}: ~$5 \cdot 10^9$ /s (using in target yields from ***App. D.4***)

A multi-user facility as an advantageous alternative to SPIRAL2 phase 2
The original SPIRAL2 phase 2 was considering the usage of a 200 kW deuteron beam on a graphite wheel as neutron converter to produce about $3 \cdot 10^{13}$ fissions per second in a voluminous target: about 2.3 kg of UCx, while e.g. SPES will use a 30 g target. As developed in [***spnu4***] it has been proven in numerous collaborations the last years that such a solution, while optimized for the production of relatively long lived isotopes such as ^{132}Sn, would strongly penalize the production of short-lived isotopes:
- The high density material considered for the nominal target was found to have limited release properties compared to standard (or historical) UCx targets (used at ISOLDE/CERN and ALTO) and optimized target materials with lower densities, as demonstrated in [***spnu5, spnu6***];
- The large volume of the target and the target unit give potentially orders of magnitude lower yields for exotic short lived isotopes, for elements where the effusion time is penalizing, see ***App.D.3*** for a more detailed discussion.
In comparison, the use of a direct beam impinging on a compact target as SPES or ISOLDE is expected to give better yields for exotic isotopes, such as ^{134}Sn, as intensities relates with power-laws of the release parameters compared to a linear dependence on the number of fissions/s. Photofission is another reaction mechanism for which a very compact target is convenient, even when using an e- to photon converter due to the short range of photons in heavy material such as UCx, as exemplified in the design used for the ARIEL facility.
The original motivation for phase 2 was the re-fragmentation of ^{132}Sn to produce even more exotic isotopes. The yield estimate for phase 2 for this isotope was of the order of 10^{10}/s of ^{132}Sn^{1+}. Such an intensity was found out to be too small by 1 to 2 orders of magnitude for the re-fragmentation to be competitive with direct fragmentation at facilities such as RIKEN, FAIR of FRIB. At the same time, this yield is considered to be more than enough for the electromagnetic probe, and many nuclear structure studies that could be undertaken with other probes at DESIR or with an optional reacceleration scheme, requiring at most a few 10^8/s.
For these reasons, the French nuclear community represented in [***sp2Gan***] and [***spnu4***] advocates the use of the alternative production methods as proposed here as an alternative to phase 2. Considering the original production building envisaged in the scope of phase 2, the large volume foreseen for the production building to be able to house the production cave, transport lines and its maintenance servitudes, the specific remote

handlings and the biological protections around these areas, this can advantageously be replaced by the processes presented here. Three production sites (3 in total as shown in the conceptual sketch of Fig. **V.2.2**, including 2 for fissions) and a Rhodotron. Safety handling of the < 10^{13} fissions/s targets and environment will be simplified in many respects, partly due to the smaller size of the objects, lighter weights, less fissile materials, less neutron flux, of the order of 10^{13}, compared to ~10^{16} /s in the case of phase 2 from the stripping of neutrons from deuterons. **The multiple caves and additional drivers enable a parallel operation of the GANIL facilities for experiments and beam R&D.** This parallel operation has been identified as the critical prerequisite in *Refs.* [*sp2Gan*],[*spnu4*] for carrying out ambitious programs at S³, DESIR and the electromagnetic probe facility.

V. 2 General Layout

The layout of the facility enabling all the reaction mechanisms for RIB production and separation at GANIL is presented in *Fig. V.2.1.* It is given with a simplified scheme including a production building close to the SPIRAL2 LINAC. The production building would permit to benefit from the intense beams from the LINAC and would possibly host a Rhodotron from IBA well suited for photofission, as detailed in *Fig. V.2.2.*
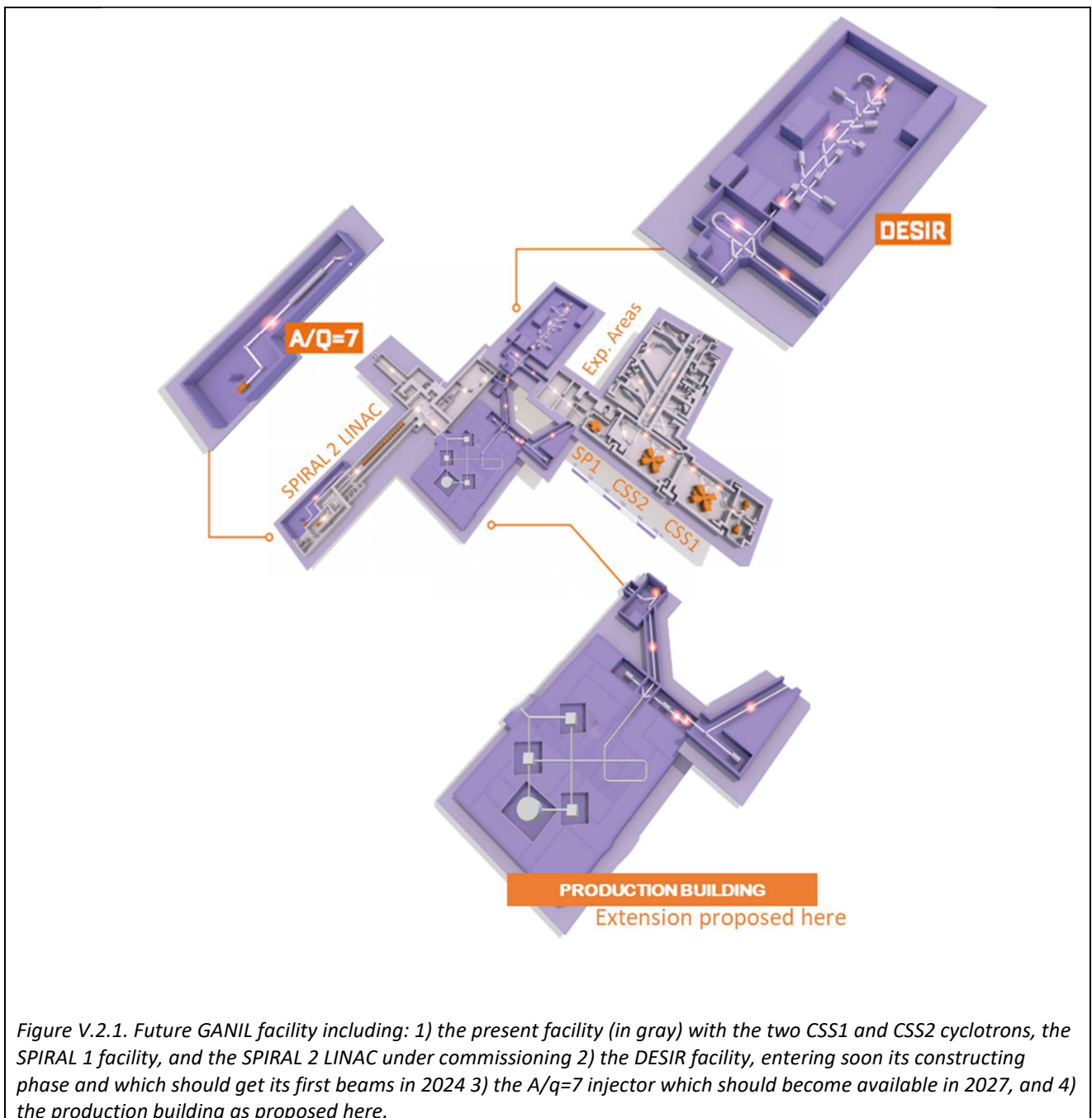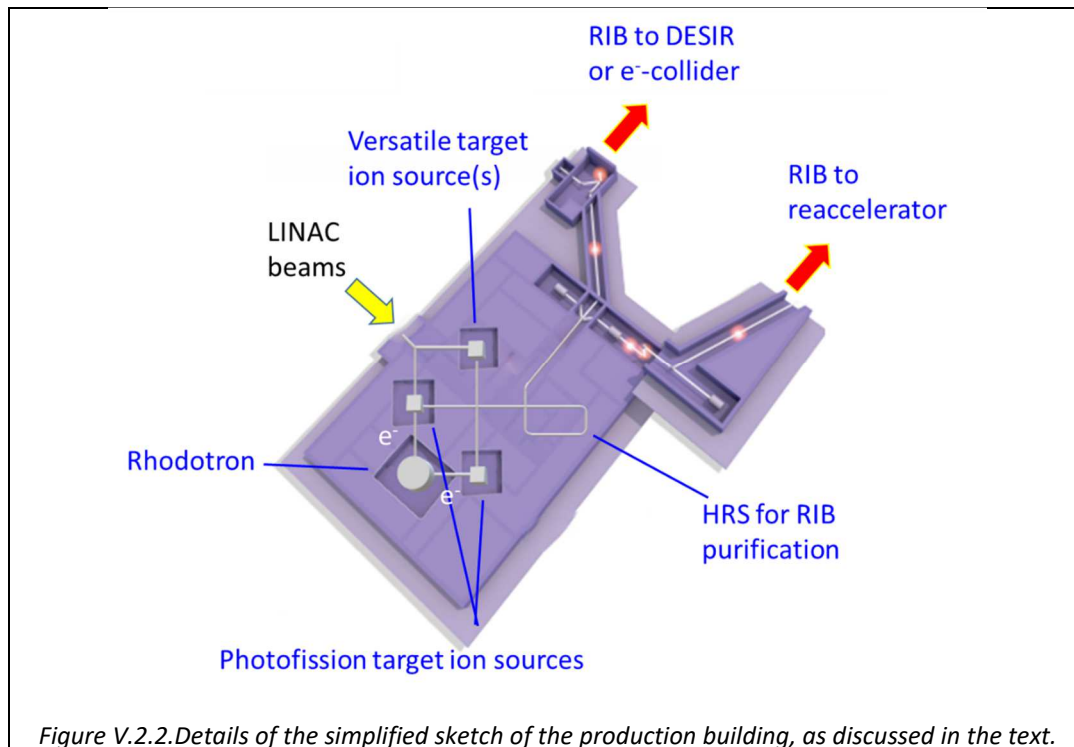

Figure V.2.1. Future GANIL facility including: 1) the present facility (in gray) with the two CSS1 and CSS2 cyclotrons, the SPIRAL 1 facility, and the SPIRAL 2 LINAC under commissioning 2) the DESIR facility, entering soon its constructing phase and which should get its first beams in 2024 3) the A/q=7 injector which should become available in 2027, and 4) the production building as proposed here.

Figure V.2.2.Details of the simplified sketch of the production building, as discussed in the text.

The general layout of the future GANIL facility including the electron-ion collider will be discussed at the end of 2021, when the preliminary design studies of the ion trap and electron accelerator are completed. The discussion will also integrate the question of the detection system in the experimental area of the electron-ion machine.

Note that it should be convenient (mandatory…) to have the accelerator close to DESIR, to take advantage of the separation power and purification devices of the DESIR facility.

We need to check the optimized compromise for the location of the ion source, and we have to consider the question of the accelerator location/ length with respect to the LINAG and to the DESIR cave.

It will be also one of the objectives of the detailed project (presented in the future possible technical design report TDR in the years 2022-2025) to investigate precisely the questions related to the radioprotection safety and the consequences for the infrastructure requirements, with the corresponding budget.

V.3 Estimated budget of the RIB production building and radioprotection issues

This part was elaborated from discussions with H. Franberg and X. Hulin (GANIL).

The possible cost for the production building has to be estimated completely including beam lines and radioprotection issues, once the technical options are fixed as well as the choices for the RIB production modes. Global considerations extrapolated from previous studies done at GANIL for SPIRAL2-phase 2 and for the S^3 experimental areas will be useful to give an estimate of the project.

To give the order of magnitude of the building cost, we can underline that compared to the SPIRAL2 phase 2 (designed with a cave classified 'Red" for radioprotection constraints) the future plan is to have 3 "yellow" caves, which reduces the operation costs for and the complexity of the operations for the beam production and for the experiments.

At first order, the budget and manpower required will scale as the volume/surface of the production building. According to the very first analysis done, the 3 caves proposed here and the Rhodotron from IBA can fit in the building which was originally studied for SPIRAL2 phase 2.

As an order of magnitude, we can recall that the SPIRAL2 phase 2 cost amounted to around 60-80 M€ [*SP2dr12*] as the end of 2012. To our knowledge, these costs did not include the full estimation of manpower needed for the internal GANIL development on the project itself.

The overall cost of phase 2 was also revaluated in the framework of the GANIL prospective initiative 2025 [*SP2dr15*] reaching around 150 M€, accounting for the inflation on the building estimation, aleas (27 M€) and an externalization of a part of the manpower (11 M€).

Costs estimates for the proposed building only.

For the discussion on the various costs, we could start from an initial estimate around 45 M€ which was given in the APD phase in June 2011. This estimate should not be retained at this early stage. The various costs have to be updated. However, it is interesting to see the sharing of the costs between the various types of technical devices included in the project:

Site preparation VRD / 0.6 M€	
main building operation (GC structural works) 13 M€ →29%	Classic ventilation 1 M€ Nuclear ventilation 6 M€ → 13.3%
Conventional fluids / 1.2 M€	Strong/low currents 1. 8 M€
General (handling operation) / 1.6 M€ Specific equipments (doors) / 1.6 M€	Cells 12 M€ → 26.7 % Radiological surveys /safety 1.7 M€ Special fluids 2.2 M€

The Rhodotron extra cost, including beam lines, will be of the order of 7 M€ according to recent exchanges IBA.

A detailed project study has also to launched in parallel to the electron machine in order to fix precisely the parameters related to the beam transport between production caves and new experimental areas, including the facility for electron-ion collisions.
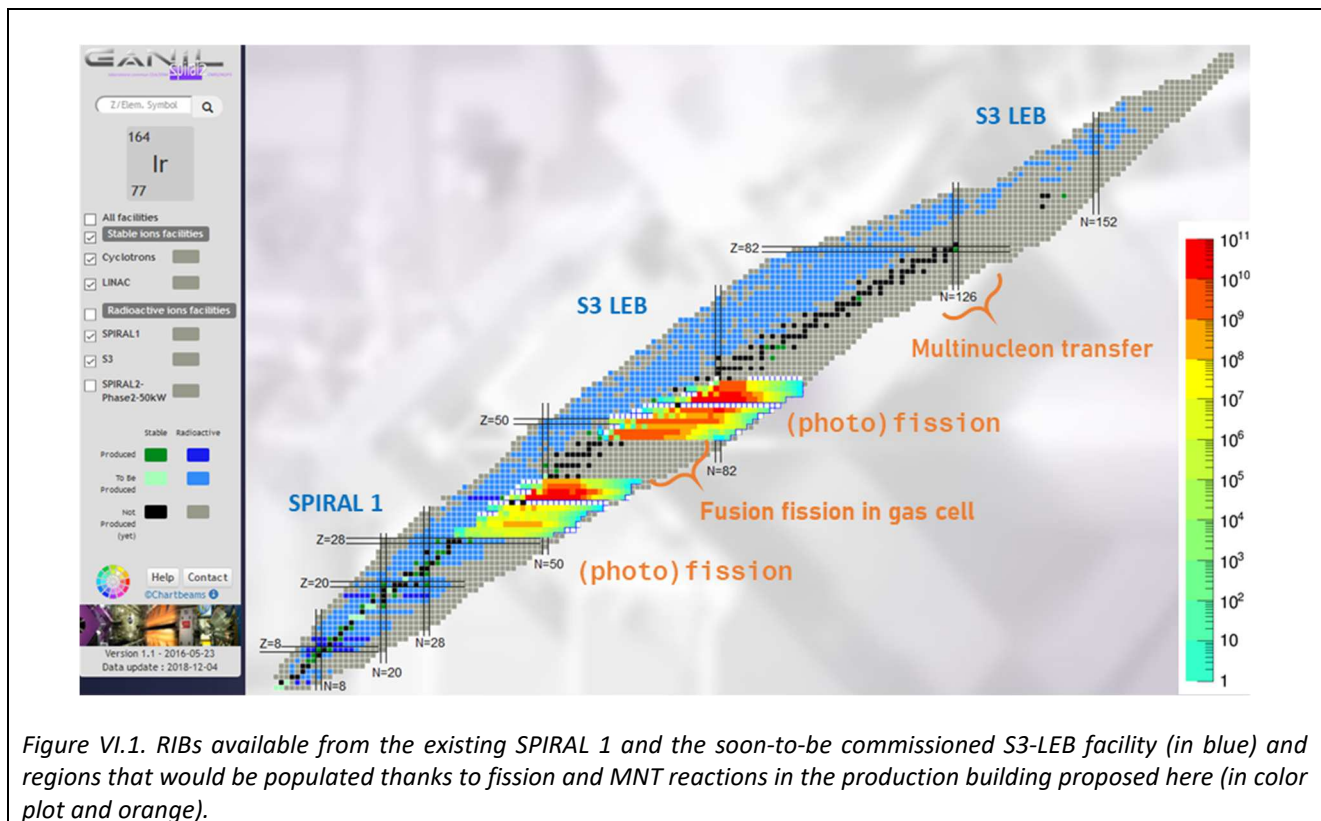
Finally, taking into account the constraints similar in terms of infrastructures, we may expect a cost for the future RIB building, around 100 M€. We outline that the cost of the production building should be completely estimated including human resources request during the TDR phase. The manpower needs have to be fully estimated for the whole phase of development project.

.

VI. Grand Accélérateur National d'Ions Lourds et Lepton (GANIL[2])

VI.1 Regions of the nuclear chart covered by the facility

Fig. VI.1 illustrates how the fission fragments and beams produced by Multi-Nucleon Transfer (MNT) in this extension would complement on the neutron-rich side the regions of the chart of nuclei covered by SPIRAL1 and S3, on the other side of the valley of stability. The region covered by fission would permit to cover four shell closures from N=50 to N=82, starting at Z = 28 and covering Z = 50. Nuclear densities could be probed all the way from neutron-deficient to neutron-rich exotic isotopes for isotopic chains such as $^{76-96}$Kr, using complementary productions from SPIRAL 2 and from the production building.

Figure VI.1. RIBs available from the existing SPIRAL 1 and the soon-to-be commissioned S3-LEB facility (in blue) and regions that would be populated thanks to fission and MNT reactions in the production building proposed here (in color plot and orange).

VI.2 Projected Day 1 physics case and requirements for the beams

Range of unstable nuclei accessible for investigation via electron scattering.
Over the nuclear chart, the RI which will be considered for the electron-ion collisions are the ones with long enough lifetimes: long enough to allow the transport from the production area and the implantation into the interacting region. We may consider a few 100 ms as the lowest manageable half-lifes ($T_{1/2}$), but this has to be further studied and precise conditions can also be fixed depending on the other beam characteristics.
Typical cycles for cooling and accumulation, mass separation in traps take a few tens of ms, which sets this general limit. Possible processes that are being investigated for manipulating the charge state distribution of ions in the trap, which develops with time and eventually limits the trapping capacity, would also take a few tens of ms.
However, in a first step we can identify the easy, "Day1" test cases for which we should be able to perform the (e,e), (e,e') and (e,e'p) studies and the ones requiring a dedicated R&D to overcome the ion trap limitations for half-lives approaching a few 100 ms.

Straightforward measurements can be seen for the beginning of the machine operation with luminosities from 10^{26} up to 10^{28}: elastic scattering on light nuclei and nuclei in the region of shape coexistence (Sr, Kr) and of the

change of charge distributions at the crossing of the N=82 shell effects (^{132,134}Sn isotopes) with long half-life times and high intensities.

^{132}Sn and ^{90}Kr are easy test cases with long lifetimes and they could be produced at large intensities (>10^7 /s).

Examples of possible beams are listed in **Tables VI.1A-B**, showing the isotopes that could be produced and trapped as rate higher than 10^7 ions/s for the Day1 experiments. They correspond to (e,e) scattering measurements with enough luminosity to reach the form factors of the charge densities, not only the rms charge radii. In some cases, this offers the possibility to investigate alpha-clustering configurations in mid-heavy and heavy nuclei. In a first step, we can focus on the even-even isotopes, presenting a low density level of excited states, which means that the separation between gs and excited states will be more favourable for the (e,e) detection without inelastic background contributions, and the conditions are better to separate the inelastic channels in the (e,e') measurements. These isotopes are considered as first physical cases, because it would be easier to produce them with improved techniques and in principle, the expected yields should be greater than the 10^7/s requested value for the good conditions of the ion trapping. Also their long lifetime makes them easier to confine in the electron beam cloud.

These isotopes represent the "benchmark" of the first physical cases studied in the R&D.

They are also the ones, which should be measured successfully in the electron-ion machine, before requesting higher luminosities. In these cases representing the most favourable conditions, we should be able if the machine requirements are satisfactory to trap them efficiently to insure the required luminosity.

The considered yields are the ones that can be expected with the most adequate production technique identified in the previous sections. The numbers are the order of magnitude indicated in *the GANIL web site [sp2beams]*. We can expect to reach beam sizes for these ions around 0.5^{H,V}mm, and in some cases down to 0.2^{H,V} to ensure the performances in terms of beam overlap and to reach the number of trapped ions needed for the luminosity requirements (**see Table III.4**).

However, the emittance conditions have to be checked as well as the beam purity to ensure that they constitute good physics cases, "easy beams" for the first experiments.

Elastic scattering on mid-heavy neutron-rich nuclei to measure charge distributions

Sn *Z=50*	^{104}Sn 20.8 s 10^5/s ^{108}Sn 10.3 min 5 x 10^5/s	^{130}Sn 3.72 min > 10^9 /s *(LEBd)* *(PhF)* ^{131}Sn 56.0 s	^{132}Sn **N=82** 39.7s **9 x 10^8** /s *(LEBd)* **3·10^9** /s *(PhF)* ^{133}Sn 1.45s	^{134}Sn 1.05 s 3 x 10^6 /s *(LEBd)* **> 10^7** /s *(PhF)* ^{135}Sn 530 ms
Kr *Z=36*	^{90}Kr N=54 32.3 s **6.4 x 10^8**/s > 10^9 /s *(PhF)*	^{92}Kr 1.84 s **2.6 x 10^8**/s > 10^9 /s *(PhF)*	^{94}Kr 212 ms **1.2 x 10^7**/s > 10^9 /s *(PhF)*	^{96}Kr **N=60** *80 ms* ~5·10^9 /s *(PhF)*
Se *Z=34*	^{84}Se **N=50** 3.1 min *(LEBd)* **9.5 x10^7**/s *(postAcc* 1.2 x 10^6)	^{86}Se 14.3 s *(LEBd)* **3.1x10^7**/s *(postAcc* 3.9 x 10^5)	^{88}Se N=54 1.5 s	

Table VI.1.A. *Characteristics of the medium heavy isotopes for the Day-1 physical cases: halftimes t$_{1/2}$, expected yields in part/s and production modes are indicated, LEBd for LEB DESIR (postAcc for post-acceleration yields) and PhF for photofission.*

The investigation of the nuclear densities in the heavy nuclei (neutron-deficient or neutron-rich) via (e,e) and (e,e') could also be considered, if these nuclei could be produced with enough intensities (see production modes in V).

Am Z=95	Bk Z=97	Ra Z=88
^{239}Am N=144 11.9 h 2·10^6/s (S3-LEB)	^{248}Bk N=151 > 9 y 3.3·10^6/s (MNT)	^{214}Ra N=126 2.44 sec 6.3·10^9/s (MNT)
Sm Z=62	^{160}Sm N=98 9.6sec (?S3-LEB)	^{162}Sm N=100 9.6 sec	^{164}Sm N=102 1.43s
Cs Z=55	^{118}Cs N=63 14 sec 3·10^6/s (S3-LEB)	^{116}Xe N=62 59 s 1.2 x 10^5/s	Te Z=52 ^{112}Te N= 60 2 min 3.4 x 10^5/s

Table VI... Same as previous table, for isotopes produced via S3-LEB or MNT techniques, with potential nuclear studies of charge densities ρ$_{ch}$ and of alpha cluster states in the neutron-rich isotopes.

Ni Z=28 refractive	^{68}Ni 29 s ^{70}Ni 6.0 s	^{72}Ni 1.57 s ^{74}Ni 0.68 s
S Z=16 ^{30}S 1.18 sec 2·10^8 /s (transfer)		Ar Z=18 ^{44}Ar 11.87 min ^{45}Ar 21.5 s >10^7/s (transfer) ^{46}Ar N= 28 8.4 s > 10^6/s ^{47}Ar 1.23s > ~5. 10^5/s ^{48}Ar 415 ms ~4. 10^4/s
Si Z=14 refractive	^{34}Si N=20 2.77 s	^{36}Si N= 22 0.45s ^{35}Si 780 ms

Table VI.1.C. Same as table VI.1A for isotopes of interest between Z=12 to 28 for which the production mode has to be determined to reach the needed intensities. Their lifetimes are long enough to a priori ensure the feasibility of the trapping technique.

Kr	^{74}Kr 11.5min > 1.5 10^6/s	^{76}Kr 14.8h > 4. 10^7/s	
Ar	^{44}Ar 11.87 min >10^6/s ^{45}Ar 21.5 s > 8. 10^5/s	^{46}Ar N= 28 8.4 s > 10^5/s	2pF par from (e,e) up to 2.5 fm^{-1} with I ~10^7
Mg Z=12	^{23}Mg 11.3 sec 2·10^8		
Ne Z=10	^{18}Ne 1.7 sec 1.7 x 10^7/s	^{19}Ne 17.3 sec 1.5 x 10^8/s	Form factors from (e,e) q ~0.5-3 fm^{-1} with I ~10^8
O Z=8	^{14}O 70 s 10^7/s	^{22}O 2.25 s ^{21}O 3.4 s ^{20}O 13.5 s ^{19}O 2.4 s Yields to be studied	
He Z=2	^{6}He 806 ms 2 x 10^8 /s (5 x 10^7)	^{8}He 119 ms 10^5 /s	

Table VI.1.D. Same as table VI.1A for the isotopes of Day-1 with SPIRAL1 production mode.

VI.3 Physical cases expansion: projected improvements

Improvements will be planned in various experimental axis:
-for (e,e) measurements, enlarging the range of nuclei, in particular to reach the isotopes produced at low intensity, or with small lifetimes at the limit of the feasibility for the ion trap techniques. Technical solutions have to be investigated to overcome the most complicated cases.
- for the **(e,e) and (e,e') scattering**, improving the detection system to make coincidence measurements to separate gs and excited contributions in the cases of high density levels (odd nuclei); this will be of particular interest for the measurement of the magnetic form factors from (e,e) from odd nuclei (**see I.1 and Appendix A**) To perform (e,e'p) measurement in order the study nucleon correlations, we need to reach the luminosity at 10^{29} (for heavy nuclei) up to 10$^{30-31}$ (for medium-light nuclei). It means that the ion trap techniques should be improved to handle ion beam size below 100 μm size with a specific R&D work, including all the physical effects which limit the size reduction of the ion beam cloud: ion heating, recirculation.

VI.4 Tentative budget and timeline for the facility and the experimental areas

Here, we do not include the cost for the RIB production building, which was already estimated in part *V.*3 around 100 M€ (for investment only, not taking the human resources)

We establish here a rough estimation, taking into account either the realistic numbers of similar facilities, accelerator machine and detection systems which exists, or the cost estimates done for the future machines including electron accelerator devices (e.g. ERL at PERLE or synchrotron-type device from the costs of element known from SOLEIL, cryomodules devices built for SPIRAL2) and experimental areas (estimates of the ELIse project at FAIR, DERICA at Dubna; spectrometer costs from MAMI, detection set-up, electronics and DAQ, costs from GANIL, VAMOS,..).This budget remains to be completed by the global estimate of the infrastructure costs due to the radioprotection safety issues.

We have integrated the whole costs from the machine, infrastructure, experimental areas (with the detection) and the human resources corresponding to the R&D project phase and to the operation during the exploitation phase of the machine, for the experiments. The details of the estimates can be found in *App. E*.

The total amount for the electron-ion collider machine is around 150 M€.

The human resources to be considered over the 12 years development represent at least 40 FTE (accelerator), 12 FTE (ion trap design and measurements), 8 FTE (spectrometer, mechanical integration, detections), 4 FTE (electronics, DAQ). The human resources for the conceptual and technical design phases as well as for the commissioning and for the realization starting phase will have to be carefully estimated at the beginning of the project, including both the engineer works and the crucial work of the technical teams in support of each operation during the integration phase for the machine. This has to be examined in details in the Technical Design Report.

VII. 1 Work plan 2021, key –questions (feasibility) to investigate in details

Our objectives are to carry out extensive electron-RIB studies to measure the structure form factors from electron-ion scattering. For the Day 1 experiments, the structure properties of the medium-heavy nuclei could be extracted from the measurements done at luminosities from 10^{24} to 10^{28}, which correspond to the potentially achievable performances of the future electron-ion collider machine.

As underlined in our March 2020 contribution, part of the crucial questions related to the technical difficulties are already identified and should be investigated quantitatively in a detailed project undertaken in the next years.

In summary, from the studies presented in this document:

-We started preliminary works on the ion trap characteristics and on the electron machine parameters, to know which typical dimensions could be attained. As discussed in *Sec.III.4*, this is a necessary input for the discussions of the electron-ion beam overlap, which rules the luminosity performances. The ion cloud sizes is one of the main constraints for the design of the electron-ion trap machine.

- We concluded that a **minimal electron beam intensity at 200 mA is requested**, and that the typical achievable dimension of the ion cloud is around **0.2 mm**. From these figures the goal of the luminosity of 10^{29} could attained, in principle (*cf III.4 and App.B)*.

- We have identified the technical issues of the electron accelerator project and of the ion trap (*III.5*);

- We obtained a first layout of the electron machine at 500 MeV, synchrotron or ERL (*cf III.5 and App.C)*.

- We discussed the feasible physics cases for radioactive ions with **lifetimes above 100 ms** (*cf VI.2*). Depending on the domain of the nuclear chart, we have identified the appropriate techniques of production (*part V*) insuring the requested intensities for the beams of interest.

However, to know if we can reach the 10^{29} luminosity in practice, we still need to solve various issues related to the ion trap and interaction region conditions. This requires phases of technical studies completed by benchmark of ion trap efficiency, which is also mandatory for the whole range of luminosities above 10^{28}.

We outline that, despite the fact that a synchrotron-type could be suitable for the electron machine, insuring to reach the intensity goal, we still need the comparison to the single –turn ERL possibility to compare both solutions and reach a final conclusion on the sets of optical beam parameters realistic for the future machine. This means having a dedicated study for the comparison, undertaken by two experts (one on synchrotron, the other on ERL) during a half-year full time for the project, to be started in 2021.

The main issues are related to the spatial charge distribution and confinement effects of the charge densities of the RIB and to the ways of reaching optical beam qualities enough to proceed to the collisions in a reduced vertex area.

We also need to identify potential paths of improvement for the increase up to 10^{30-31}. To overcome the limitations for the luminosity, we need to **work on the optimization of the ion trap techniques.**

Several paths of R&D are identified (see *III.4*) and would require dedicated works during a few years in collaboration with experts of the field to progress on the technical key questions: on beam instabilities, ion heating phenomena, ion charge state distribution with electron-ion beam interactions.

The project should examine in particular how to overcome the problems of the spatial charge effects of the plasma in the ion trapping area.

In parallel, we need to have **benchmark phases with an electron beam at high energy** (>few 100 MeV) and enough intensity (> few 10 mA) **to test an ion trap prototype**, to study the physical phenomena at play, and to measure the evolution of the number of trapped ions, depending on the beam stability conditions.

For the electron machines R&D studies, the main issues are related to the spatial charge distribution and confinement effects of the charge densities of the RIB and to the ways of reaching optical beam qualities enough to proceed to the collisions in a reduced vertex area.

To examine the technical issues of the e-RI project, it is mandatory to constitute a group of physicists and engineers experts of these questions, and to define a work plan between the technical divisions of IRFU and

IN2P3 with an international team of experts interested in the physics of the future project. Starting in 2021, the time scale would be:

i) one year for a team of two experts pushing forward the studies on the two options for the electron accelerator machine to define the achievable performances, finally selecting the best option for the physics requirements;
ii) In parallel one year to start the design study of the ion trap techniques and benchmark tests;
iii) 4-5 years for the conceptual design report,
iv) Construction phase to be ready for the e-RI physics in the years 2035.

If the whole project for the future of GANIL is launched in 2021, the detailed questions and preliminary studies related to the **design of production building** (*see V.3*) including radioprotection safety issues and technical constraints should be given in a complete project report which could be foreseen for the end of 2021.

For the momentum of the electron machine project we should start the phase of the detailed R&D as soon as possible in 2021, and constitute a task force of physicists and engineers devoting their time during one year to explore completely the technical issued and give final answer at the end of 2021.

The characteristics of the machine defined in *Section III* will be refined/optimized in the preliminary studies, which are planned to include some test calculations of the beam optics*,* with simultaneous considerations on the IBS constraints, for typical physical cases-a few selected radioactive ion beams. As outputs, more extensively in the global project phase in 2021, we would like to better quantify the feasibility in terms of luminosity and to figure out the quality of the possible measurements for the cross section observables.

VII. 2 International competitors and collaborators

The physicists of our community, gathered in the present proposal, are willing to develop physics cases for a future dedicated electron-RIB machine at GANIL for the years 2030s, exploiting the radioactive ion beams produced by the existing facility or by the next production scheme of RIBs (*the scenario of the RIB productions is discussed in the other contributions*). **The assets of the GANIL facility would be the local expertise existing in ion trap and all the purifying tools available at DESIR, as well as the required cryogenic infrastructures and the INB framework allowing continuous luminosity upgrades.**

All the main questions addressed in the field of exotic nuclei have been treated up to now by the most advanced accelerators and will be treated in the future with machines which are significantly ahead in the production of exotic nuclei: nowadays, RIKEN is at the forefront of the production of rare exotic nuclei, and with RIBF which started in 2007, it is a unique machine to delineate the neutron dripline. In 2019, at RIBF "the boundaries of nuclear chart have been updated for the first time in 20 years", with the newly established limit in the Ne isotopic chain, ^{34}Ne being the last bound isotope [*RIBF34Ne*], the previous limit was ^{24}O. The advances obtained by the current machines like RIBF is such that in the international context of the 2035s GANIL, as of today, will not be able to compete in the scientific field of the very neutron-rich exotic nuclei.

With the e-RI project, GANIL would still be in the run for a unique and exciting program: it would open a new era for nuclear physics with long-awaited structure studies of exotic nuclei by electron scattering gradually becoming accessible. Starting the project in the early 2020's would make GANIL **a world competitive machine with unique observables** in the scientific context of the years 2035, regardless of the evolution of the RIB machines around the world. Moreover this would be a very appealing machine project within the international community, in particular for physicists who proposed e-RI programs at their own facilities, but who have made the choice of different techniques. These programs based on ion beam-electron beam collisions were left aside or postponed due to the complexity to explore in parallel the expansion of their present facilities (GSI/FAIR, DERICA at Dubna), requiring already important resources.

At RIKEN, the SCRIT technical solutions was the most promising to develop an operational system for RIB but there are constraints which now require a higher level of R&D to increase the luminosity, and it is clear that their developments could be complementary to the ones we foresee for our project.

In 2015, the first attempt in France to envision a facility for e-RIB collisions was within the ETIC project proposed for the GANIL 2025 horizon.

Now, as presented in this document, the physicists gathered on the e–RIB physics has revisited this project to check the constraints and to identify the solutions allowing us to get rid of the limitations in terms of luminosity of the present SCRIT, and also to develop the ion trap able to confine at least 10^7/s ions.

We contacted physicists at GSI/FAIR, at TUD and at JINR Dubna who would be interested in joining an alternative European project with a shorter-term time scale, like the one we propose for the years 2030 at GANIL. We plan to involve them more deeply when the time comes for the detailed conceptual design for the electron accelerator and the detection devices.

In Japan, the physicists who developed SCRIT at RIKEN are in search of new technical solutions for their physics program. They would be interested in collaborating to the discussions on the ion trap techniques and the R&D program to improve the efficiency of trap would benefit from crossed expertise at RIKEN and at GANIL. In the long-term range if the Japanese physicists develop an upgrade of the SCRIT device, we would envision complementary studies on isotopic chains done by international collaborations at GANIL and at RIKEN, as done in the past for the successful studies of the Ca, Ni, stable isotopes, at the Stanford, MIT and at ALS Saclay (Orme).

VII. 3. National and International strategies

GANIL is the ideal place for the project, having a large variety of RI beams, already or soon available (SPIRAL1, Desir, S^3) or which could be delivered with the various modes of production foreseen in the possible projects explained by the other groups working on the plans at GANIL: photofission, Multi-nucleon transfer (MNT) reactions for heavy nuclei. The renewal of this project represents a new strategy for the nuclear physics at the international level. For the detailed project phase, we plan to gather the experts of the field, and possibly work hand in hand with them, by forming task force collaborations with the following groups:
- The *TU Darmstadt group* (*O. Boine-Frankenheim*) for the Electron beam machine studies and the questions of the intra-beam scattering phenomena;
- The *SCRIT group*, *T. Suda* (*RIKEN*) and *M. Wakasugi* (*Kyoto Univ.*), for the questions related to the trap confinement of ions in the electron beam;
- Groups working in Ion trap techniques at LPC Caen and CENBG, and also at *KU Leuven* (*T.E. Cocolios*).
- Groups working on electron spectrometer detection (like the ones working on hadronic physics at MAMI and at JLab), experts of the detection and spectrometer design for the (e,e') scattering.
At the national level the e-RI project for GANIL requires an official agreement at the highest level: from the research ministry, to ensure that the human resources, the R&D budget and the operating costs will be correctly dimensioned and allowed on a stable (sustainable) basis.
It should be underlined that for the periods of R&D and building of the projected facility both the size of the groups and the timescale of the project have to be sharply defined with a fixed period of roughly 10 years, to ensure that the community is gathered and focused on the common project, and that the teams designing the machine would also be in the first line to exploit the beams and make the starting experiments.
For the future operation, the request is also to extend the perimeter (human resources, regular budget) of the GANIL facility to include the needs for the RI production and for the e-RI facility, both for the operations of the accelerators and for the experimental areas.Taking into account all possible nuclei produced at GANIL, matching our requirement for luminosity (intensity for ions above 10^7/s) and purity (> 95 %) it will be possible to scan and determine the charge density for all these species.
We need to conclude on the various key questions outlined in the present document, in order to check the feasibility of the machine at the high luminosity (10^{29}).
In itself the project at luminosities 10^{27-29} is enough to justify the launching of the R&D for the future facility: it opens a new window on the nuclear structure with a direct access to the proton nuclear densities. Moreover for a range of heavy nuclei the (e,e) cross sections would be high enough to give access to the magnetic form factor – that is an access to the neutron form factor.

Physics cases will be enlarged gradually: production when the e-RIB machine rises, Day 1 experiments with the existing beams at GANIL/SPIRAL1 and 2, then there will be the Day2 experiments at higher luminosities and for heavy nuclei, following the progress of the new developed beams at GANIL. *Such a facility would thus offers to GANIL bright scientific perspectives for several decades.*

References

[*Ae91*] *B. Frois, C.N. Papanicolas, S.N. Williamson, Nucleon distributions and the nuclear many-body problem, pp. 352-391, in Modern Topics in Electron Scattering, B. Frois, I. Sick (Eds.), World Scientific Singapore (1991).*

[ALS80] Ph. Leconte et al., Nucl. Instr. Meth. 169, 401 (1980).

[ALSLec76] Ph. Leconte, Ph.D. thesis, Centre d'Etudes Nucléaires, Orsay, 1976.

[ALSNi75] I. Sick, *et al.*, Phys. Rev. Letters 35, 910 (1975).

[*ANDT87*] H. De Vries, C.W. De Jager, and C. De Vries, *Nuclear charge-density-distribution parameters from elastic electron scattering*, Atomic Data and Nuclear Data Tables **36**,495-536 (1987).

[*BA74*] R.C. Barrette, *Nuclear charge distributions*, Rep. Prog. Phys. **37** (1974) 1

[Bau2020] *A. Bauswein, N. Stergioulas, Spectral classification of gravitational-wave emission and equation of state constraints in binary neutron star mergers,* J. Phys. G: Nucl. Part. Phys. **46** 113002 (2019). *https://doi.org/10.1088/1361-6471/ab2b90*

[*Bec81*] IPNO_81_05, (Saclay, Orsay) EBIS workshop proceedings, 1981, p. 185.

[*Ca41m90*] H. Baghaei, *et al.,* Elastic Magnetic Electron Scattering from ^{41}Ca, Phys. Rev. C **42**, 2358 (1990)

[*ChRms*] B. A. Brown, *Mirror Charge Radii and the Neutron Equation of State,* Phys. Rev. Lett. **119**, 122502 (2017). *https://doi.org/10.1103/PhysRevLett.119.122502*

*P.-G. Reinhard and W. Nazarewicz, Nuclear charge and neutron radii and nuclear matter: Trend analysis in Skyrme density-functional-theory approach, PRC **93**, 051303 (2016). https://doi.org/10.1103/PhysRevC.93.051303*

[*Diffpp*] A. E. Feldman, J. J. Kelly, *et al., Neutron transition densities for 48Ca from proton scattering at 200 and 318 MeV,* Phys. Rev. C **49**, 2068 (1994) *and ref. therein.*

*32S(p, p') at 318 MeV: J. J. Kelly et al., Phys. Rev. C **44**, 1963 (1991). 30Si(p, p'), ibid. **41**, 2525 (1990).*

[*Don73*] T.W. Donnelly and J.D. Walecka, Nucl. Phys. **A201**, 81 (1973).

[*Don75*] T. W. Donnelly and J.D. Walecka, *Electron Scattering and Nuclear Structure,* Ann. Rev. Nucl. Part. Sci., 329-405 (1975). https://doi.org/10.1146/annurev.ns.25.120175.001553

[*Don84*] T.W. Donnelly and I. Sick, Rev. of Mod. Phys., **56**, No.3, 461 (1984).

[*Dubna18*] A.S. Fomichev, L.V. Grigorenko, S.A. Krupko, S.V. Stepantsov, G.M. Ter-Akopian, *The ACCULINNA-2 project: The physics case and technical challenges,* Eur. Phys. J. A **54**, 97 (2018) *doi: 10.1140/epja/i2018-12528-0.* DERICA *LoI: http://aculina.jinr.ru/pdf/DERICA/DERICA-for-ufn-11-en-resubmit.pdf*

[*Elise07*] H. Simon, *The ELISe experiment at FAIR*, Nucl. Phys. A**787**, 102 (2007). *https://doi.org/10.1016/j.nuclphysa.2006.12.020* ; *https://fair-center.eu/for-users/experiments/nustar/experiments/elise.html*

The ELISe project at FAIR, H. Simon (GSI FAIR) presentation on: *http://esnt.cea.fr/Phocea/file.php?class=page&file=58/HaikSimon_eRIB_Esnt16.pdf*

[*EIC2019*] "*Electron-Ion Collider User Group Meeting*" 22 -26 July, 2019 in Paris, co-organized by IN2P3/IPNO and CEA DPhN: *http://indico.in2p3.fr/event/EICUG2019*

[*eRIB17*] Toshimi Suda, Haik Simon, *Prospects for electron scattering on unstable, exotic nuclei,* Progress in Part. and Nucl. Phys. **96**, 1-31 (2017). *https://doi.org/10.1016/j.ppnp.2017.04.002*

[*ERIB2020*] Collaboration "electron-RIB for GANIL future", *Nuclear structure from electron-ion collisions, proposal n°9 submitted on March, 16th 2020 to the international scientific committee for Ganil future*: *https://indico.in2p3.fr/event/20534/contributions/81059/*

[**Erl14**] C. Mayes, IPAC2014, *http://accelconf.web.cern.ch/AccelConf/IPAC2014/talks/frxbb01_talk.pdf*

[**ESNT16**], 25-27 April 2016 *Electron-radioactive ion collisions: theoretical and experimental challenges* *http://esnt.cea.fr/Phocea/Page/index.php?id=58*

[**ETIC15**] *Electron-Trapped Ion Collider*, A. Chancé *et al.* (CEA Saclay), ETIC project within GANIL-2025 (2015). *A. Chancé (CEA, IRFU, SACM), presentation on:* *http://esnt.cea.fr/Phocea/file.php?class=page&file=58/Chance_electronEsnt16.pdf*

[**FO66**] T. de Forest and J.D. Walecka, *Advances in Physics*, **15** (1966) 1

[Fro83] B. Frois, *et al., A Precise Determination of the 3s Proton Orbit,* Nucl.Phys. A396, 409c (1983). https://doi.org/10.1016/0375-9474(83)90035-0

[*FroP87*] B. Frois, C. N. Papanicolas, *Electron Scattering and Nuclear Structure,* Ann. Rev. Nucl. Part. Sci. **37**, 133-176 (1987). *https://doi.org/10.1146/annurev.ns.37.120187.001025*

[GoBJ11] S. Goriely, A. Bauswein, H.-T. Janka, r-process nucleosynthesis in dynamically ejected matter of neutron star mergers, ApJL **738**, L32 (2011). *https://doi.org/10.1088/2041-8205/738/2/L32*

[GW2017] B. P. Abbott, et al., GW170817: Observation of Gravitational Waves from a Binary Neutron Star Inspiral, Phys. Rev. Lett. **119**, 161101 (2017). *https://doi.org/10.1103/PhysRevLett.119.161101*

[*Hel66*] R. H. Helm, *Inelastic and Elastic Scattering of 187 MeV Electrons from Selected Even-Even Nuclei,*

Phys Rev 104, 1466 (1966).

[*Hof53*] R. Hofstadter, H. R. Fechter, and J. A. McIntyre*, High-Energy Electron Scattering and Nuclear Structure Determinations,* Phys. Rev. **92**, 978 (1953). *https://doi.org/10.1103/PhysRev.92.978*

[*InelExp*] J. Heisenberg, *Nuclear Transition Density determination from inelastic electron scattering*, Adv. in Nucl. Phys. **12**, 61 (1981) ; Bazantay, *et al.*, Phys. Rev. Lett. **54**, 7 (1985);
B. Frois et al., Phys. Lett. B **122**, 347 (1983).

[*LRP2017*] *NuPECC Long Range Plan 2017 Perspectives in Nuclear Physics, p118.*
http://www.esf.org/fileadmin/user_upload/esf/Nupecc-LRP2017.pdf

[*LumT*] A. Wu Chao, K.H. Mess, M. Tigner and F. Zimmermann, *Handbook of Accelerator Physics and Engineering, Eds.* World Scientific (2013) *https://doi.org/10.1142/8543*

[*Mami98*] K.I Blomqvist et al., *The three-spectrometer facility at the Mainz microtron MAMI,*
Nucl. Instr. and Meth. A, 403 (1998) 263-301 *https://doi.org/10.1016/S0168-9002(97)01133-9*

[*Mou80*] J. Mougey *et al.,* Nucl. Phys. A **335**, 35 (1980).

[Mue07] P. Mueller *et al.*, *Phys. Rev. Lett.* **99** 252501 (2007).

[*NIK98*] D. J. J. de Lange et al., *The optical properties of the BigBite spectrometer at NIKHEF,*
NIM **412**, 254-264 (1998). *https://doi.org/10.1016/S0168-9002(98)00476-8*

[**NimERL19**] A Khan, O Boine-Frankenheim, F Hug, C Stoll, *Beam matching with space charge in energy recovery linacs,*
Nucl. Instr. Methods in Phys. Res. A **948**, 162822 (2019) *https://doi.org/10.1016/j.nima.2019.162822*

[*PERLE18cdr*] *PERLE. Powerful energy recovery linac for experiments. Conceptual design report,*
J. Phys. G: Nucl. Part. Phys. 45 (2018) 065003. DOI: https://doi.org/10.1088/1361-6471/aaa171

[Pha88] X.H. Phan et al., Electron scattering studies of the ground state rotational band of 152Sm,
Phys. Rev. C 38, 1173 (1988).

[PRC82TiSr] S. Platchkov *et al.*, Phys. Rev. C **25**, 2318 (1982)

[*Pb208ex*] D. Goutte, J. B. Bellicard, J. M. Cavedon, B. Frois, M. Huet, P. Leconte, Phan Xuan Ho, and S. Platchkov, J . Heisenberg, J. Lichtenstadt and C. N. Papanicolas, I. Sick, *Determination of the Transition Charge Density of the Octupole Vibration in 208Pb,* Phys. Rev. Lett. **45**, 1618 (1980)

[projE] 4GLS: CDR 2006.
BERLinPro: J.Knobloch et al.,IPAC2012, *http://accelconf.web.cern.ch/accelconf/ipac2012/papers/moppp015.pdf*
eRHIC11: D. Kayran et al., RHIC & AGS Annual Users' Meeting (2011)
LHeC12: LHeC-Note-2012-002 GEN (2012), *http://arxiv.org/pdf/1206.2913v2.pdf*

[RIBF34Ne] D. S. Ahn, N. Fukuda *et al.*, *Location of the Neutron Dripline at Fluorine and Neon*,
Phys. Rev. Lett. **123**, 212501 (2019). *https://doi.org/10.1103/PhysRevLett.123.212501*

[*SCMF03*] M. Bender, P.-H. Heenen, P.G. Reinhard, *Self-consistent mean-field models for nuclear structure, Rev. Mod. Phys. 75, 121 (2003). https://doi.org/10.1103/RevModPhys.75.121*

[*Scrit04*] *M. Wakasugi, T. Suda, and Y. Yano, A new method for electron-scattering experiments using a self-confining radioactive ion target in an electron storage ring,*
*Nucl. Instrum. Methods Phys. Res., Sect. A **532**, 216 (2004). https://doi.org/10.1016/j.nima.2004.06.047*

[*Scrit05*] T. Suda, M. Wakasugi, *Structure studies of unstable nuclei by electron scattering (Review)*,
Prog. Part. Nucl. Phys. **55,** 417 (2005). *https://doi.org/10.1016/j.ppnp.2005.01.008*

[*Scrit09*] M. Wakasugi *et al.*, *Novel Internal Target for Electron Scattering off Unstable Nuclei,*
Phys. Rev. Lett. 100, 164801 (2008). https://doi.org/10.1103/PhysRevLett.100.164801
T. Suda *et al.*, *First Demonstration of Electron Scattering Using a Novel Target Developed for Short-Lived Nuclei,* Phys. Rev. Lett. **102,** 102501 (2009). *https://doi.org/10.1103/PhysRevLett.102.102501*

[*Scrit16w*] The SCRIT facility at RIKEN, M. Wakasugi (RIKEN, Kyoto Univ.) presentation on
http://esnt.cea.fr/Phocea/file.php?class=page&file=58/Wakasugi_electronEsnt16.pdf

[*Scrit17*] K.Tsukada *et al.*, *First Elastic Electron Scattering from ^{132}Xe at the SCRIT facility*,
Phys. Rev. Lett. **118,** 262501 (2017). *doi: 10.1103/PhysRevLett.118.262501*

[**scriTAC05**] *https://ribf.riken.jp/RIBF-TAC05/14_SCRIT.pdf*

[*Sick74*] Ingo Sick, "*Model-independent nuclear charge densities from elastic electron Scattering*",
Nucl. Phys. **A218,** 509-541 (1974). *https://doi.org/10.1016/0375-9474(74)90039-6*

[sp2beams] The GANIL web site for the beam intensities: https://u.ganil-spiral2.eu/chartbeams/

[*SP2dr12*] Document stratégie scientifique GANIL/SPIRAL2 DIR-005-A19/12/2012 by the deputy head for the scientific coordination of SPIRAL2 (H. Savajols) and the Ganil Deputy director (M. Lewitowicz).

[*SP2dr15*] Une vision d'avenir pour l'installation de recherché GANIL – SPIRAL 2, GANIL 2025, GANIL internal report, 2015, H. Savajols and M.Lewitowicz.

[sp2Gan] P. Delahaye et al., *GANIL-SPIRAL2 as a Multifaceted Radioactive Ion Beam Facility*,
https://indico.in2p3.fr/event/20534/contributions/81850/

[sp7RFQ] C. Theisen *et al.*, *RFQ injector A/Q = 7 for the production of exotic nuclei using fusion-evaporation and multinucleon transfer reactions, https://indico.in2p3.fr/event/20534/contributions/81871/*

[spActar] ACTAR Active Target https://www.ganil-spiral2.eu/scientists/ganil-spiral-2-facilities/instrumentation/actar/

[specG] H. Savajols, VAMOS collaboration, *VAMOS: A VAriable MOde high acceptance spectrometer for identifying reaction products induced by SPIRAL beams,*
Nucl. Instrum. Meth. B **204**, 146 (2003). *https://doi.org/10.1016/S0168-583X(02)01908-0*

[*specR*] T. Kobayashi, N. Chiga, T. Isobe, Y. Kondo, T. Kubo, K. Kusaka, T. Motobayashi, T. Nakamura, J. Ohnishi, H. Okuno, H. Otsu, T. Sako, H. Sato, Y. Shimizu, K. Sekiguchi, K. Takahashi, R. Tanaka, K. Yoneda, *SAMURAI spectrometer for RI beam experiments*, Nucl. Instrum. Meth. B **317**, 294 (2013). *http://dx.doi.org/10.1016/j.nimb.2013.05.089*

[*specS3*] R. Ferrer, B. Bastin, D. Boilley, P. Creemers, P. Delahaye, E. Liénard, X. Fléchard, S. Franchoo, L. Ghys, M. Huyse, Y. Kudryavtsev, N. Lecesne, *et al., In gas laser ionization and spectroscopy experiments at the Superconducting Separator Spectrometer (S3): Conceptual studies and preliminary design,* Nucl. Instrum. Meth. B **317** (2013) 570.

[*spes08*] A. Andrighetto *et al.*, *The SPES multi-foil direct target*, Nucl. Instrum. Meth. B **266,** 4257 (2008).

[*spFa17*] The FAZIA collaboration, *Isotopic identification using Pulse Shape Analysis of current signals from silicon detectors: Recent results from the FAZIA collaboration,*
 Nucl. Instrum. Meth. B **860**, 42 (2017). *https://doi.org/10.1016/j.nima.2017.01.048*

[*spGrit18*] M. Assié, A. Matta, B. Le Crom, M. Chabot, D. Mengoni, D. Beaumel, Y. Blumenfeld, J.-J. Dormard, B. Genolini, F. Hammache, J. Guillot, A. Jallat, E. Rauly, N. de Séréville, D. Suzuki, *New methods to identify low energy 3He with Silicon-based detectors,* Nucl. Instrum. Meth. B **908**, 250 (2018).   *https://doi.org/10.1016/j.nima.2018.08.050*

 [*spnu4*] *Issues discussed in the presentation given in the Nuclear physics and nuclear astrophysics Town Hall Meeting accessible here:* https://indico.in2p3.fr/event/19748/contributions/78693/

[spnu5] S. Tusseau-Nenez et al., Characterization of uranium carbide target materials to produce neutron-rich radioactive beams, Nucl. Instrum. Meth. B **370** (2016) 19

[spnu6] J. P. Ramos, Thick solid targets for the production and online release of radioisotopes: The importance of the material characteristics – A review, Nucl. Instrum. Meth. B, **463** (2020) 201

[spnu7] Y. Hirayama, Y.X. Watanabe, M. Mukai, M. Oyaizu, M. Ahmed, H. Ishiyama, S.C. Jeong, Y. Kakiguchi, S. Kimura, J.Y. Moon, J.H. Park, P. Schury, M. Wada, H. Miyatake, *Doughnut-shaped gas cell for KEK Isotope Separation System*, Nucl. Instrum. Meth. B **412** (2017) 11.

[spnu8] G. Savard, M. Brodeur, J.A. Clark, R.A. Knaack, A.A. Valverde, *The N = 126 factory: A new facility to produce very heavy neutron-rich isotopes*, Nucl. Instrum. Meth. B **463** (2020) 258.

[spnu9] M.-G. Saint-Laurent, A. Pichard, G. Lhersonneau, F. de Oliveira Santos, F. Pellemoine, P. Delahaye, M. Fadil, H. Frånberg, R. Leroy, L. Serani, P. Alfaurt, C.-E. Demonchy, A. Fournier, M. Hass , T. Hirsh, T. Stora , R. Hodak and the GANISOL group, *Comparison of expected yields for light radioactive beams at SPIRAL-1 and 2,* AIP Conf. Proc. 1224 (2010) 482.

[spUcx] M. Fadil, *Taux de production dans la cible UCx à basse densité pour une puissance du courant de deuton de 50 kW*, internal GANIL note SP2_NT_I-021053_v1.0.

[**Th132Xe]** P. Arthuis, C. Barbieri, M. Vorabbi, P. Finelli, *Ab initio computation of charge densities for Sn and Xe isotopes,* https://arxiv.org/abs/2002.02214

[**TheRI08**] X. Roca-Maza, M. Centelles, F. Salvat, and X. Viñas, *Theoretical study of elastic electron scattering off stable and exotic nuclei,* Phys. Rev. C **78**, 044332 (2008). *https://doi.org/10.1103/PhysRevC.78.044332*

[**Th34Siab**] T. Duguet, V. Somà, S. Lecluse, C. Barbieri, and P. Navrátil, *Ab initio calculation of the potential bubble nucleus 34Si, Phys. Rev. C* **95**, *034319 (2017).* *https://doi.org/10.1103/PhysRevC.95.034319*

 [**Theo34Si**] M. Grasso et al., *Nuclear "bubble" structure in 34Si,*
Phys. Rev. C **79**, 034318 (2009). *https://doi.org/10.1103/PhysRevC.79.034318*

J.-M. Yao, S. Baroni, M. Bender, and P.-H. Heenen, *Beyond-mean-field study of the possible "bubble" structure of 34Si*, Phys. Rev. C **86**, 014310 (2012). *https://doi.org/10.1103/PhysRevC.86.014310*

 [**TheoLRC09**] C. Barbieri, *Role of long-range correlations in the quenching of spectroscopic factors,*
Phys. Rev. Lett. **103**, 202502 (2009). *https://doi.org/10.1103/PhysRevLett.103.202502*

C. Barbieri and W.H. Dickhoff, Int. Jour. Mod. Phys. A **24**, 2060 (2009).

 [**TheoNS11**] X. Roca-Maza, M. Centelles, X. Viñas, and M. Warda, *Neutron Skin of ²⁰⁸Pb, Nuclear Symmetry Energy, and the Parity Radius Experiment,* Phys. Rev. Lett. **106**, 252501 (2011). *https://doi.org/10.1103/PhysRevLett.106.252501*

[**Wan04**] L.-B. Wang et al., *Phys. Rev. Lett.* **93** 142501 (2004).

[**WARPweb**] *https://sites.google.com/a/lbl.gov/warp/home*

GLOSSARY

BBU beam break-up instabilities	ERL Energy Recovery Linac
IBS intra beam scattering	
IP Interaction Point	MNT Multi Nucleon Transfer

Appendix A. Electron-ion Kinematics and cross sections, detection systems

Elastic (e,e)

In the regime below 200 MeV, it has been possible to extract the main parameters of the charge densities for a selection of even-even nuclei, see for instance for ^{24}Mg, ^{28}Si, ^{32}S, ^{40}Ar and ^{88}Sr, at 187 MeV in Ref. [*Hel66*]. However, to obtain the form factor in an extended range and access to the densities inside the nuclear interior (below 2-3 fm) the incident energies have to be increased.

For instance, before the experiment done at the Saclay ALS [*ALSLec76, ALSNi75*] it was not possible to extract unambiguously the charge densities for ^{58}Ni, due to the lack of high transfer data, above 3 fm^{-1}. With the data set at 500 MeV, with the higher momentum reached at 3.9 fm^{-1}, it was possible to obtain the charge densities at small radii (see figure below). Note that in this experiment, the limitation to q ~3.9 fm^{-1} lies in the small counting rates for the cross sections below 8x 10^{-38} cm^{2}" (*down to 8. 10^{-11} mb/sr*). **This corresponded to a mean counting rate of one event every 6 hours for an incident current of 25 µA.** At this rate, no background noise appears above the elastic peak nor between the first excited state and the ground state.

FIG. 2. The full curve represents the error band for the experimental ^{58}Ni charge density, the dashed and dotted curves correspond to the theoretical HF densities. The density-dependent HF calculations of Ref. 21 include pairing for the neutrons above the $1f_{7/2}$ shell.

Charge density distibutions obtained from the measurement of the form factor of 58Ni using 58Ni(e,e) cross section at 449.5 MEV for q range between 0.5 to 3.9 fm^{-1} [*ALSNi75*].

Data from the experiment done at the ALS (accélérateur linéaire de Saclay) reported in Refs. [*ALSLec76, ALSNi75*].

INELASTIC (e,e')

*Excitation energy spectra from electron elastic and inelastic scattering on [49]Ti [**PRC82TiSr**], for the extraction of F_T form factor and of the valence nucleon densities. Magnetic electron scattering and valence nucleon radial wave functions were extracted also for [51]V, [59]Co, [87]Sr, [93]Nb, [209]Bi in the same studies, combining results of experiments done between 175 and 325 MeV (theta between 0 and 155 deg.) and at 500 MeV (angles between 39 and 73 deg).*

"The lowest cross section measured in this experiment was 2.17 X 10^{-37} cm²/sr, which corresponds to three counts in the elastic peak without any background." [**PRC82TiSr**].

[PRC82TiSr]

Fig 3 [**Scrit17**] from SCRIT measurements in the years 2015 of 132Xe(e,e').

Comparison of the spectra obtained at 150, 201 and 301 MeV.
« *At Ee = 301 MeV, the enhanced tail suggests some inelastic processes. In the high-momentum transfer region (0.9–1.4 fm^{-1}), the magnitude of elastic scattering diminishes and inelastic scattering processes (such as the giant dipole resonance) gain prominence.* »

Inelastic (e,e') at 500 MeV

---

*Electron scattering studies of the ground state rotational band of ^{152}Sm [**Pha88**].*
""The data were collected in the HE1 experimental hall at the Saclay electron linac. Scattered electrons were analysed using the SP900 magnetic spectrometer.… capable of measuring very small cross sections (as low as 7 10^{-36} cm^2 /sr for the ^{152}Sm 6+ state.".
"" the results of high momentum transfer electron scattering experiments in which cross sections for the first four states (0$^+$, 2$^+$, 4$^+$, 6$^+$) of the ground state rotational band of ^{152}Sm were obtained. These measurements extended the q range of the existing data sufficiently to permit the charge and transition charge densities to be determined precisely and unambiguously throughout the nuclear volume. "
The transition charge densities for 0$^+$, 2$^+$, 4$^+$, 6$^+$ can be directly compared with a triaxial DD HFB calculation.

152Sm 0+ gs
2+
4+
6+
3-
momentum resolution
 typically $\Delta E/E = 1\ 10^{-4}$
incident energies 251 MeV ; 500 MeV range of scattering angles, 0, corresponding to effective momentum transfers 0.6 < qeff < 2.9 fm^{-1}."
beam current varied from 5 to 15 μA
20 and 52 mg/cm thick targets were enriched to 98.3% 152Sm

FIG. 3. Measured form factors for elastic ($\lambda=0$) and inelastic ($\lambda=2$, 4, and 6) electron scattering from the ground state rotational band of ^{152}Sm. The solid curves are based on a fit to these data using Fourier-Bessel expansions for the nuclear charge densities.

*Figures extracted from [**Pha88**].*

47
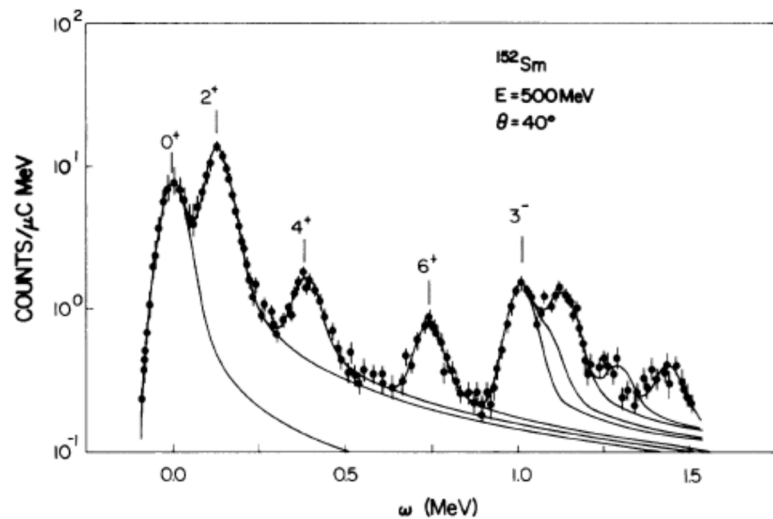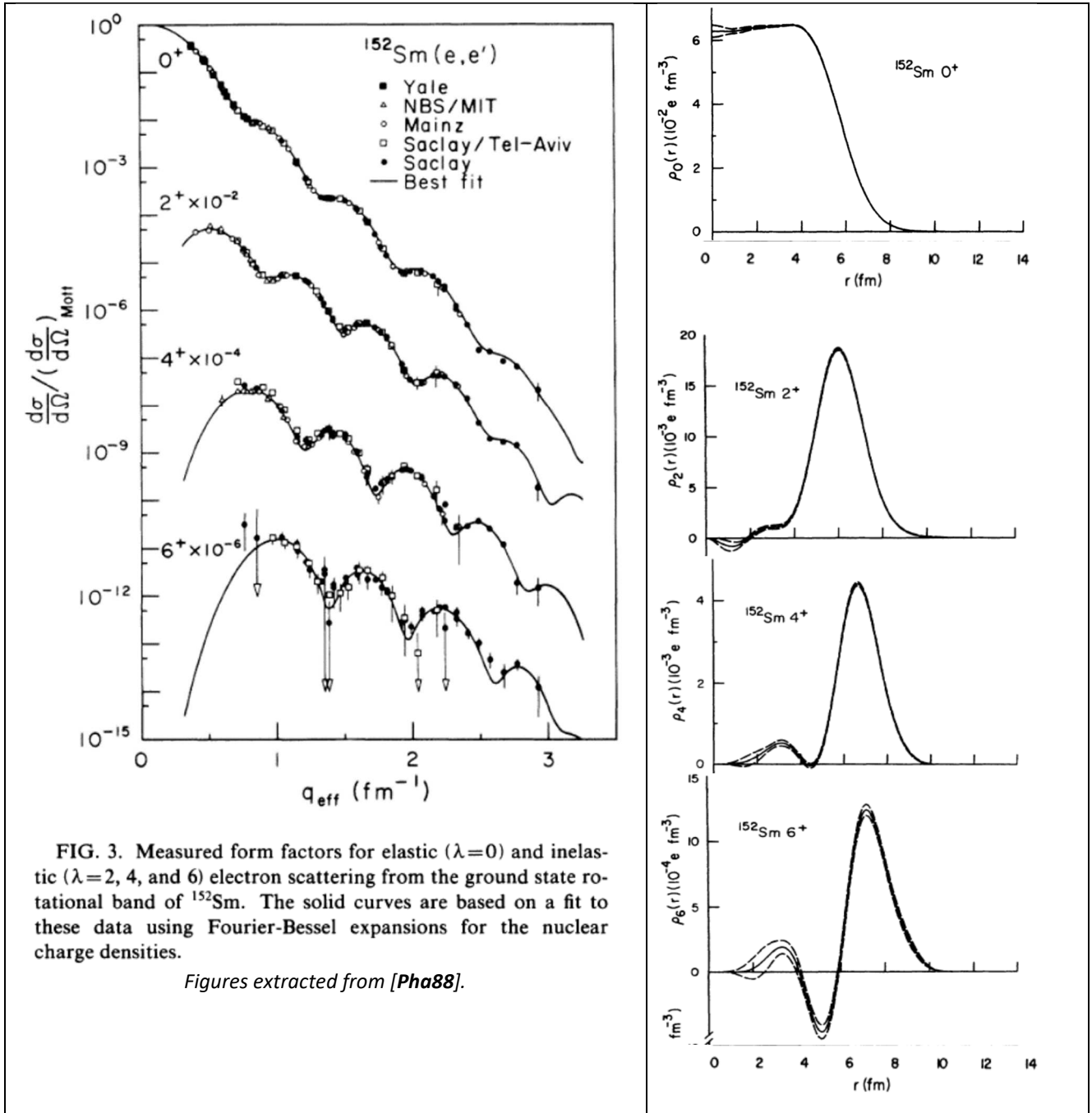
(e,e'p) measurements

Spectroscopic strength of ^{15}N obtained from ^{16}O(e,e'p) [Mou80].
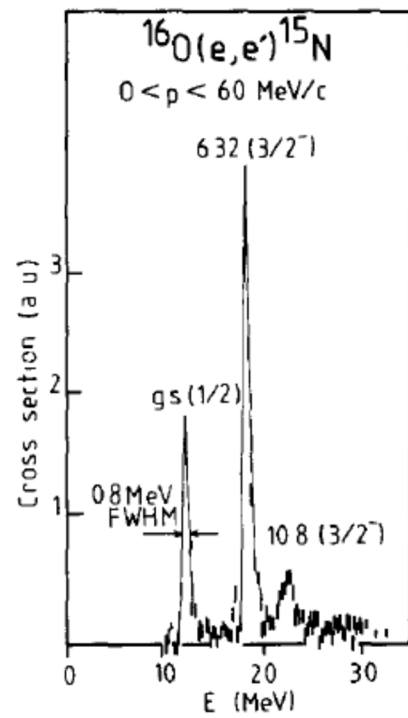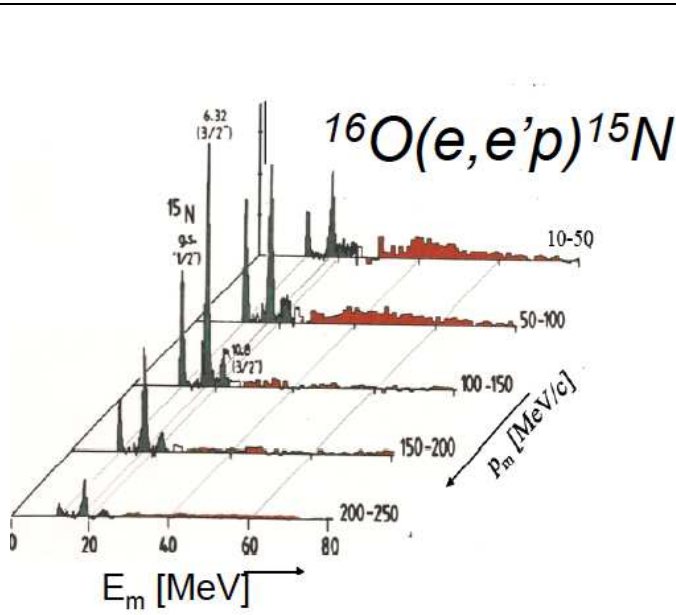
$^{16}O(e,e'p)^{15}N$

Fig 16 Missing energy resolution in the ^{16}O(e, e'p)^{15}N reaction [ALS80]

Appendix B. Simulations of ion trap performances for the luminosities

Maximal ion capacities for the luminosities

Simulations of the ion trap capacities have been performed using the code WARP [WARPweb]. The trap design is assumed to be a cylindrical box with axial symmetry along the electron beam axis. A set of three electrodes is defined (see Fig. B.1): two external electrodes assuring confinement in the longitudinal direction and one electrode in the middle slowing injected ions down to a few eV of longitudinal energy. One of the two external electrodes can be switched on and off allowing the injection of the ion beam into the trapping region.

Figure B.1. Typical setup of an ion trapping simulation with WARP. The colored areas denote the electrode fields. The potential of the leftmost electrode is initially at zero and then increased to its nominal value after all ions have reached the trapping area.
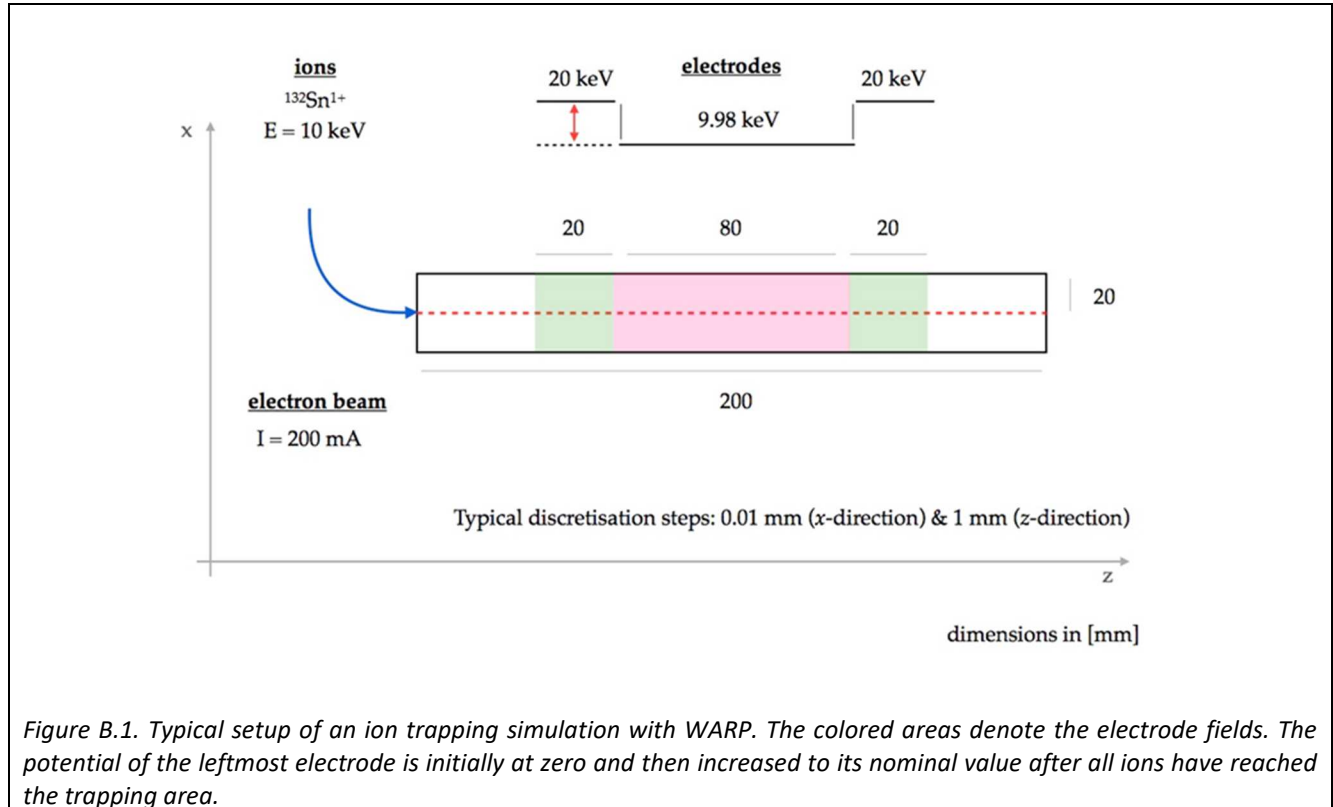
The type of ion beam, charge state, initial velocity, beam size, bunching etc. are parameters of the calculations. The electron beam is modelled with analytical expressions, under the assumptions of a Gaussian and continuous beam. Given that the ions should not be sensitive to high frequency variations of the electric field, this analytical model should be sufficiently accurate in the present case. Simulations are performed over typical times of 0.5-1 ms. At around 0.2-0.3 ms the ion cloud settles in some equilibrium configuration (in terms of number of ions and their spatial distribution). At each time step, the full 3D distribution can be printed out. Typical integrated information on the ion cloud (at a given time step) include i) the total number of ions in the simulation box, ii) the number of ions in the overlap region and iii) the rms radius of the ion distribution. For a given number of injected ions, the final number of trapped ions depends on the injection radius, the size and intensity of the electron beam. Several parameters were tested.

Below we illustrate some typical results, focusing on three points: the maximum number of trapped ions (saturation phenomenon), the overlap between the electron beam and the ion cloud and the effect of higher charge states. All the simulations shown here were carried out for a trap length of 10 cm and with ^{132}Sn ions. (Other isotopes were tested and gave qualitatively similar results.) In **Fig. B.2** the number of trapped overlapping ions and the rms size of the corresponding ion cloud are shown as a function of time for different values of injected ions. One observes a saturation of the number of ions that can be trapped at around 3×10^8 ions. This is close to the maximal theoretical value deduced assuming full charge compensation between ions and electrons (4×10^8).

In **Fig. B.3** the evolution of the number of trapped ions is studied varying the rms size of the initial ion beam. As expected, more and more ions are lost as their initial size increases and departs from the size of the electron beam. Nevertheless, some reasonable fraction of the initial ions ends up being captured in the section of the electron beam. In the right panel one sees how the rms size of the ion cloud eventually evolves towards the radius of the electron beam. From these results we conclude that, even starting with unfavourable initial conditions (ion size 10 times larger than electron size) a good fraction of ions can be trapped and overlap with the electrons.
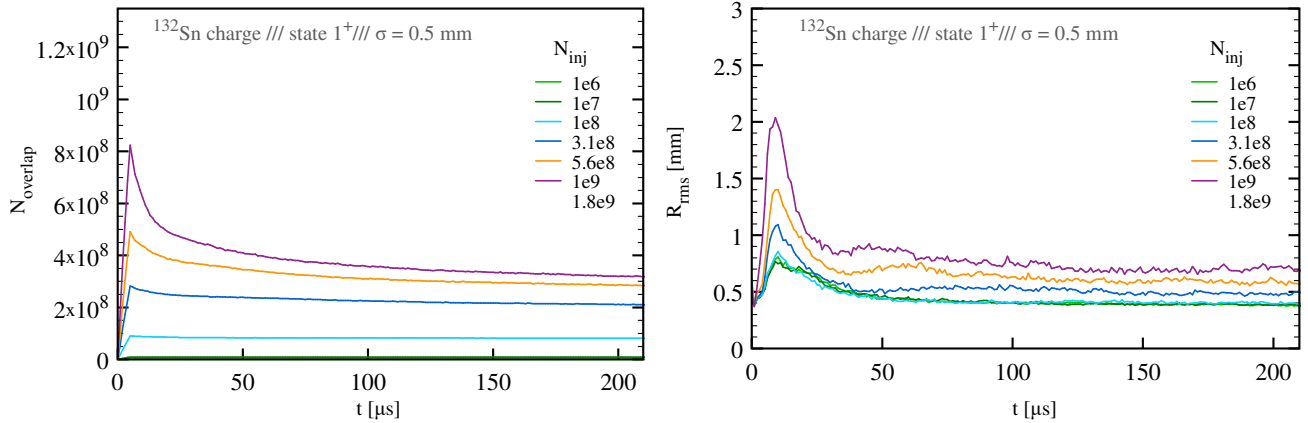
Figure B.2. (Left) Number of ions overlapping with the electron beam as a function of time, for different numbers of injected ions. (Right) Rms radius of the ion cloud as a function of time, for different numbers of injected ions. The grey area represents the region of the electron beam. Simulations were carried out for $^{132}Sn^{1+}$ ions and electron and ion beams having a rms radius of 0.5 mm.
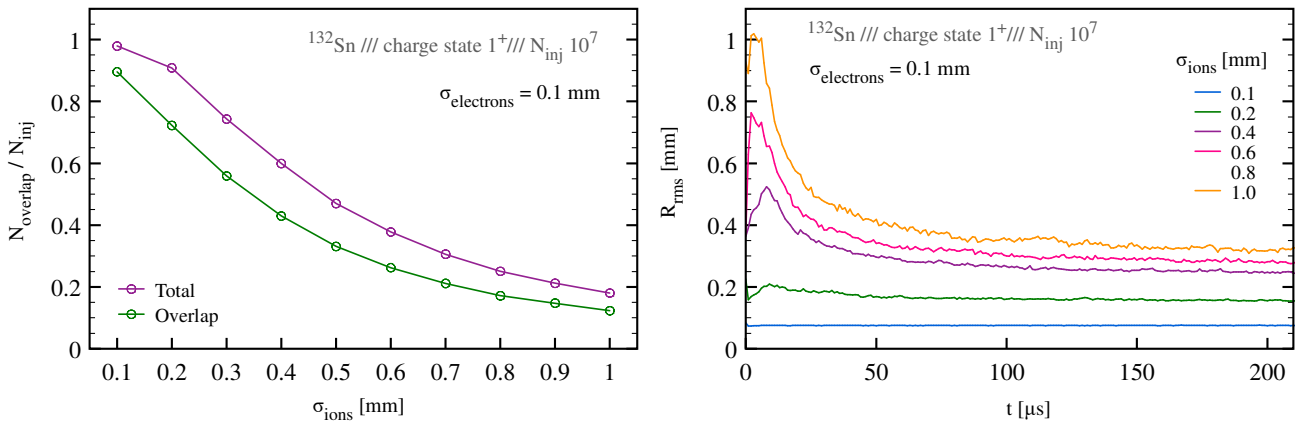
Figure B.3. (Left) Total number of ions and number of ions overlapping with the electron beam as a function of the initial size of the ion beam. (Right) Corresponding rms radius of the ion cloud.
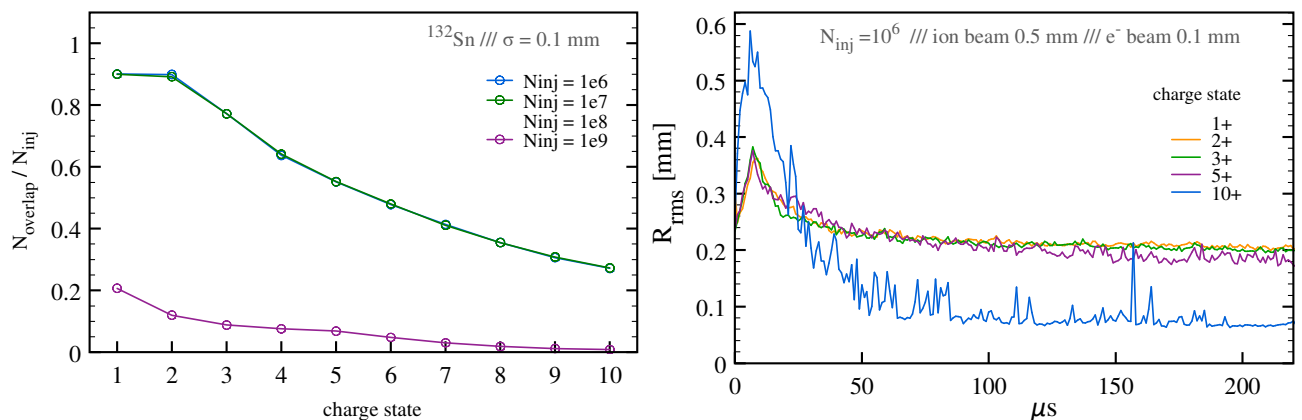
Figure B.4. (Left) Number of ions overlapping with the electron beam as a function of the ion charge state. (Right) Rms radius of the ion cloud for different charge states.

Finally, the effect of ion charge states higher than 1+ was examined. In Fig. B.4 the evolution of the number of trapped ions as a function of their charge state is studied. We conclude that, up to 10^8 injected ions, no degradation of the trapping properties is observed, with about $2\ 10^7$ 10+ ions at equilibrium (cf. $4\ 10^7$ maximal theoretical limit). Further, by looking at the radial distribution one observes how higher charge states tend to concentrate closer to the electron beam, as expected, especially when the ions initially have a larger radial size. Notice that in the preliminary simulations performed so far, the charge state is not evolved with time but determined at the injection. Therefore, the number of trapped ions can be viewed a conservative estimate (given that a large number of them evaporates during the simulated injection).

In conclusion, no showstopper has been identified from the present simulations. In all the considered trap conditions, the number of ions overlapping with the electron beam is close (at most a factor 2) to the theoretical limit inferred from full charge compensation. This is encouraging and supports the luminosity estimates of ***Table III.4***.

In the future, more refined simulations are required with several possible paths for improvement:
- the injection process can be better modelled (ion bunches, different injection times, sizes, position, energy spread…);
- a more realistic electric field could be envisaged for the electron beam (checking also the possible differences of this field in the case of the synchrotron or ERL solutions);
- the effect of ion heating (due to electron collisions) should be included;
- the limitations of the radial trapping have to be well understood taking into account ion-ion Coulomb interactions, and ionisation to different charge states (the latter should be introduced dynamically in the course of the simulation).

Appendix C. Possible design of the electron synchrotron

The choice of the parameters for the potential solutions of the electron-ion collider machine was discussed in section III. Here we present a possible design of the electron synchrotron corresponding to the parameters sets presented in Table III.5.

The layout is made of 6 sections, each one with:
- A straight section of 5 m
- 2 matching sections
- 2 dispersion suppressors
- 4 cells with a dipole with gradient and 2 quadrupoles.

MAGNETS

Type	Number	Length [m]	Max Field
Dipole 1	12	0.29	1 T, −9.26 T/m
Dipole 2	24	0.29	1 T, −10.5 T/m
Quadrupole 1	48	0.2	45.7 T/m
Quadrupole 2	60	0.12	17.9 T/m
Sextupole	90	0.15	1244 T m^{-1}

Layout
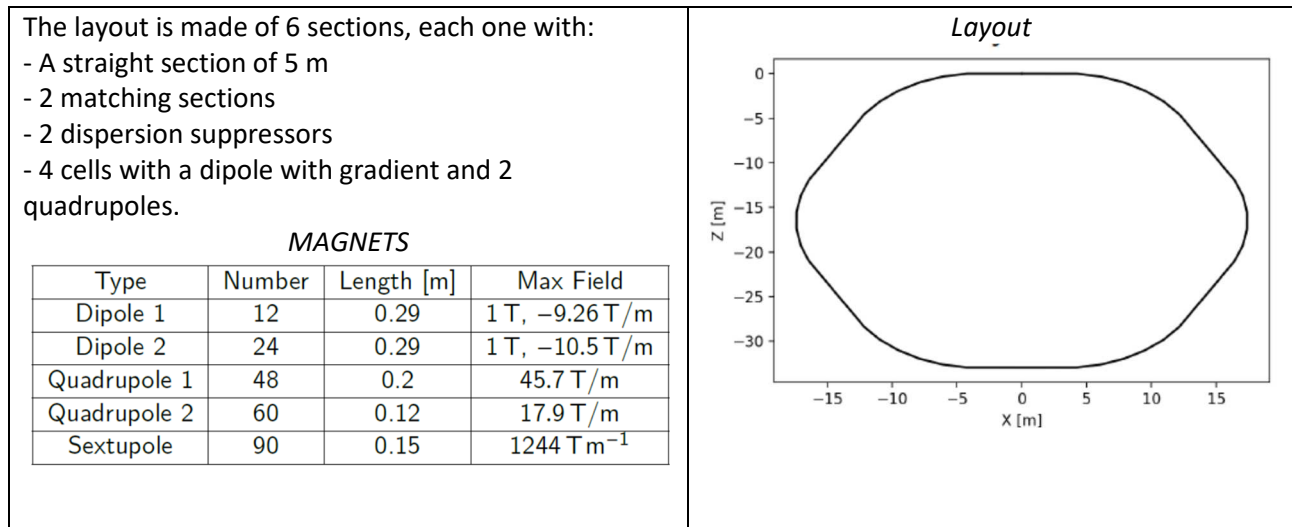
The equilibrium emittance and damping time (synchrotron radiation) only depend on the ring optics.
The bunch length σ_z is deduced from σ_E and from the RF voltage.
The Touschek lifetime (momentum transfer in the longitudinal plane, losses because of large Coulomb collision angles) Tl is a non-linear and complex function.
It is inversely proportional to the beam current.
It increases with the RF acceptance, beam energy, and beam sizes.
The RF acceptance increases with the RF voltage (depends on the optics).
The IBS is also a non-linear function.
 The lifetime (should be large) decreases with the beam current.
 It increases with energy, emittance, bunch length, energy spread.

(On the curves below, the point are for the values corresponding to the electron beam energy of 500 MeV).

Dependence with beam energy

The optimum beam quality is at 700 MeV.
The lifetime is also minimum (smaller beam size) but is still manageable.
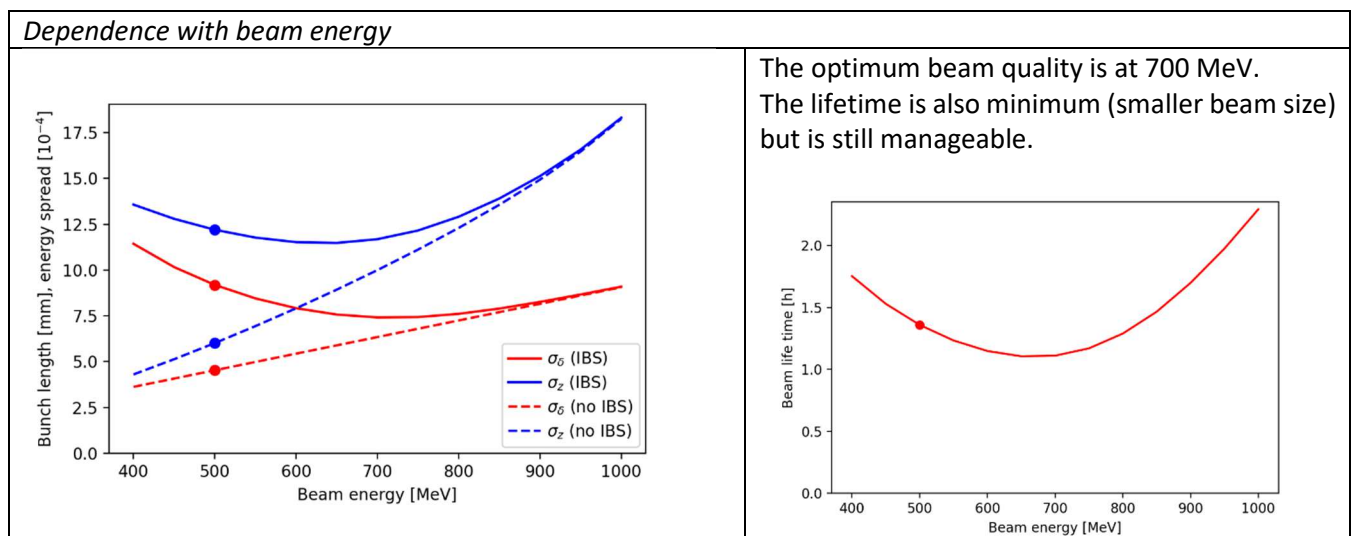
Dependence with beam current
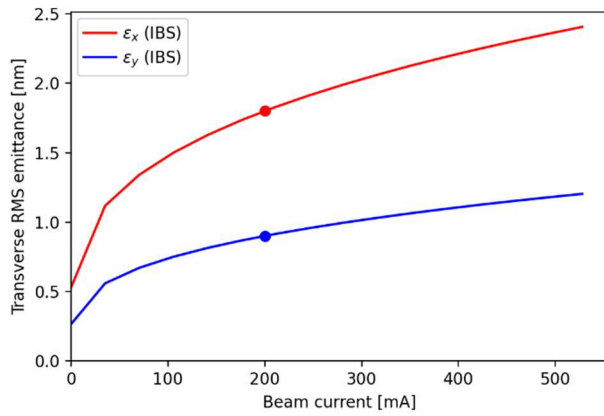
The beam emittance significantly increases with beam current. Beam lifetime dramatically decreases also.
Reaching 500 mA has a cost on beam quality.
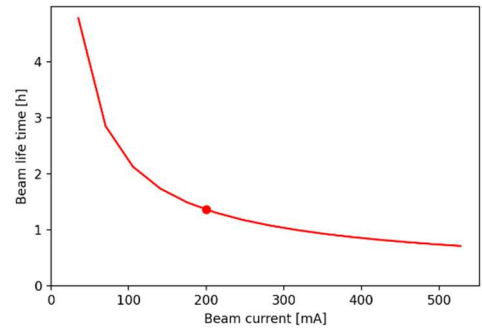
Dependence with coupling factor
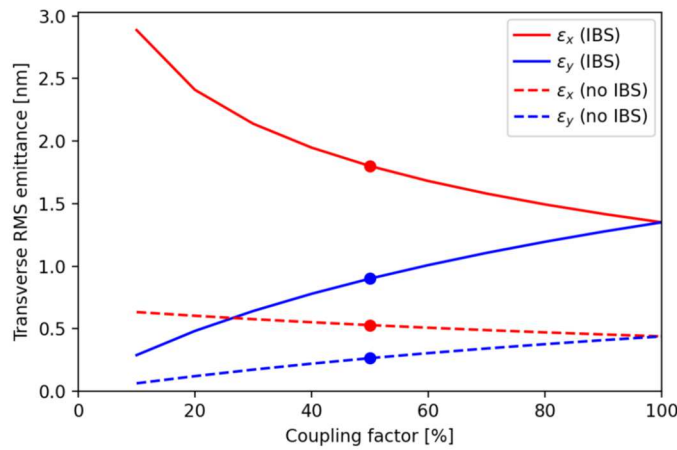
With no coupling, IBS is a big issue.
We need to couple both planes. It can be done by different ways:
- Strong coupling with a dedicated section.
-Exciting the resonance $\nu_x - \nu_y$
(enables to use weak skew quadrupoles).
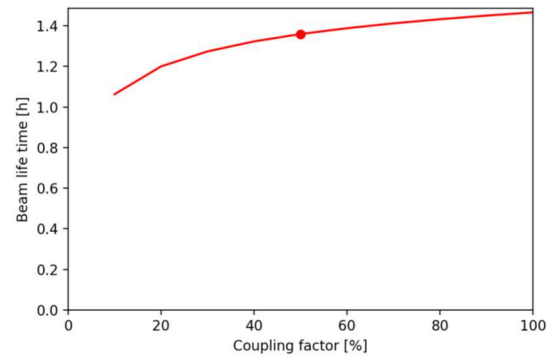
Twiss functions (1/6)

Beam sizes with IBS	
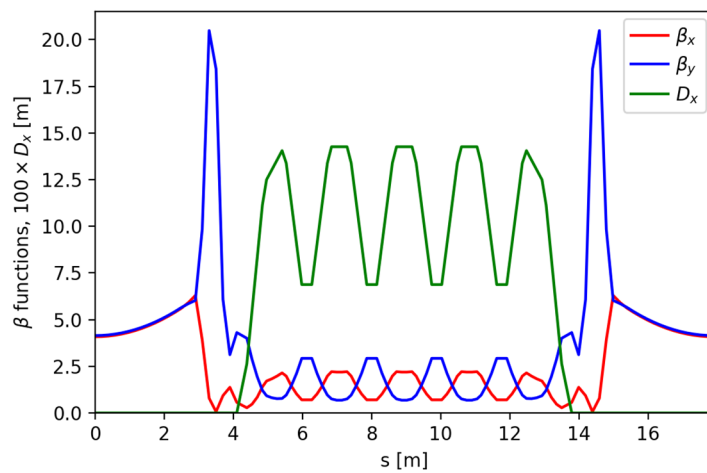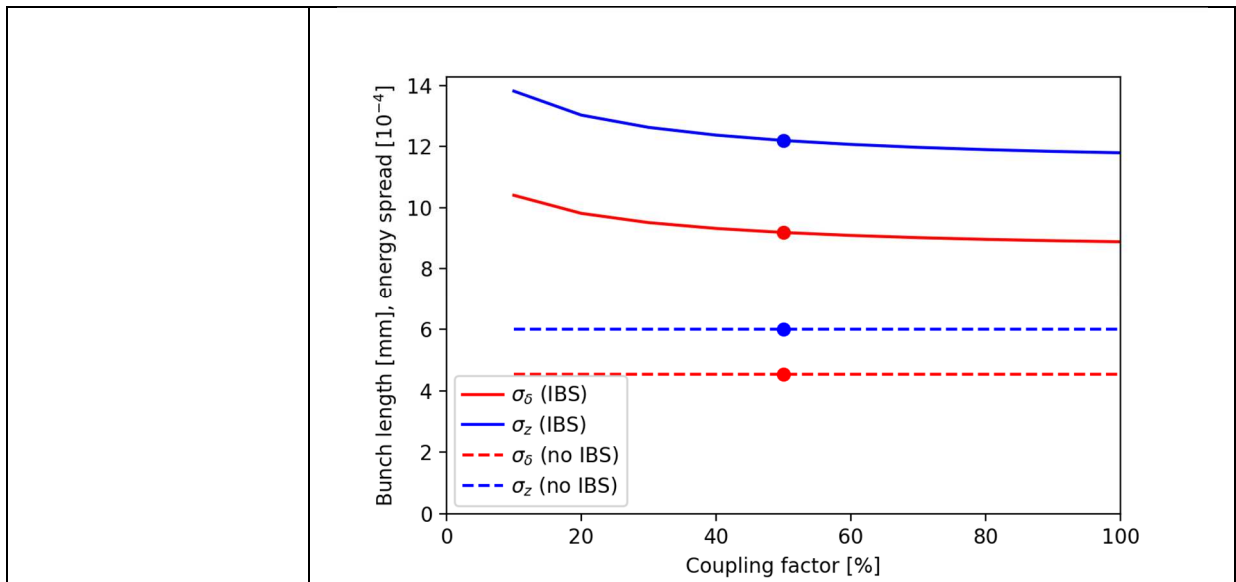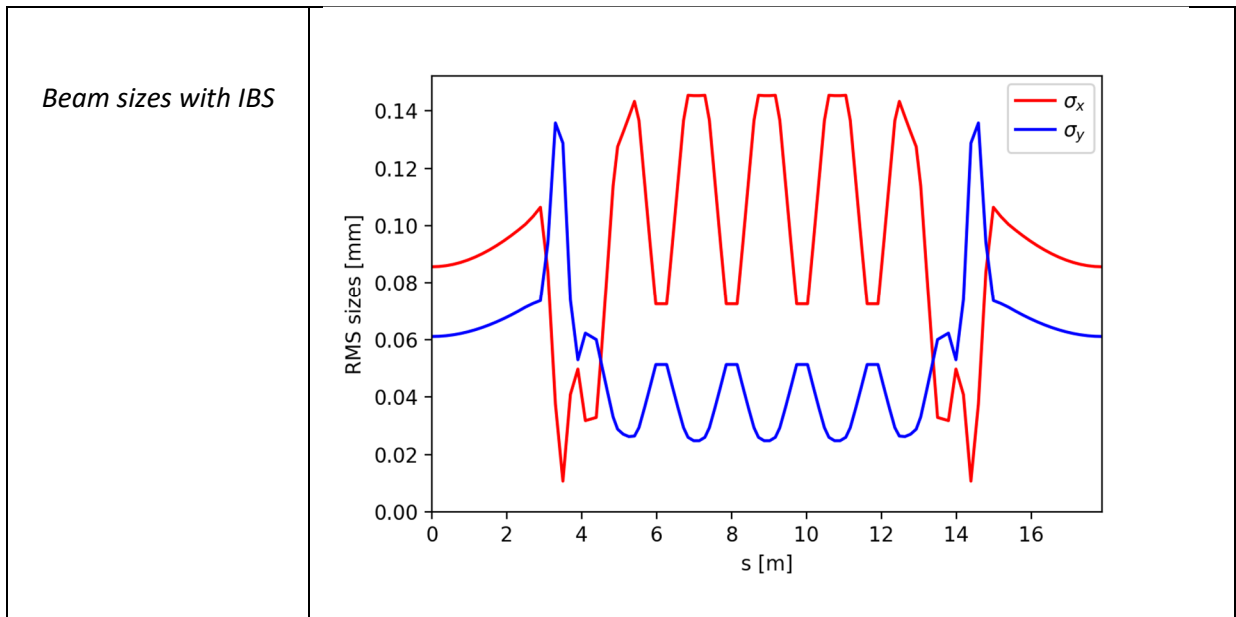
The IBS is indeed an issue but at 500 MeV and a beam current of 200 mA, we can achieve the target values:

Size at the IP **$\sigma_{x,y}$ < 0.1 mm** ; energy dispersion (**σE)/E < 10^{-3} and beam Touschek lifetime T$_l$ > 30 min.**

There is still room for optimization and possible improvements are identified on optics, RF voltage, etc…
We have to check the magnets characteristics, they should be feasible (depends on the inner aperture, determined by injection). The lengths and optics can be optimized.

A smaller momentum compaction could enlarge the RF acceptance and thus the beam lifetime.
Several studies are needed to make evaluations of:
- the dynamic aperture (transverse stability region), it can be a limitation for injection.
- the energy acceptance (and off-momentum dynamic aperture); an energy acceptance of over 2% should be reached (to keep a large beam lifetime).
- on the skew quadrupoles to introduce the coupling.

Appendix D. RIB production modes.

D.1 Target-ion source and A/Q=7 LINAG beams for heavy (trans-lead and actinide) nuclei

Contribution from C. Theisen, CEA DPhN.

We discuss here the opportunities for producing trans-lead and actinide nuclei using an upgraded SPIRAL facility. The ions of interest would be produced using fusion-evaporation or (multi-nucleon)-transfer reactions. While the possibility of using S^3 as a production and separation facility has extensively been discussed, it presents severe limitations for MNT and inverse kinematics reactions in terms of transmission and rejection. Having for objective the highest possible production and thus the highest beam intensities, S^3 also presents limitations in terms of target, notably thickness. It would be therefore advantageous to benefit from a new target ion-source devoted to fusion-evaporation and MNT reactions, installed in a dedicated yellow cave. It would be dedicated to the study of nuclei with long (≥100ms) lifetime and high to moderate production cross-section (≥100μb). Devices suitable for MNT reactions have been already proposed as N=126 factories by the Argonne National Laboratory [G. Savard et al., NIMB 463 (2020) 258] and KEK [Y. Hirayama et al., NIMB 412 (2017) 11][KISS Web page]. These devices are typically a gas catcher followed by a mass separation (magnet, MR-TOF). Adaptations, or even a new concept, are needed for fusion-evaporation reactions.

In a broad approach, we consider the objective of studying actinides in a multifaceted fashion as discussed at the SPIRAL2 2025 think tank: ground state properties (mass measurement, laser spectroscopy), Coulex / inelastic scattering (spectroscopy, quadrupole moment measurements, spectroscopy of the second/third well), transfer reactions (detailed spectroscopy, spectroscopic factors, fission barrier measurement, fission dynamics, spectroscopy of the second well), or more simply spectroscopy after implantation. The minimum intensities needed for these studies are about 10^3 pps (Coulex), 10^3-10^4 pps (detailed spectroscopy using transfer reactions), 10^4 pps (fission probabilities) and 10^6 pps (fission fragment distribution characteristics).
The opportunities of performing electron-ion scattering experiments is presently discussed within the "Spiro committee" for the future of Ganil. Ion-electron scattering studies require typically 10^7 ions trapped and thus production rates at the 10^8 pps level assuming a gas cell extraction efficiency of ~ 10%. These production figures can be lower in case of long (> 1s) half-lives.
The examples provided in the following are intended to discuss the feasibility as well as to give constraints on beams and targets. For the sake of simplicity, we have not considered here the beam slowing down in the target, and thus the variation in production rate as a function of the target depth. However, the target thickness is adjusted approximately to allow the ions to escape. Radioprotection issues are also not considered.

It is important to note that the beam intensities provided are for guidance only and will need to be adjusted according to the injector performance.

Fusion-evaporation reactions using heavy ions

Let us consider as a first example the direct kinematics reaction ^{206}Pb(^{12}C,4n)^{214}Ra, E_{beam} = 70 MeV, σ ~ 400 mb. The target has to be not too thick because of the low recoil velocity, i.e. ≤1 mg/cm^2.
Assuming 50 pμA beam (3.5 kW, A/Q=7 injector not needed in this specific case), the ^{214}Ra production rate will be about 3.6 10^8 pps. A specific high-power target would be required to sustain such high intensities (*e.g.* PbS, or liquid/gas targets)
This reaction would highly benefit from inverse kinematics although the beam intensity will be lower: ^{12}C(^{206}Pb,4n)^{214}Ra, E_{beam} ~1.2 GeV. First the C target will better withstand the intense beam. Second, a thicker target of 10 mg/cm^2 can be used because of a larger recoiling nuclei velocity and lower stopping power.
Assuming a Pb beam intensity of 5 pμA (6 kW), the production rate should be at the order of 6.3 10^9 pps.

Other examples of inverse kinematics reactions are the following:
- ^{9}Be(^{208}Pb,4n)^{213}Rn σ ~ 450 mb [M. Dasgupta et al., PRC 81 (2010) 024608]

- ^{9}Be(^{209}Bi,4n)^{214}Fr σ ~ 400 mb [M. Dasgupta et al., PRC 81 (2010) 024608]
- ^{12}C(^{208}Pb,4n)^{216}Ra, ~ 400 mb [K. Kalita et al., JPG 38 (2011) 95104]

Other examples using direct kinematics:
- ^{208}Pb(^{18}O,4n)^{222}Th, E_{beam} = 95 MeV, σ ~ 5 mb [W. Bonin et al., ZPA 322 (1985) 59], target thickness 1 mg/cm^2, I_{beam} = 50 pµA (4.75 kW). ^{222}Th production ~ 9 10^6 pps. This case is at the limit since the half-life is only 2.8 ms.
- ^{197}Au(^{22}Ne,5n)^{214}Ac, E_{beam} = 114.5 MeV, σ ~6.5 mb [A.V. Yeremin et al., NIM A 350 (1994) 608], target thickness 2 mg/cm^2, I_{beam} = 20 pµA (2.3 kW). ^{214}Ac production ~ 5 10^6 pps. Still at the limit but half-life of 8.2 s allows a longer accumulation time.

In general, the production is higher using inverse kinematics, and benefits greatly from the intense heavy beams delivered by the A/Q=7 injector. Using direct kinematics, production rates $\gtrsim$ 10^8 pps correspond to cross sections $\gtrsim$ 200 mb while in inverse kinematics the cross section can be ~50 times lower to reach similar production rates.

Proton induced fusion-evaporation reactions

Protons will be available at LINAG up to 33 MeV with potentially very high beam intensity. There is an abundant literature on fusion-evaporation cross-sections using proton beams, some of which being of interest for the production of radioisotopes for medicine (see e.g. among many examples [Morgenstern et al., Appl. Radiat. Isot. 66 (2008) 1275]). Theses cross sections can be retrieved using the EXFOR database [https://www-nds.iaea.org/exfor/, N. Otuka et al., NDS 120 (2014)272].
Reactions using a 33 MeV proton beam may not be the adapted to the production of the most exotic actinides. However, the cross sections for few neutrons evaporation channels already offer large opportunities. It should be noted that a program on actinides studies based on p-induced reactions is being pursued a the University of Jyväskylä using the IGISOL facility (therefore a gas-cell). The feasibility of such studies is therefore proven. Obviously these reactions would not benefit from the A/Q = 7 injector.

Two examples are provided for illustration purpose.
^{232}Th(p,3n)^{230}Pa, E_p = 20 MeV, σ ~ 200 mb (see
- *Figure 1*-left), target thickness = 2 mg/cm^2, I_{beam} = 10 µA (0.2 kW). ^{230}Pa production ~ 6.5 10^7 pps (half-life 17.4 d).
^{238}U(p,3n)^{236}Np, E_p = 20 MeV, σ ~ 80 mb (see
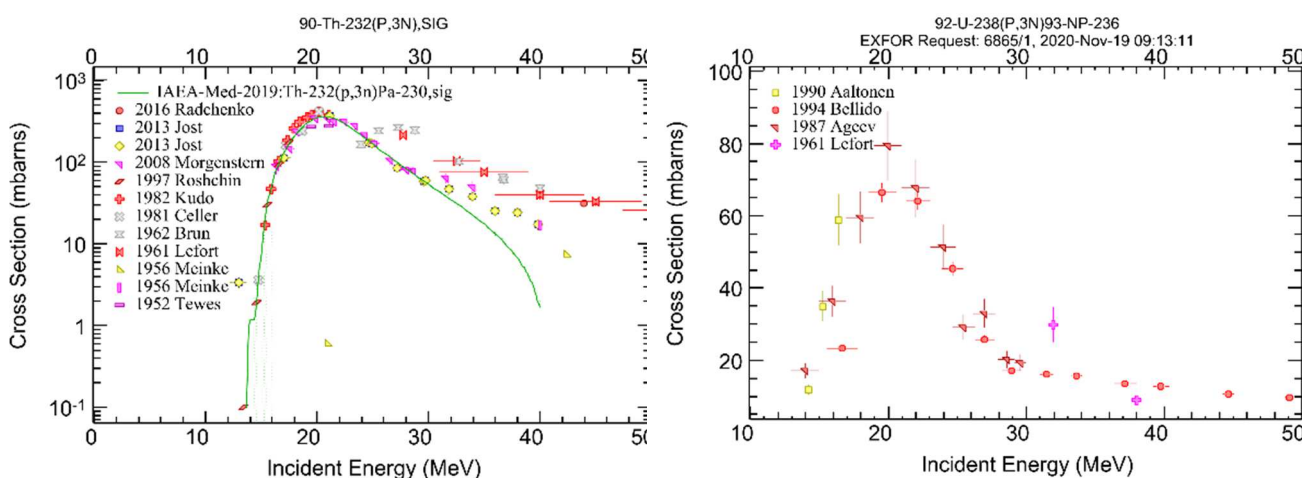- *Figure 1*-right), target thickness = 2 mg/cm^2, I_{beam} = 10 µA (0.2 kW). ^{236}Np production ~ 2.5 10^7 pps (half-life 0.153 My).

Figure 1. Fusion-evaporation reaction cross sections for the reactions ^{232}Th(p,3n)^{230}Pa (left) and ^{238}U(p,3n)^{236}Np (right) extracted from the EXFOR database.

MNT reactions

There is a fairly extensive literature on actinide production using multinucleon transfer reactions: see e.g. [Magda and Leyba, Int. J. Mod. Phys. E 01 (1992)221][Kratz, Loveland and Moody, NPA 944 (2015) 117]. It is not the purpose of the present document to discuss the details of the reaction mechanism as a function of the beam specie and energy. As a rule of thumb however, the heaviest target should be used to produce the heaviest actinide nuclei. For the production of SHE, the heaviest beam should be used as well, but this turns out to be less sensitive for isotopes near the target (i.e. not too many transferred nucleons). As an example, Bk isotopes can be produced with few mb cross-sections using a ^{248}Cm target and either a ^{18}O, ^{86}Kr, ^{136}Xe [Moody et al. PRC 33 (1986) 1315], ^{31}P [Leyba et at al., PRC 46 (1992) 1364], ^{40,48}Ca [Hoffman et al., PRC 31 (1985) 1763] or ^{238}U [Schädel et al. PRL 48 (1982) 852] beam: see Figure 2.

Let us consider for example a ^{40}Ca beam, which is a good compromise between the power dissipated in the target and the residue velocity (and thus the target thickness).
E_{beam} = 240 MeV, I_{beam} = 20 pµA (4.8 kW), target thickness 2 mg/cm^2, σ(^{248}Bk) = 5,4 mb → I(^{248}Bk) = 3.3 10^6 pps. Note that the ^{248}Bk half-life is larger than 9 y.
As shown in Figure 2, nuclei heavier than Bk can be produced with production rates larger than 10^4 pps for other applications listed in the introduction (e.g. 6 10^4 pps ^{250}Es).
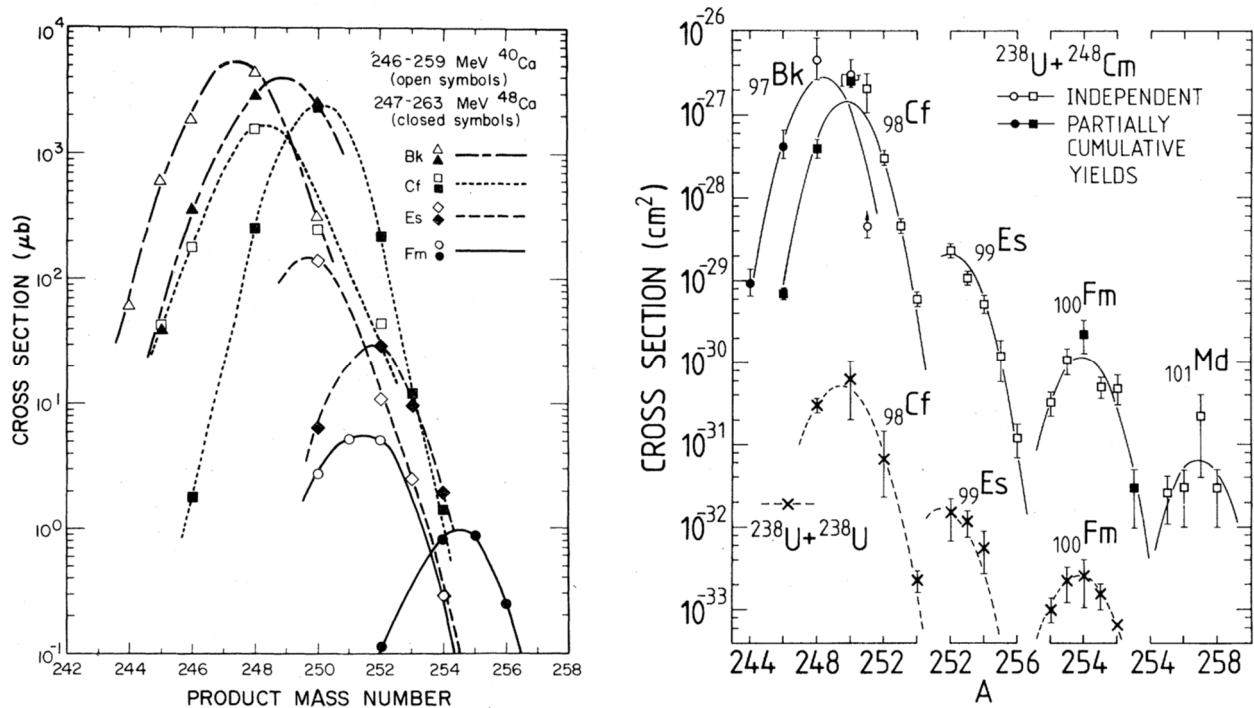
Figure 2. (Left) ^{40,48}Ca+^{248}Cm reaction [Hoffman et al., PRC 31 (1985) 1763].
(Right) ^{238}U+^{248}Cm@7.4-7.5 MeV/u reaction [Schädel et al. PRL 48 (1982) 852].

For the production of lighter actinide nuclei, the ^{238}U+^{238}U reaction is well adapted see *e.g.* [M. Schädel et al. PRL 41 (1978) 469]. As shown in Figure 3, a large variety of Pu, Am and Cm isotopes can be produced with cross-section at the trans-µb level. The advantage of the ^{238}U beam compared to ^{136}Xe is also obvious.
Consider I_{beam} = 2.5 pµA (4.4 kW), E_{beam} = 1.76 GeV, target thickness = 10 mg/cm^2, the production rate is ~ 4 10^5 pps for a 1 mb cross section.
Productions rates at the 10^8 level is challenging. However, the panel of isotopes available with production rates above ~10^4 is larger: Cm, Am and Pu isotopes.
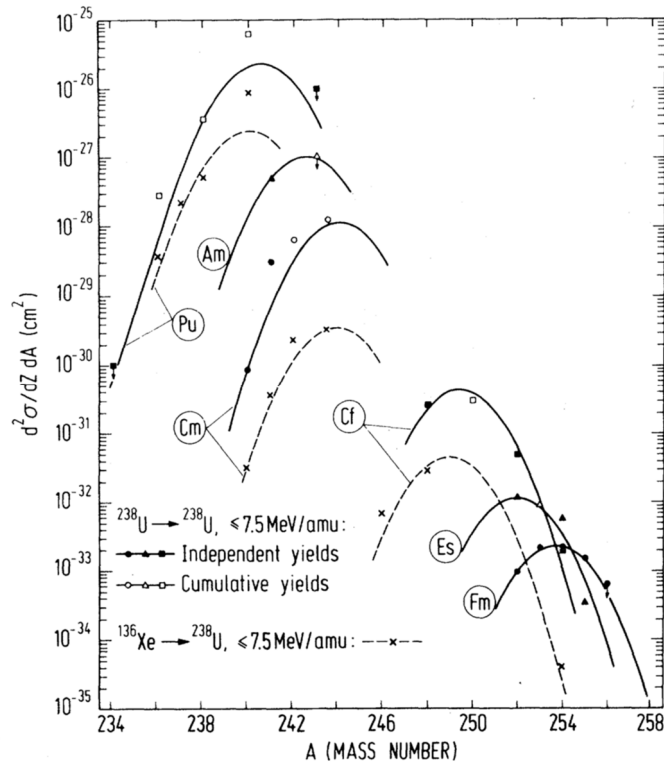
Figure 3. Actinide production using the ^{238}U+^{238}U and ^{136}Xe+^{238}U reactions [M. Schädel et al. PRL 41 (1978) 469].

Few nucleon transfer reactions are not discussed in the present document, but are also valuable tools for producing exotic actinides with relatively high cross-section of several mb. Like in the case of fusion-evaporation reactions, advantage can be taken from inverse kinematics for a larger production (thicker target, higher transfer products velocity). An example, among many other, is the reaction ^{12}C(^{238}U, ^{240}Pu)^{10}Be (σ = 2.8 mb [Rodrìguez-Tajes et al. PRC 89 (2014) 024614]).

To summarize, several trans-lead and actinide nuclei can be produced at the 10^8 level or higher using fusion-evaporation, MNT or few nucleon transfer reactions. Using heavy beams (Kr, Xe, Pb, Bi, U) is mandatory to reach these rates. The use of proton-induced few neutrons fusion-evaporation reactions on actinide targets provide production rates up to ~10^8 pps. In a broader approach, a very large number of trans-lead and actinide isotopes up to Fm[1] can be produced with production rates higher than 10^4 pps for a wide range of physics case.

---

[1] using e.g. a ^{86}Kr beam [Moody et al. PRC 33 (1986) 1315].

Contribution from I. Stefan, IJCLab.

Production potential of light and medium neutron rich nuclei by deep inelastic reactions with Linag

The production potential presented here is extrapolated using the experimental results presented in reference [1] and [2]. In reference [1] are presented the measured double differential cross-sections for the beam-like fragments obtained from a 10 MeV/A 48Ca beam impinging on a 0.17 mg/cm2 238U target. The measurement was performed at Ganil using Vamos spectrometer and covered all the phase space in angle and energy except the most forward angles for the beam-like fragments. In reference [2] are published the measured double differential cross-sections at 0° for the beam-like fragments obtained from a 8.5 MeV/A 18O beam impinging on a 1 mg/cm2 238U target. The measurement was performed at Ganil using Lise 0° spectrometer. Two theoretical calculations are presented for all other angles.
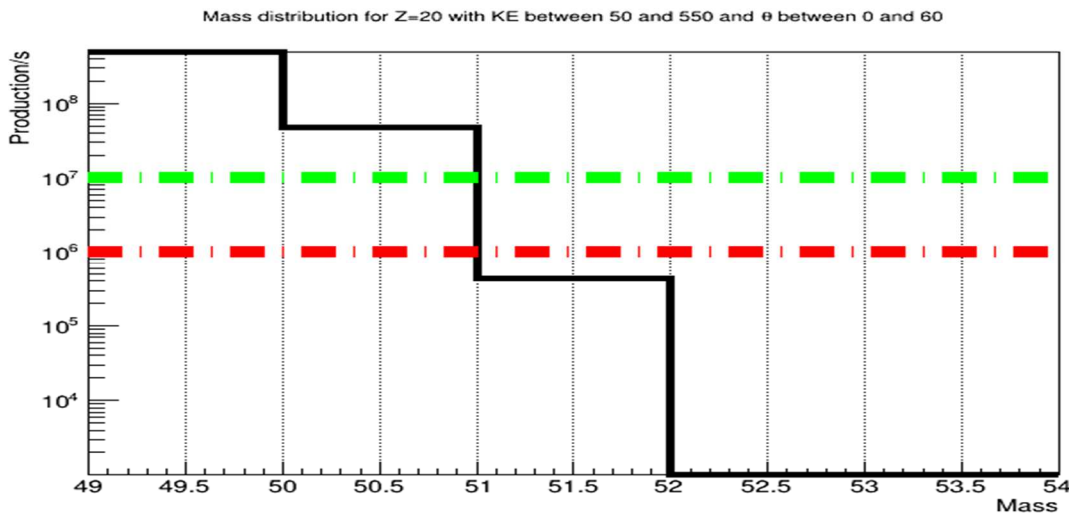
Figure 1. Estimated counts/s for different neutron-rich Ca isotopes (in black), obtained from using a 10 puA ^{48}Ca beam impinging on a 1 mg/cm^2 ^{238}U target. Estimation obtained using ref [1] and [2]. The green and red dash-dotted lines show the 10^7 counts/s and 10^6 counts/s limits respectively.
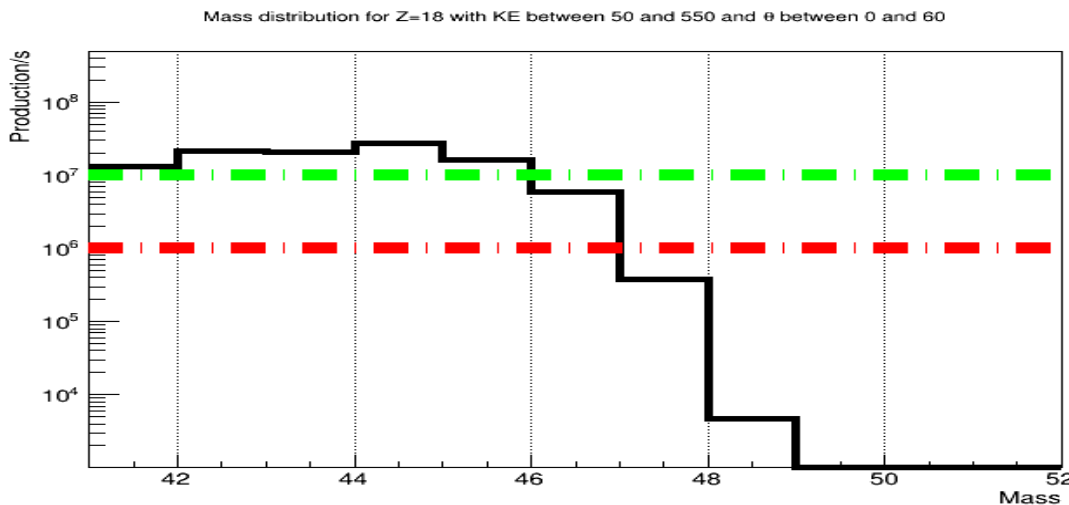
Figure 2. Same as in Fig.1 for different neutron rich Ar isotopes (in black).
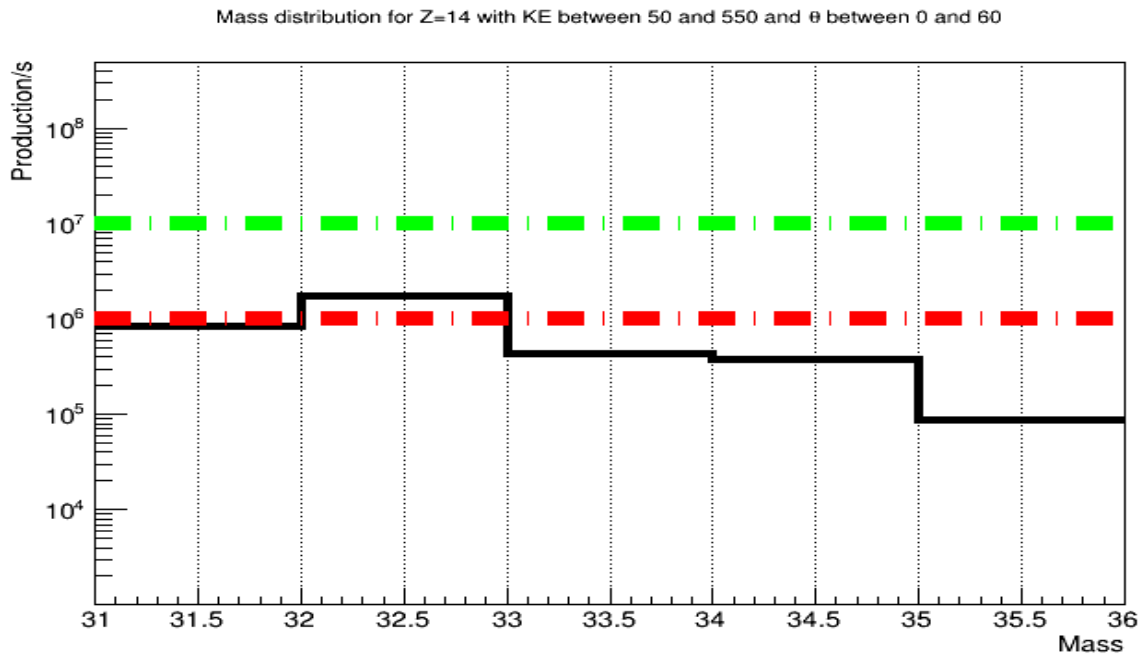
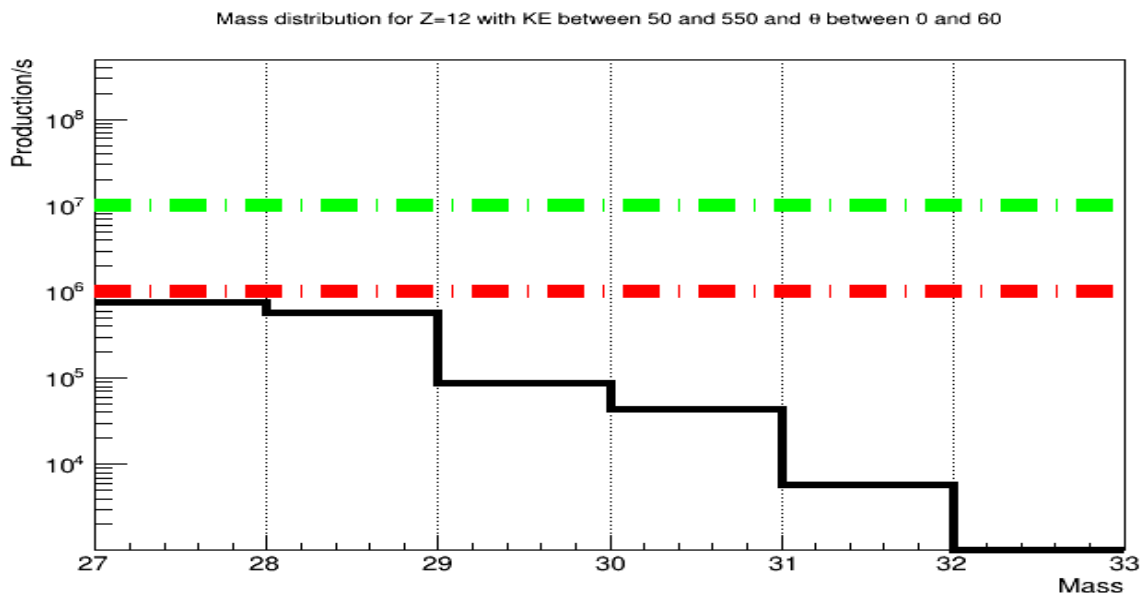Figure 3. Same as in Fig.1 for different neutron-rich Si isotopes (in black).

Figure 4. Same as in Fig.1 for different neutron-rich Mg isotopes (in black).

Assuming a 10 puA of ^{48}Ca beam delivered by the LINAG and a 1 mg/cm^2 thick ^{238}U target the total production/s of some neutron reach nuclei is estimated in the figures 1 to 4.

The same pattern is expected for a different incident beam. I such a case the A and Z shown in the figures is expected to shift by the same difference in A and Z between the beam and the ^{48}Ca taken as example.

[1] C. Portail phd thesis 2017 https://hal.archives-ouvertes.fr/tel-01630850
[2] I. Stefan et al Phys. Lett. B **779**, 456 (2018) https://doi.org/10.1016/j.physletb.2018.02.037

D.3 Discussions on the fission production techniques

Contribution from P. Delahaye with M. Fadil, GANIL

Release characteristics of the SPIRAL2 phase 2 target compared to standard compact UCx targets

The SPIRAL2 phase 2 nominal target was designed to attain a number of fissions/s of the order of $3 \cdot 10^{13}$ using a high density target of a relatively large volume, compared to standard ISOLDE CERN or ALTO targets. Its characteristics are compiled and compared to the SPES target in the following table.

Target design	Target density (g/cm3)	Target weight (g)	Disks dimensions Diam. X thick. (mm)	Number of disks N_d	Total target surface S_t (cm²)	Rough estimate number of contacts (S_t/10mm²)
SPIRAL2 phase 2	10.7	2300	15 x 1	19 x 70 = 1330	9300	93000
SPES	2.5	30	40 x 1.3	7	88	880

*Table 1. Characteristics of the SPIRAL2 phase 2 target [**spUcx**] as compared to SPES [**spes08**]. Each target is composed of a stack of disks of different dimensions, whose overall surface differs by 2 orders or magnitude. A rough estimate of the average number of contacts required for effusion is obtained from the ratio of the latter surface to an open area fixed to a typical value of 10 mm².*

The overall efficiency of an ISOL target ion source system relies on three main types of processes: diffusion of the radioactive atoms from the target material, effusion (transport by successive contacts on materials to the ion source) and ionization. The target material and geometry will affect the two first processes, whose efficiency product is usually referred as release efficiency.

Diffusion efficiency.
The release from high density UCx synthetized in Gatchina (reference material for phase 2) and other newly synthesized targets with different compositions were compared to commonly used target materials from ISOLDE/CERN and ALTO in the frame of ENSAR/Actilab [*spnu5,spnu6*]. It resulted from on-line measurements at PARNNE and ISOLDE that the high density material has inherently modest diffusion efficiencies compared to the classical target materials, but also compared to the other newly designed target pellets. At ISOLDE, the secondary beam intensities measured with the high density material were mostly lower for the shorter lived products, and only equivalent to the standard ISOLDE target material for the produced isotopes with longer half lives, despite 4x more fissions in the target [*spnu6*]. This argument alone already weakens the case of SPIRAL2 phase 2, for which targets with $3 \cdot 10^{13}$ fissions/s may result in essentially the same secondary beam intensities as in ISOLDE or SPES with a 3 times less fissions in the target.

Effusion efficiency.
The effusion efficiency is determined by the number of contacts required for the radioactive atoms to be transported from the target to the ion source. Each contact results in a sticking time (adsorption of the atom onto the surface) which delays the transport of the radioactive atom to the ion source. Effusion losses occur by radioactive decay when the transport time becomes non negligible with respect to the radioactive half-lives. The number of contacts can be roughly determined from a ratio of open surfaces (through which the atoms will escape and reach the ion source), to closed surfaces (sum of target disks and container surfaces). Owing to the much more complicated path in the case of the SPIRAL2 phase 2 target, the average number of contacts will be significantly higher than in the case of a simple target such as the one of SPES. *Table 1* gives orders of magnitude for this number considering:
- an open surface of 10 mm², corresponding to typical dimensions of transfer tube orifices connecting the target to the ion source, and,

- a closed surface mainly determined by the target disks dimensions.

In the case of the SPIRAL2 phase 2 target, a number of contacts roughly 100 times more important than in the SPES target is expected. The impact of this significantly enlarged number of contacts in case of the SPIRAL2 phase 2 target requires a case-by-case study, as the sticking times significantly vary from element to element. Sticking times can be estimated from adsorption enthalpies that can be found in the literature (see [5a]).

Figs. 1 and 2 show qualitatively the difference in terms of secondary beam intensity one would expect between, on one hand the SPIRAL2 phase 2 target (930000 contacts, $3\cdot10^{13}$ fissions/s), and on the other hand an optimized target geometry for photo-fission, resembling the one of SPES (1000 contacts, $1\cdot10^{13}$ fissions/s), for two examples of isotopic chains, Ge and Sn respectively. The 1+ beam intensities were calculated using a similar procedure as described in ref. [5a]. The orders of magnitudes are correct provided that:

- the estimate of number of contacts given in Tab. 1 is not too crude. A rigorous determination of the number of contacts would require the use of an ad-hoc Monte Carlo simulation with a detailed target ion source design.
- the A,Z distribution is equivalent for both reaction mechanisms. An A,Z distribution as expected from neutron induced fission was used for both cases. As shown in annex β the A,Z distribution may differ for the most exotic isotopes (from PHITS this difference seems to be favorable to photo-fission).
- The diffusion and effusion coefficients found from literature as well as typical ionization efficiencies are correct. For both cases an equivalent diffusion coefficient was used, despite the observation done in [*spnu6*] of a more modest diffusion efficiency from the high density UCx material. This material served as reference for the design of the SPIRAL 2 phase 2 target. In this respect, the red curves correspond a priori to an optimistic estimate for this target.

-

It is remarkable that Ge is particularly sensitive to effusion, according to the coefficients found in literature. Example of other elements found to be particularly sensitive to effusion are Cu As, Y, Ag, Cd, In, La. Considering as in [5a] a typical flight time of 10 µs between each contact, effusion becomes a limiting process for all elements irrespective of their chemical properties for half-lives approaching 1 s in the case of the SPIRAL2 phase 2 target, and 10 ms in case of the SPES target. This is exemplified by *Fig. 2* for which the ^{134}Sn yields become more advantageous for the SPES target than from the SPIRAL2 phase 2 target. For the long-lived isotopes, the yields are potentially higher in the case of SPIRAL2 phase 2 target by a factor of 3, provided that this advantage is not hampered by a modest diffusion from the high density UCx material [*spnu6*].
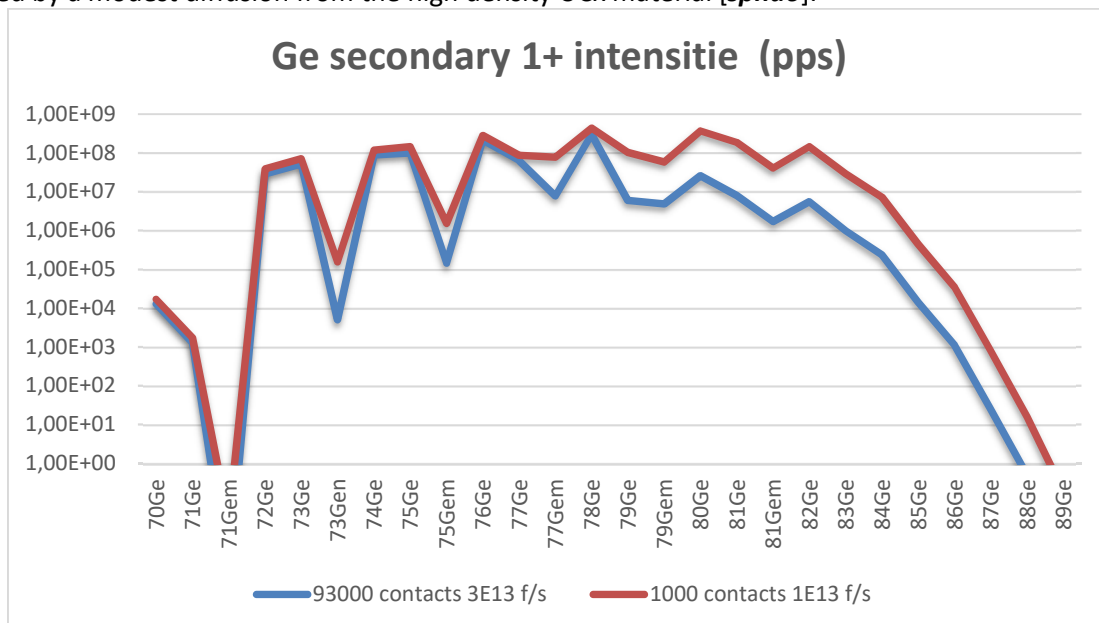

Figure 1. Secondary beam intensities estimated for the Ge isotopic chain with different number of contacts and fissions/s, using A,Z distribution as calculated for neutron-induced fission, and diffusion and effusion coefficients from literature. See text for more details.
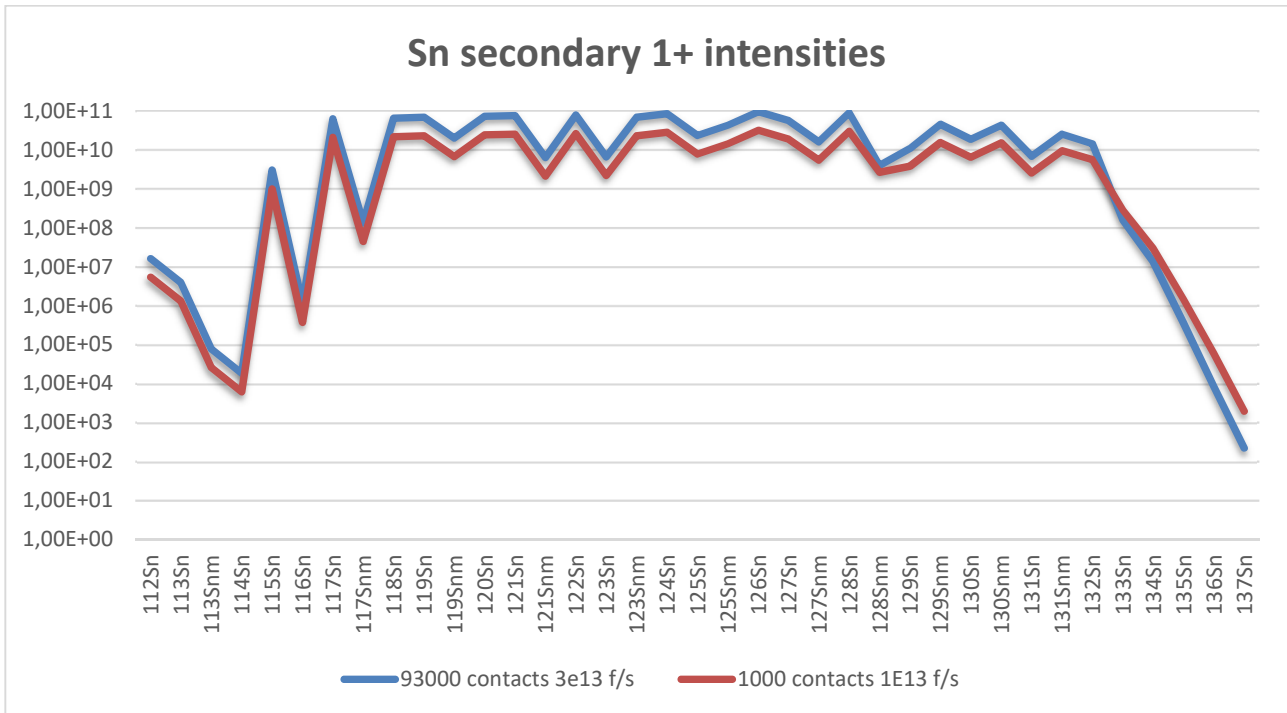
Figure 2. Secondary beam intensities estimated for the Ge isotopic chains with different number of contacts and fissions/s, using A,Z distribution as calculated for neutron-induced fission, and diffusion and effusion coefficients from literature. See text for more details.

Conclusion.

The original design of the SPIRAL2 phase 2 target is quite cumbersome when compared to other simpler and more compact designs if one considers the objectives of in terms of intensities defined for the electromagnetic probe:

- It strongly penalizes the production of many short-lived isotopes with half-lives approaching 1s, and above for certain elements for which effusion is the limiting process,
- It does not bring any significant advantage for longer lived beams which are produced in all cases at intensities, which are way beyond the space charge capacities the ion trap ($>> 10^8$ /s)

In contrast, the use of optimized target designs for photo-fission or light-particle fission at a reasonable level ($5 \cdot 10^{12}$ - 10^{13} fissions/s) seems to yield a good compromise for long and short-lived isotopes production, as developed in this document.

D.4 Photofission production
Simulation of photofission with a 40 MeV electron beam in a low density UCx target, with/without converter

Contribution from M. Fadil with P. Delahaye, GANIL

Input data :
-Electron beam at 40 MeV) ; 10 kW
- Target of UC4 material at low density 3.5 g.cm^{-3}; total mass of 277 g;
- Shape : 7 series of pellets piled-up on a 7 cm-length (hexagonal distribution);
- Pellets: r = 0.75 cm, thickness: 1 mm, distance between 2 of them = 0.3 mm;
- UCx density in the spill= 3.5 g.cm^{-3}; apparent density in each serie: 3.2 g.cm^{-3}, in all target: 2. 5 g.cm^{-3}
- Converter: tungsten (W); thickness: 5 mm; distance converter-target : 5 mm

Fission rates
The simulations are performed with the physics models of the PHITS code, for a direct beam of 2.0 10^{12} fissions/s ; with converter: 1.6 10^{12} fissions/s.
The comparison with the previous SPIRAL2 project (electron option) [**SP2eOpt**] is done below.
(Ee- = 45 MeV, distance between converter and target = 4 mm). Note that there are no detailed information on the UCx target in the previous report (mass ? density? shape ?).
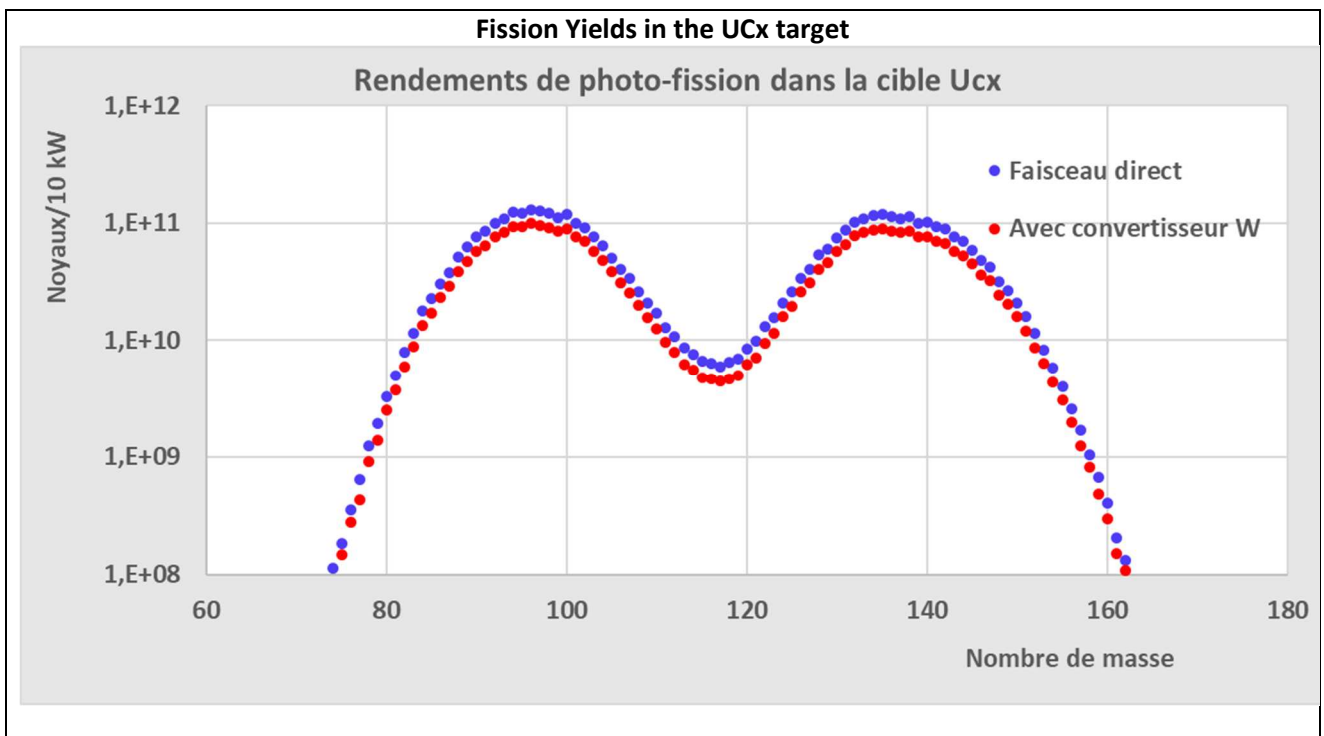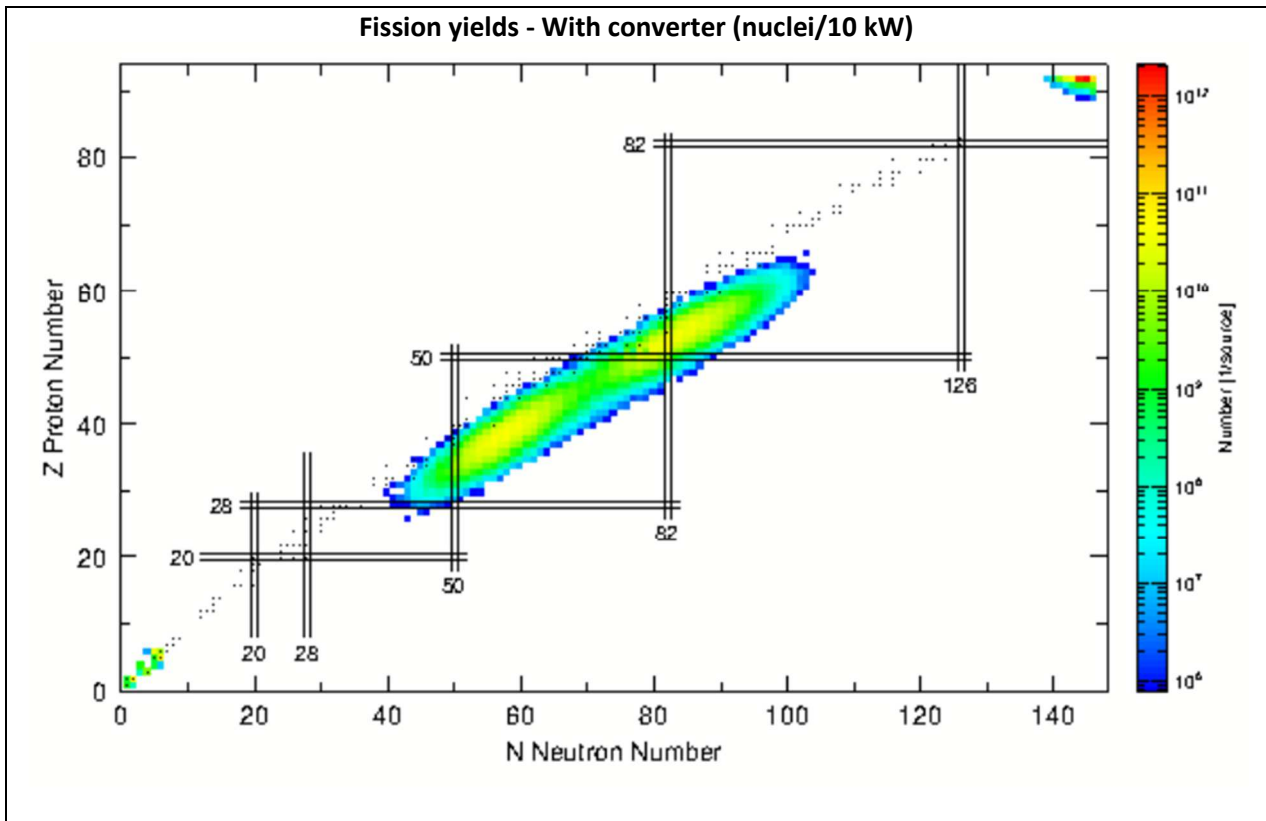Direct beam: 10^{13} fissions/s for Pe-= 22,5 kW; With converter: 10^{13} fissions/s for Pe- = 225 kW.

[**SP2eOpt**] Preliminary Design Study (PDS) of the project SPIRAL II (electron option) GANIL/SPI2/007-A.
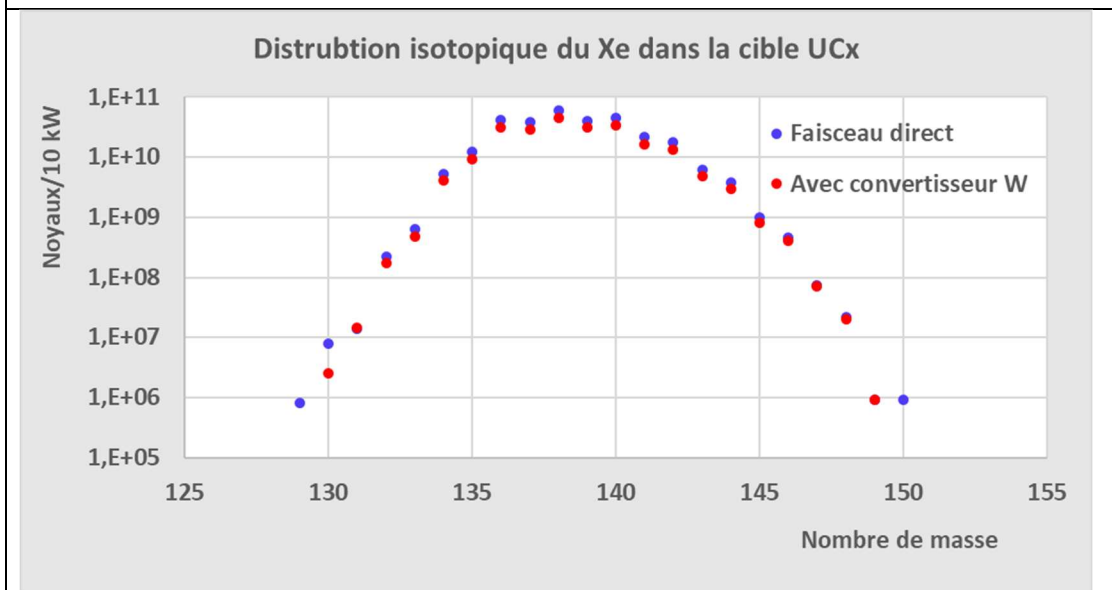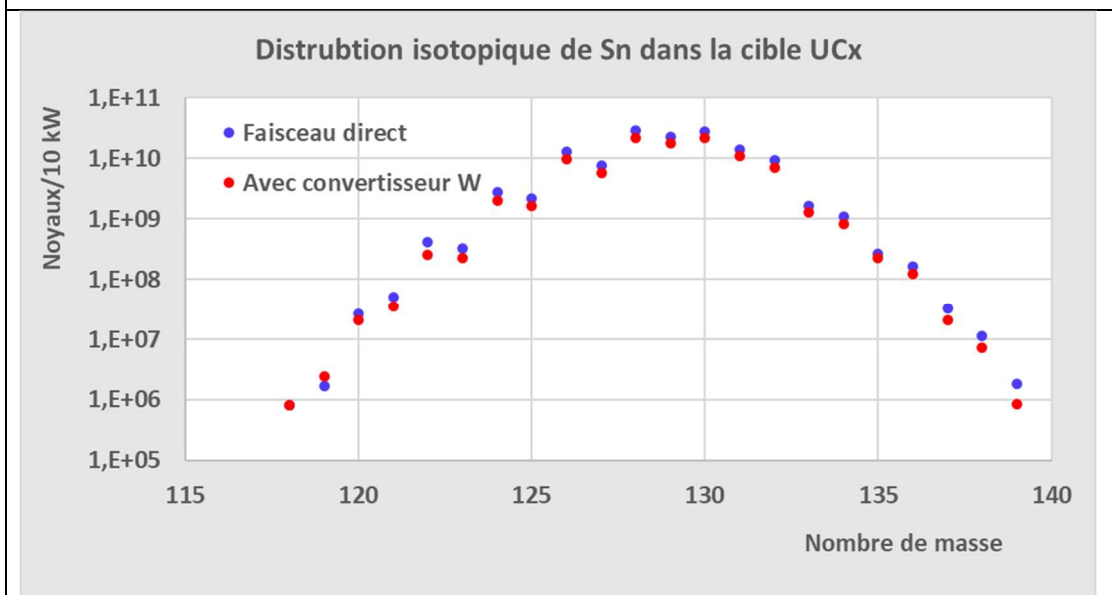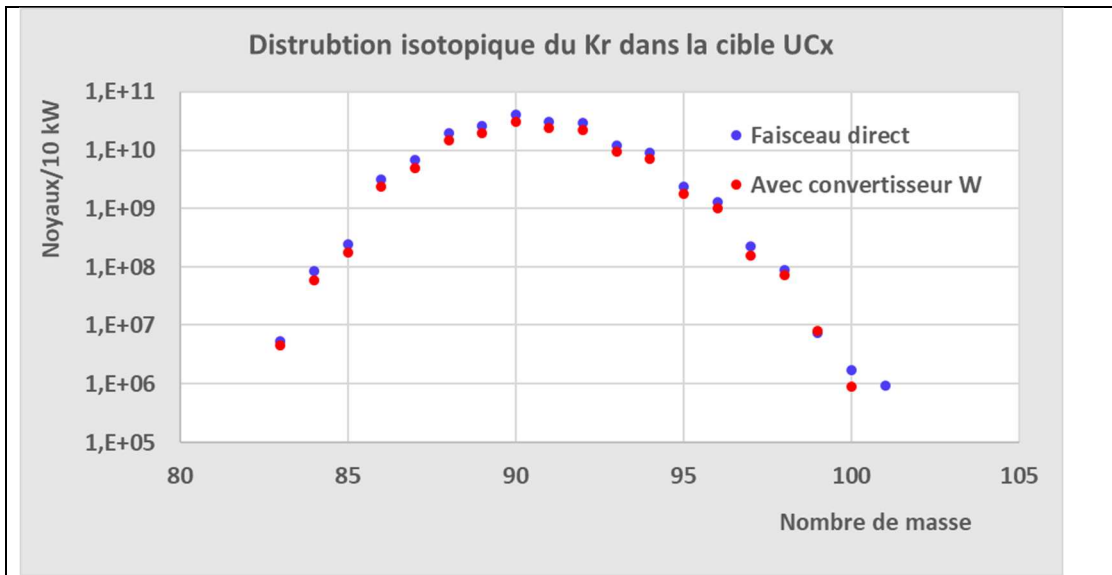
Normalisation at 1 kW incident beam

	This works (40 MeV)	SPIRAL2-electron option (45 MeV)
Direct beam	2.0 10^{11}	4.4 10^{11}
With converter	1.6 10^{11}	8.9 10^{10}

Fission yields - Direct beam (nuclei/10 kW)

Fission yields - With converter (nuclei/10 kW)

Fission Yields in the UCx target

Rendements de photo-fission dans la cible Ucx

- Faisceau direct
- Avec convertisseur W
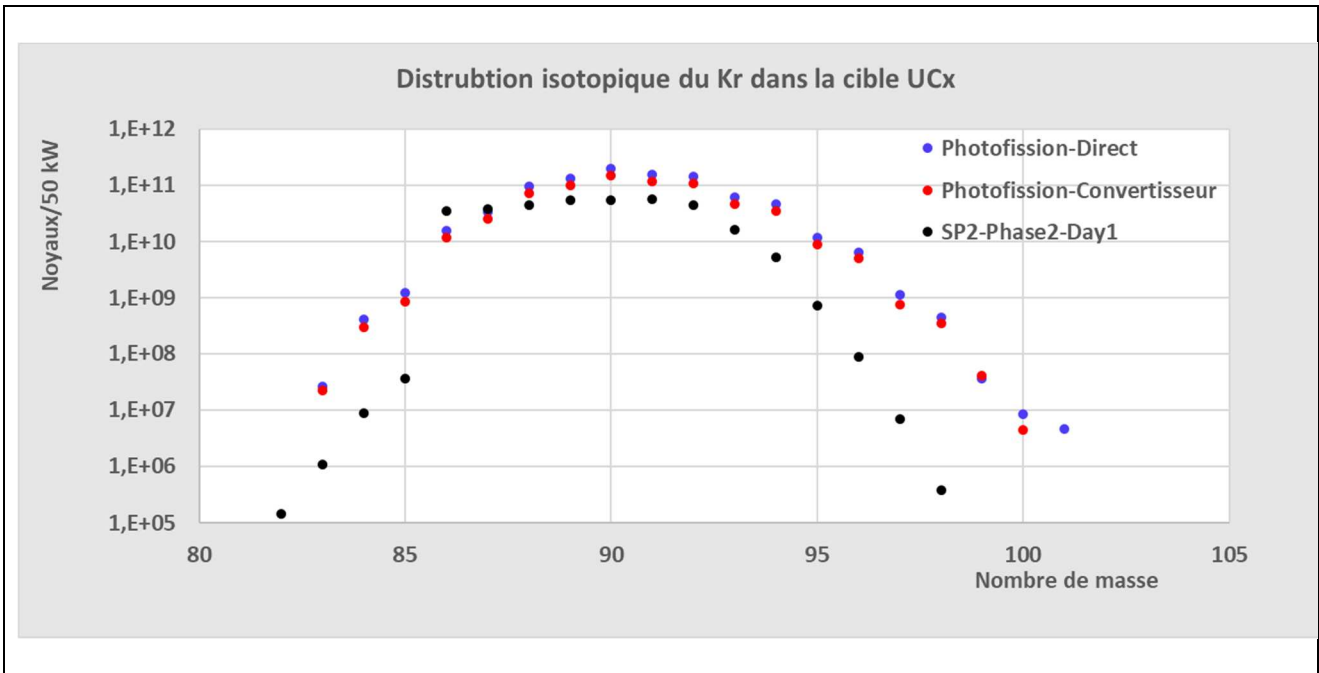
Noyaux/10 kW

Nombre de masse
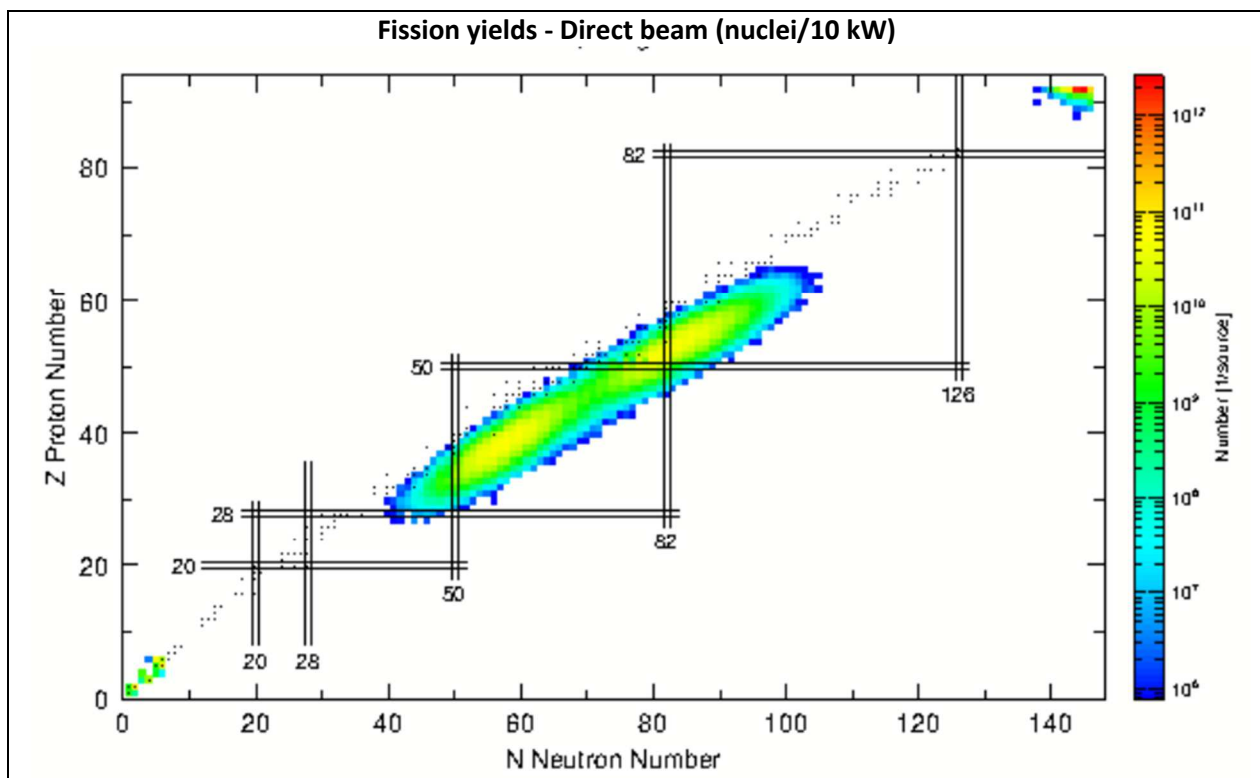
Production rates of a few selected fission products, Kr (Z = 36), Sn (Z = 50) and Xe (Z = 54) isotopes

Comparison Photofission / SPIRAL2-Phase2-Day1

Distrubtion isotopique du Kr dans la cible UCx

	Photofission (40 MeV)	SPIRAL2-Phase2-Day1
Beam characteristics	Electron 40 MeV - 50 kW	deuton 40 MeV - 50 kW
Target characteristics	low density target UCx 277 g	
Converter	W	Graphite
Direct beam	$1.03\ 10^{13}$	- - -
With converter	$7.8\ 10^{12}$	$1.7\ 10^{12}$

Comparison between SPES target with the SPIRAL2-Phase2-Day1 target

Rendements de photo-fission dans la cible UCx
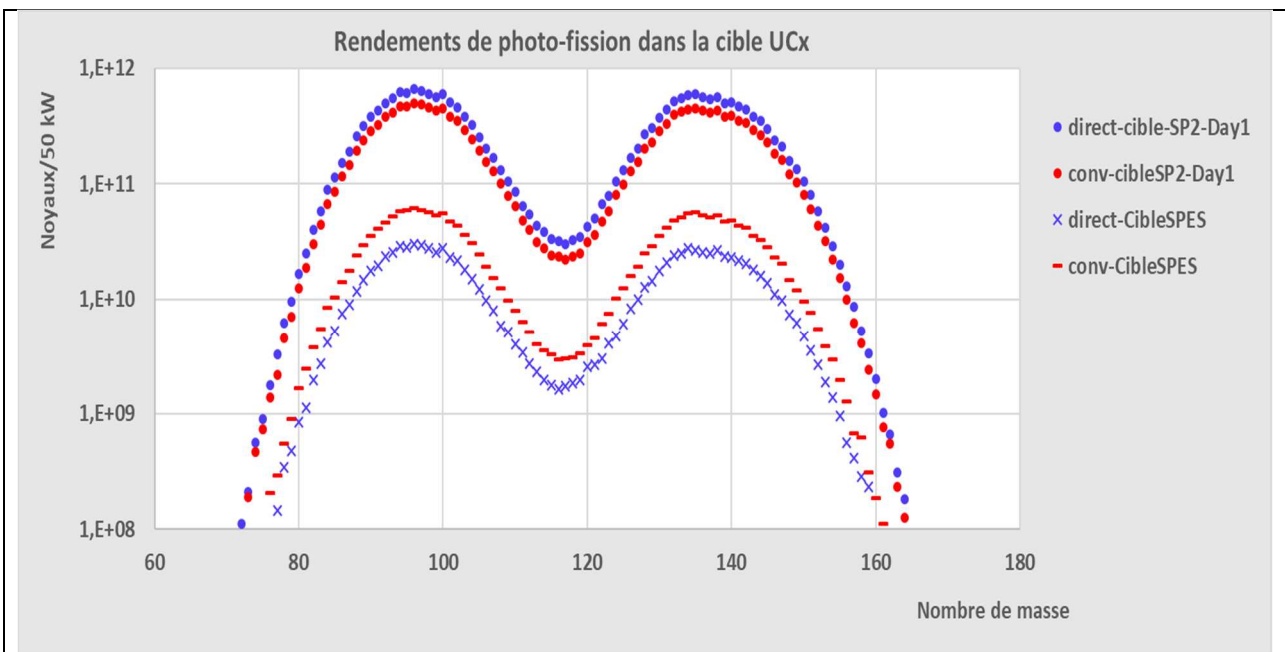
Appendix E. Tentative budget and manpower requests, timelines

Based on the similar machine project (electron accelerators, spectrometers) and taking into account the development for the ion trap and for the beam production building, we establish the following preliminary schematic project schedule (*CDR: conceptual design report*):

	Y1	Y2	Y3	Y4	Y5	Y6	Y7	Y8	Y9	Y10	Y11	Y12
e-RI	CDR	CDR	CDR	CDR	Ion trap test	Electron Machine building Spectrometers Detection				Integration Trap-RI-electrons	Electron beam tests	Electron-ion tests
RIB	> 10^7 /s RI from SPIRAL1, SP2 DESIR, S3				> 10^7/s RI from new production schemes photofission, MNT…							

Estimate of the total cost of the project for the electron-ion machine
Here we do not include the cost of the RIB production building, it is discussed in **V.3.**

We detail the required resources over 12 years, with a 1st phase (4 years), 2nd phase (8 years).
We give the number of full Time equivalent (FTE) for the manpower and we precise also the domain of expertise and the time required for the given task ("half time means half time period for a given expert over the years indicated in the column).

e-RIB Day1 with existing RIB Cost +/-10%	Resources: R&D, manpower Expertise/Design report 4 years	Resources: Technical report & realization, commissioning manpower Expertise 8 years	OPERATION PERIOD Resources and manpower for the running conditions
Electron accelerator E ~500 MeV ~100 M€[§] *Including the experimental area building for the exp (spectrometers, detection)*	Design Report: 2 experts, *full time* 8FTE	8 experts (*RF, vacuum, beam dynamics, mechanics…*) *half time* > 32 FTE	+ 2 beam operators/technicians of the machine + 1 beam optics engineer
Ion trap techniques Beam injection X 10 ? M€ between 30 and 40 M€	2 experts *half time* 4 FTE	Test experiments varying the ion species 3 experts, *1/3 time* > 8 FTE	2 Ion source/ion trap expert
2 spectrometers[µ] Focal plane detectors Mechanics 8 M€	2 (spectrometer expert with 1 CAO engineer) *half time*; 4 FTE	2 (spectrometer + CAO engineer) *1/4 time* ; > 4 FTE	2 (1 technician/1 engineer) of the area
Particle detection Electronics and DAQ 2 M€	2 (1 DAQ/electronics engineer; 1 Control Command) ¼ time; 2FTE	1 *1/4 time*; > 2 FTE	1
TOTAL ~ **64 FTE (4+8 years)** **Budget ~ 150 M€**	18 FTE	> 46 FTE ***(without the support teams, to be defined)***	Running operations: See estimate from other electron facilities Eg MAMI, Jlab

[§] *As a reference for the cost of the various elements for an electron machine, considering for instance the cost estimates for PERLE at Orsay the beam lines, equipment for accelerator are of the order of 25 M€ (this amount does not include the Human Resources, infrastructures and experimental areas) taking account 5 M€ for the magnets, 4-5 M€ for the cryomodules, 5 M€ for the injector, 10 M€ for the cryogenics power supply*
Taking into account the standard order of cost for the infrastructures, we have ~40-50 M€ for the building areas.

The total amount for the electron-ion collider machine is around 150 M€.
The human resources to be considered over the 12 years development represent 40 FTE (accelerator), 12 FTE (ion trap design and measurements), 8 FTE (spectrometer, mechanical integration, detections), 4 FTE (electronics, DAQ).
Note that we would need technical teams in support of each operation in the integration phase of the equipments for the machine. This should be examined in the detailed Technical Design Report.

As a reference, one can consider the overall cost of the upgrade of the European Source RF ESRF around including the 6 GeV machine, the building and the various elements (magnets, ondulators, etc…).
Amongst the possible references, looking for instance at an APD in 2019 for an electron synchrotron of a few GeV in South East Europa (*SEEIIST project [SEEIIST]*): "The average investment cost for the machine, using the experience from previous projects ALBA, SOLEIL, DIAMOND and MAX IV is roughly 0.25 M€ per meter."
"For the design, following up the contracts, installation and commissioning roughly 40 people are needed (6 specialist from other SRL (100 k€/year), 15 engineers (50 k€/year) and 20 technicians (30 k€/year)."
For our case with a circumference of about 100 m, we get a cost of 25 M€ for the machine.

Note that here we only give overall numbers for the cost of the machine (reasonable estimation within 10% error) and the global expected number of FTE. For the FTE, there could be aleas due to specific problems, to be identified in the CDR, and solved during the TDR phase.
Therefore, we should wait for the CDR phase to obtain a reliable estimate of the human resources for the whole period of the project.

The cost for an upgrade of our machine for the luminosity 10^{30-31} has also to be estimated. This can be done once the detailed study can indicate if the gain in luminosity can be reached directly from the electron part of from the optimization of the ion trap efficiency.

[SEEIIST] Web site of the SEEIST project: http://seeiist.eu ; document mentioning the cost estimates: http://seeiist.eu/wp-content/uploads/2018/05/Basic-concepts-for-a-SOUTH-EAST-EUROPE-INTERNATIONAL-INSTITUTE-FOR-SUSTAINABLE-TECHNOLOGIES.pdf

Appendix F. ERL scientific, medical and industrial applications

We first indicate potential applications. In the second part we develop the medical applications of very high energy electron (VHEE) beams.

I. List of potential applications.

An ERL device is the appropriate instrument to produce intense photon backscattering beams resulting from intense laser light collisions with high-energy electron beams.

This opens a variety of possible applications for therapy and for material science researches.

For therapy purposes, using flash dose deposit and micromesh techniques [*Thmed1*] requires accelerator of high-intensity electrons at energies between 150 and 300 MeV. This was part of the programme [*Thmed2*] intended for the PRAE facility project (*Platform for Research and Applications with Electrons*) [*Thprae*], "a multidisciplinary platform based on a high-performance new generation linear accelerator delivering a pulsed electron beam in the energy range 30–70 MeV, upgradable to 140 MeV".

The GANIL site would be also interesting **for R&D medical studies**, since it is ideally located for the pre-clinical tests on animals (small and large-sized) which are already part of studies done at ARCHADE and CYCERON. The developments of the dedicated instrumentation and areas for the preclinical test studies would represent an interesting aspect of the application of the electron beams at GANIL.

- **Use of the beam dump for radioisotope production**, similar to the photofission performed at ARIEL [*Thmed3*].

This would require a new building, for the (hot) chemical processes needed to extract the radioisotopes. GANIL is an optimum site since it is located near-by the "Francois Baclesse" oncology centre. This would also constitute a complementary installation for the R&D radioisotope room, which is proposed to be associated with the LINAG (*in the work plans for the interdisciplinary applications at GANIL).*

- **Other applications** may be envisioned and will be discussed, **for solid-state physics and chemistry**, with colleagues from CIMAP and CRISMAT; **for industry**, for instance for micro-satellite irradiation.

References
[*Thmed1*] *Flash:* V. Favaudon et al., Sci.Transl Med 6, 245ra293, 2014.
GRID and micro-beam: P. Regnard, G. Le Duc, E. Bräuer-Krisch *et al.,* Phys Med Biol.2008; 53(4):861-878, *https://doi.org/10.1088/0031-9155/53/4/003*
F.A. Dilmanian, T.M. Button, G. Le Duc *et al.,* Neuro. Oncol. 2002; 4(1):26-38.
https://doi.org/10.1093/neuonc/4.1.26
[*Thmed2*] Medical programme at PRAE: A. Faus Golfe *et al.,* IPAC2018, Vancouver, BC, Canada, *https://doi.org/10.18429/JACoW-IPAC2018-MOPML051*
 [*Thmed3*] Robertson AKH, Ramogida CF, Schaffer P, Radchenko V., *Development of 225Ac Radiopharmaceuticals: TRIUMF Perspectives and Experiences.* Curr Radiopharm. 2018; 11(3):156–172. *https://doi.org/10.2174/1874471011666180416161908*
[*Thprae*] (PRAE Collaboration) D. Marchand et al., EPJ Web of Conf. 138 (2017) 010102.

II. Medical applications of very high energy electron (VHEE) beams

Contributions (II.1-4) from:
S. Salvador[a], R. Delorme[b], V. Favaudon[c], S. Heinrich[c], L. de Marzi[c], Y. Prezado[c]
a. Normandie University, ENSICAEN, UNICAEN, CNRS/IN2P3, LPC Caen,
b. Univ. Grenoble Alpes, CNRS, Grenoble INP, LPSC-IN2P3
c. Institut Curie, Inserm U 1021-CNRS UMR 3347, University Paris-Saclay

One of the recent challenges in conventional radiotherapy consists in the constant struggle of increasing the so-called *Tumour Control Probability* (TCP) while decreasing the Normal Tissue Complication Probability (NTCP). In other terms, finding the therapeutic window of irradiation doses that will sterilise the tumour cells and spare as much as possible the surrounding normal tissues and organs (***Figure 1***). Some modern techniques such as intensity-modulated radiotherapy using MV photon beams or light and heavy ions may have widen the therapeutic window to some extent but acute radiation reactions might still arise and be a reason for treatment interruptions or failure. Moreover, radioresistant tumours might also need higher radiation dose to control local disease progression but at the risk of intolerable acute or late toxicity. Hence, innovations in radiation therapy treatment are still required to overcome these limitations.
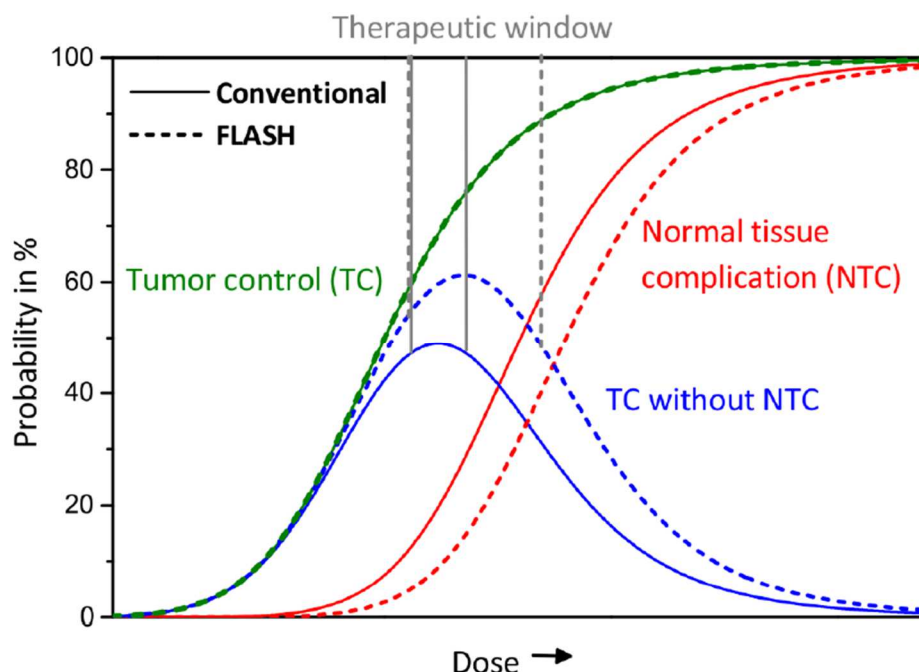

Figure 1. Illustration of dependence of tumour control probability (TCP, green) and normal tissue complications probability (NTCP, red) on dose for conventional (solid) and FLASH (dashed) radiotherapy. TCP without NTCP (blue) has its maximum in the so-called therapeutic window. Extracted from [1].

VHEE radiotherapy (very-high energy electrons, in the energy range of 100 to 250 MeV), first proposed in the 2000s, would be particularly accurate and independent of tissue heterogeneities (unlike low energy electrons or protons), and could be applicable in a large number of deep anatomical localisations due to higher dose depth profiles (as illustrated in ***figure 2***). It is also potentially much less expensive than other radiotherapy techniques, and would allow accelerated treatment, for example through *Spatially Fractionated Radiotherapy* (SFR) as well as *Ultra-High Dose Rate irradiation* (UHDR or FLASH), thereby improving its effectiveness to limit side effects to critical normal structures to an acceptable degree of toxicity.
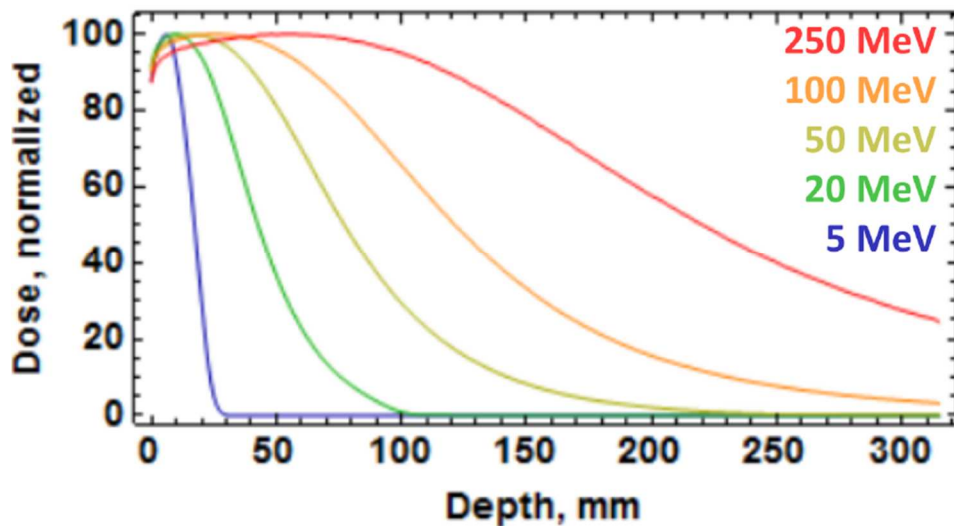
Figure 2: Example of dose depth profiles for several electron beam energies. Extracted from [2].

1. Spatially Fractionated Radiotherapy using VHEE

In SFR, the resulting dose profiles consist of a pattern of peaks and valleys, with high doses along the beam paths and low doses in the spaces between them. This have been proven safe and effective in delivering large cumulative doses without causing severe damage to healthy tissues, either with the Grid irradiation technique (centimeter-sized collimated beams) or using mini or micro-beams (beam sizes from 50 to 400—700 µm [3]). Small beams allow exploiting the dose volume effects: the smaller the beam size, the higher the tolerances of the normal tissue. For these reasons, the combination of VHEE with the benefits of Grid therapy has been proposed [4] (see *figure 3*). One advantage of using charged beams is that sub-millimetric beam sizes can be obtained with pure magnetic collimation, avoiding the degradation of the grid pattern on the accumulated dose due to secondary particles coming from a collimator. Varying physical parameters such as beam energies, grid sizes, and grid spacing, it is possible to favor tumour exposure by delivering a quasi-homogeneous dose in the tumour, or to enhance the normal tissue tolerance by enlarging the fractionated dose area.
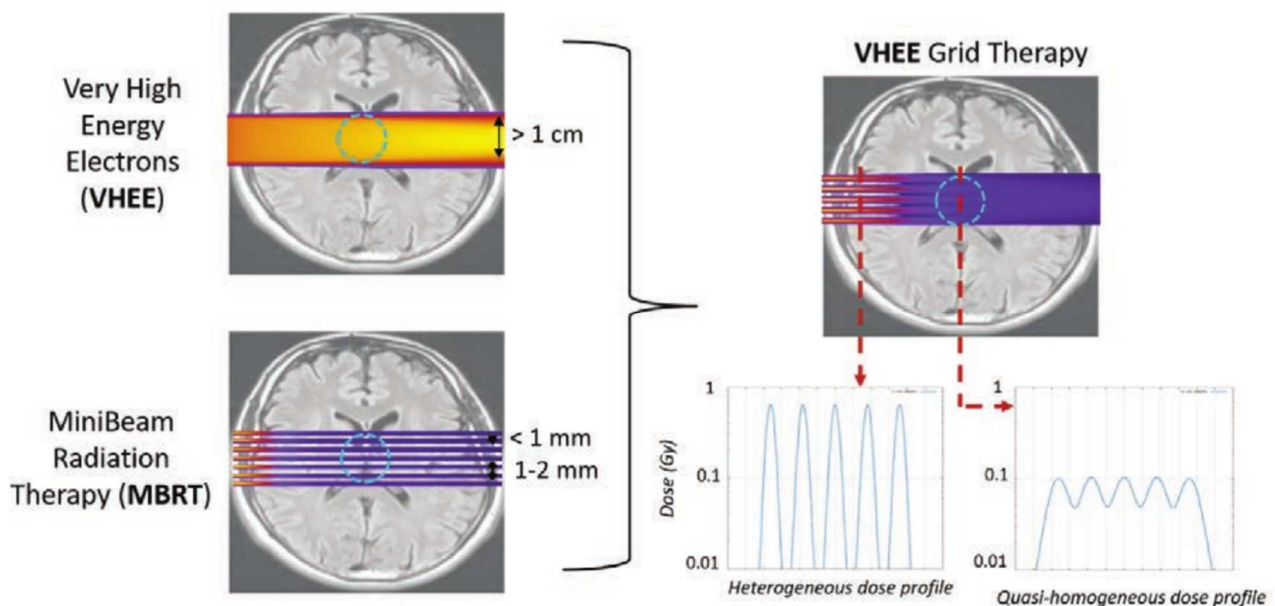

Figure 3. Principle of the spatial fractionation of dose and VHEE Grid therapy with two examples of peak and valley dose profiles. Extracted from [5].

2. FLASH-RT

UHDR used in *FLASH radiotherapy* (FLASH-RT) demonstrated in vivo to dramatically reduce adverse side effects to healthy tissues while being as effective for tumour control as *conventional radiotherapy* (CONV-RT) [6]. The therapeutic window is then further widened as illustrated in ***figure 1*** (dashed lines), opening the scope of applications of FLASH-RT for radioresistant tumours. The irradiation conditions of UHDR to observe a significant FLASH effect have been proposed in [7]. While the dose rate could be as high as 1×10^6 Gy/s, an equivalent total dose as for CONV-RT between 10—50 Gy has to be delivered. In the current state of knowledge, this can be achieved using very short pulses of few µs with doses above 1 Gy (~10 nC electrons per pulse) for a total irradiation time less than 100 ms.

Most of the pre-clinical studies investigating FLASH effect have been done so far with electron beams generated by a compact LINAC with energies not exceeding 6 MeV, which are only suitable for treatment of superficial or shallow-seated lesions. As an example, ***figure 4*** shows a mini-pig skin irradiated with both conventional (5 Gy/min) and FLASH-RT (1 Gy/µs) with the same total dose. In the case of the FLASH irradiation, the skin did not present necrotic lesions compared to the conventional irradiation, illustrating the high potential of FLASH irradiations. VHEE would allow to investigate the benefits of both modalities for deep-seated tumours but this however represents a challenge from the accelerator point of view as the electron beam current will have to be above 10 mA.

Figure 4. Irradiation of a mini-pig skin with the same total doses, delivered using 300 Gy/s (FLASH) and 5 Gy/min (CONV) dose rates. Necrotic lesions were observed at the CONV-irradiated spots whereas the skin in FLASH-irradiated spots presented quasi-normal appearance. Picture extracted from [8].

3. The dosimetric challenges

SFR as well as FLASH-RT present significant metrological challenges as there are three to four orders of magnitude either in smaller beam sizes or in higher dose rates than for conventional medical accelerators.

For SFR, the narrow beam widths (typically from 50 μm for microbeam to 400 μm for minibeam) require a detector with submillimetric dimensions to accurately measure peak doses and scattered dose between the beams (valley). The detector should also exhibit tissue equivalence in a large range of particle/particle energies (applications exists from KV X-ray spectra to protons or VHEE) and have a linear response with dose rate and beam energy. A robust dosimetry protocol is then at the core of any quality assurance or experiment for these new radiation therapy techniques, and thus presents significant challenges to dosimetric measurements.

Concerning FLASH-RT, the established active detectors for online dosimetry start to fail when the dose rate/dose-per-pulse is increased beyond what is used in CONV-RT [9]. Two aspects of the dosimetry are particularly difficult to ensure within clinical accuracy: establishing standards for the delivered dose (whether for absolute or relative dosimetry) and monitoring the beam for deviations during the irradiations. For example, significant efforts are currently made on developing and modifying calorimeters as primary absorbed dose standards but aspects of their behaviours under VHEE and UHDR irradiation still remain unknown. Concerning the beam monitoring, ionization chambers are considered the gold standard by the international codes of practice. Their reduced charge collection efficiency due to ion recombination can be corrected in the case of CONV-RT but reaches its limit for FLASH irradiation, where the high charge density in the chamber makes it non-linear and non-proportional. Those challenges will have to be thoroughly investigated before any clinical implementation of FLASH-RT.

4. Conclusion

Combining the ballistic and practical advantages of VHEE with the potential of new forms of radiotherapy such as SFR and FLASH irradiations would allow to effectively treat radioresistant and deep-seated tumours while limiting side effects compared to CONV-RT.
The construction of a dedicated machine for very-high energy electrons with SFR and FLASH capabilities ready for physics, biology and preclinical studies would allow many research groups associated to deepen our knowledge on these irradiation modalities.

References

[1] A. Schüller, S. Heinrich, C. Fouillade, *et al. The European Joint Research Project UHD pulse– metrology for advanced radiotherapy using particle beams with ultra-high pulse dose rates.* Physica Medica: European Journal of Medical Physics, 80(1):134–150, 2020.
[2] A. Lagzda. *Applications of very high energy electrons (50-250 MeV) for radiotherapy. indico.cern.ch/event/578818/contributions/2487012/attachments/1435583/2207629/strathclydeVHEE2.pdf,* 2017. EUCARD-2 Annual Meeting.
[3] Y. Prezado, M. Dos Santos, W. Gonzalez, *et al. Transfer of minibeam radiation therapy into a cost-effective equipment for radiobiological studies: a proof of concept.* Scientific Reports, 7:17295, 2017.
[4] I. Martínez-Rovira, G. Fois and Y. Prezado. *Dosimetric evaluation of new approaches in GRID therapy using non conventional radiation sources.* Medical Physics, 42(2):685–693, 2015.
[5] R. Delorme, D. Marchand, and C. Vallerand. *The PRAE multidisciplinary project.* Nuclear Physics News, 29(1):32–35, 2019. *https://doi.org/10.1080/10619127.2019.1571833*
[6] V. Favaudon, L. Caplier, V. Monceau *et al. Ultrahigh dose-rate FLASH irradiation increases the differential response between normal and tumor tissue in mice.* Science Translational Medicine, 6(245):245ra93, 2014.
[7] V. Favaudon, J.-M. Lentz, S. Heinrich, *et al. Time-resolved dosimetry of pulsed electron beams in very high dose-rate, FLASH irradiation for radiotherapy preclinical studies.* Nucl. Instr. Meth.in Physics Research Section A: Accelerators, Spectrometers, Detectors and Associated Equipment, 944:162537, 2019.
[8] M.-C. Vozenin, P. De Fornel, K. Petersson, *et al. The advantage of FLASH radiotherapy confirmed in mini-pig and cat-cancer patients.* Clinical Cancer Research, 25(1):35–42, 2019.
[9] M. McManus, F. Romano, N.D. Lee *et al. The challenge of ionisation chamber dosimetry in ultra-short pulsed high dose-rate very high energy electron beams.* Scientific Reports, 10:9089, 2020.